NASA TECHNICAL NOTE

SHEAR-FLEXIBLE FINITE-ELEMENT MODELS OF LAMINATED COMPOSITE PLATES AND SHELLS

Ahmed K. Noor and Michael D. Mathers

Langley Research Center
Hampton, Va. 23665

NATIONAL AERONAUTICS AND SPACE ADMINISTRATION • WASHINGTON, D. C. • DECEMBER 1975

1 Report No	2. Government Accession No.	3. Recipient's Catalog No.
NASA TN D-8044		

4. Title and Subtitle
SHEAR-FLEXIBLE FINITE-ELEMENT MODELS OF LAMINATED COMPOSITE PLATES AND SHELLS

5. Report Date
December 1975

6. Performing Organization Code

7. Author(s)
Ahmed K. Noor and Michael D. Mathers

8. Performing Organization Report No.
L-10414

10. Work Unit No.
506-17-21-02

9. Performing Organization Name and Address
NASA Langley Research Center
Hampton, Va. 23665

11. Contract or Grant No.

13. Type of Report and Period Covered
Technical Note

12 Sponsoring Agency Name and Address
National Aeronautics and Space Administration
Washington, D.C. 20546

14. Sponsoring Agency Code

15. Supplementary Notes

Ahmed K. Noor and Michael D. Mathers: The George Washington University, Joint Institute for Acoustics and Flight Sciences.

16 Abstract

Several finite-element models are applied to the linear static, stability, and vibration analysis of laminated composite plates and shells. The study is based on linear shallow-shell theory, with the effects of shear deformation, anisotropic material behavior, and bending-extensional coupling included. Both stiffness (displacement) and mixed finite-element models are considered. Discussion is focused on the effects of shear deformation and anisotropic material behavior on the accuracy and convergence of different finite-element models. Numerical studies are presented which show the effects of (a) increasing the order of the approximating polynomials, (b) adding internal degrees of freedom, and (c) using derivatives of generalized displacements as nodal parameters.

17. Key Words (Suggested by Author(s))
Finite elements
Fibrous composites
Anisotropy
Shells
Plates
Laminates
Stress analysis
Stability
Vibrations
Shear deformation

18. Distribution Statement
Unclassified – Unlimited

Subject Category 39

19. Security Classif. (of this report)	20. Security Classif. (of this page)	21. No. of Pages	22. Price*
Unclassified	Unclassified	111	$5.25

*For sale by the National Technical Information Service, Springfield, Virginia 22161

CONTENTS

SHEAR-FLEXIBLE FINITE-ELEMENT MODELS OF LAMINATED COMPOSITE PLATES AND SHELLS

Ahmed K. Noor* and Michael D. Mathers*
Langley Research Center

SUMMARY

Several finite-element models are applied to the linear static, stability, and vibration analysis of laminated composite plates and shells. The study is based on linear shallow-shell theory, with the effects of shear deformation, anisotropic material behavior, and bending-extensional coupling included. Both stiffness (displacement) and mixed finite-element models are considered. Discussion is focused on the effects of shear deformation and anisotropic material behavior on the accuracy and convergence of different finite-element models. Numerical studies are presented which show the effects of (a) increasing the order of the approximating polynomials, (b) adding internal degrees of freedom, and (c) using derivatives of generalized displacements as nodal parameters.

INTRODUCTION

Although the finite-element analysis of isotropic plates and shells has received considerable attention in the literature, investigations of laminated composite plates and shells are rather limited in extent. The reliable prediction of the response characteristics of high-modulus fibrous composite plates and shells often requires inclusion of the transverse shear effects in their mathematical models. This fact has been amply documented for linear static, stability, and dynamic problems. (See, for example, refs. 1 to 5.)

At present there are three approaches for developing plate and shell finite-element models which account for shear deformation. The first approach is based on the use of three-dimensional isoparametric solid elements which automatically include the shear-distortion mechanism (refs. 6 and 7). The second approach employs two-dimensional elements used with independent shape (or interpolation) functions for displacements and rotations (refs. 8 and 9). The third approach is based on the addition of effects of shear deformation to two-dimensional classical plate or shell elements through the use of equilibrium equations (refs. 10 and 11). Although it is desirable to have an element which gives accurate results regardless of how important the shear deformation is, most of the existing elements do not satisfy this requirement.

*The George Washington University, Joint Institute for Acoustics and Flight Sciences.

In the context of the stiffness method, the first approach has the major disadvantage that it leads to a stiffness matrix which is (1) very large for laminated composites consisting of many layers and (2) highly ill conditioned for thin plates or shells. If low-order interpolation polynomials are used, the second approach leads to overly stiff elements for very thin plates and shells. Although the aforementioned drawbacks have been recognized and some improvements have been suggested, the difficulties have not been overcome. (See, e.g., refs. 12 to 17.) The range of validity of the third approach has not been explored. Since the second approach provides flexibility and simplicity in fulfilling the interelement compatibility conditions and does not result in as large a stiffness matrix as in the first approach, it was adopted in the present study.

The first objective of this paper is to assess the relative merits of a number of displacement and mixed shear-flexible finite elements when applied to the linear static, stability, and vibration problems of laminated plates and shells. Emphasis is focused on the effects of shear deformation and anisotropic material behavior on the accuracy and convergence of the different models. The second objective is to study the effects of increasing the order of approximating polynomials, adding internal degrees of freedom, and using derivatives of generalized displacements as nodal parameters on the accuracy and rate of convergence of the different models. To the authors' knowledge no publication exists in which the aforementioned effects are studied in any detail.

The analytical formulation is based on a form of the shallow-shell theory modified to include the effects of shear deformation and rotary inertia. Indicial notation is used throughout this paper since it is particularly useful in identifying the symmetries and, consequently, simplifies the element development. Both triangular and quadrilateral elements are considered. The elements are conforming and satisfy continuity requirements of the type C^0 (continuity of the fundamental unknowns).

SYMBOLS AND NOTATION

$A_{\alpha\beta\gamma\rho}, A_{\alpha 3\beta 3}, B_{\alpha\beta\gamma\rho}, G_{\alpha\beta\gamma\rho}$ shell compliance coefficients, inverse of shell stiffnesses

a side length of plate or shallow shell

$C_{\alpha\beta\gamma\rho}$ extensional stiffnesses of shell

$C_{\alpha 3\beta 3}$ transverse shear stiffnesses of shell

$c^{(k)}_{\alpha\beta\gamma\rho}, c^{(k)}_{\alpha 3\beta 3}$ stiffness coefficients of kth layer of shell

c_σ, c_u portions of shell boundary over which tractions and displacements are prescribed

$D_{\alpha\beta\gamma\rho}$ bending stiffnesses of shell

E elastic modulus of isotropic materials

E_f error index (see eq. (36))

E_L, E_T elastic moduli in direction of fibers and normal to it, respectively

$F_{\alpha\beta\gamma\rho}$ stiffness interaction coefficients of shell

f rise of shallow shells

G_{LT}, G_{TT} shear moduli in plane of fibers and normal to it, respectively

H_J^i nodal stress resultants

h local thickness of shell

h_k, h_{k-1} distances from reference (middle) surface to top and bottom surfaces of kth layer, respectively

K_{IJ}^{ij} stiffness coefficients of shell element

$\overline{K}_{IJ}^{ij}$ geometric or initial stress stiffness coefficients of shell element

$k_{\alpha\beta}$ curvatures and twist of shell reference surface

$\ell_{\alpha,\alpha'}$ direction cosines, $\cos(x_\alpha, x_{\alpha'})$

M_{IJ}^{ij} consistent mass coefficients of shell element

$M_{\alpha\beta}$ bending-moment stress resultants

m number of shape functions

m_0, m_1, m_2 density parameters of shell

N^i	shape or interpolation functions
$N_{\alpha\beta}$	extensional (in-plane) stress resultants
$N^o_{\alpha\beta}$	relative magnitudes of prestress components
n	total number of elements in x_1- or x_2-direction
$\bar{n}$	total number of nodes in finite-element model
n_α	unit outward normal to shell boundary
P^i_I	consistent nodal load coefficients
p, p_α	external load intensities in coordinate directions
p_o	intensity of uniform pressure loading
Q_α	transverse shear stress resultants
R	radius of curvature
r	radial coordinate in circular cylindrical shell (see fig. 24)
$S^{ij}_{IJ}, S^{\bar{i}j}_{I\bar{J}}$	"generalized" stiffness coefficients of shell element
T	kinetic energy of shell
U	strain energy of shell
U^c	complementary energy of shell
U^o	strain energy due to prestress
U_{sh}, U_a	measures of shear deformation and degree of anisotropy
u_α, w	displacement components in coordinate directions
V	work done by internal forces

$W, \overline{W}$ work done by external forces

x_α, x_3 orthogonal curvilinear coordinate system (see fig. 1)

x_α^i nodal values of x_α

$\bar{\beta}$ dimensionless eigenvalues of stiffness matrix

ζ_r relative size of rth element in variable grid (eq. (37))

η_r, η_{r+1} dummy coordinates of ends of rth element

θ fiber orientation, angle between fiber direction and x_1-axis

κ constant defined in appendix D

λ in-plane loading parameter

$\bar{\lambda}$ nondimensional frequency $\left(\omega\sqrt{\rho a^2/E_T}\right.$ for plates; $\omega\sqrt{\rho h^2/E_T}$ for shallow spherical segments; $\left.\omega\sqrt{\rho R^2/E_T}\right.$ for circular cylinders)

ν Poisson's ratio for isotropic materials

ν_{LT} Poisson's ratio measuring strain in T-direction (transverse) due to uniaxial normal stress in L-direction (direction of fibers)

$\xi_\alpha^{(i)}$ natural coordinates of node i

ξ_α, ξ_3 natural (dimensionless) coordinate system in element domain

Π, Π_R functionals defined in equations (1) and (2)

ρ density of plate or shell material

$\rho_s^{(k)}$ density of kth layer of laminated shell

σ_o uniform extensional stress in cylindrical shell

ϕ_α rotation components

ψ_J^i nodal displacement parameters

Ω shell domain

ω circular frequency of vibration of shell

∂_α $= \frac{\partial}{\partial x_\alpha}$

Range of indices:

Lowercase Latin indices 1 to m

Uppercase Latin indices:

I,J 1 to 5

$\bar{I},\bar{J}$ 1 to 8

Greek indices 1,2

Finite-element-model notation:

SQN stiffness formulation, quadrilateral element, N shape functions per fundamental unknown

STN stiffness formulation, triangular element, N shape functions per fundamental unknown

MQN mixed formulation, quadrilateral element, N shape functions per fundamental unknown

MTN mixed formulation, triangular element, N shape functions per fundamental unknown

SQH stiffness formulation, quadrilateral element, Hermitian interpolation functions

MATHEMATICAL FORMULATION

The analytical formulation is based on a form of the shallow-shell theory, with the effects of shear deformation, anisotropic material behavior, rotary inertia, and bending-extensional coupling included. (See appendix A and ref. 18.) For stability problems, the prebuckling stresses are assumed to be given by the momentless (membrane) theory. Two finite-element formulations are considered. In the first formulation (displacement model) the

fundamental unknowns consist of the displacement and rotation components of the shell reference (middle) surface, and the stiffness matrix is obtained by using Hamilton's principle (which for static problems reduces to the principle of minimum potential energy). The fundamental unknowns in the second formulation (mixed model) consist of the 13 shell quantities: generalized displacements u_α, w, and ϕ_α and stress resultants $N_{\alpha\beta}$, $M_{\alpha\beta}$, and Q_α. (See fig. 1 for sign convention.) The generalized stiffness matrix is obtained by using a modified form of the Hellinger-Reissner mixed variational principle.

The functionals used in the development of displacement and mixed models are given by the following equations:

Displacement models

$$\Pi(u_\alpha,w,\phi_\alpha) = U + U^O - W - T \tag{1}$$

Mixed models

$$\Pi_R(N_{\alpha\beta},M_{\alpha\beta},Q_\alpha,u_\alpha,w,\phi_\alpha) = V + U^O - U^c - W - \overline{W} - T \tag{2}$$

where

$$U = \frac{1}{2}\int\Big\{C_{\alpha\beta\gamma\rho}\left[\partial_\alpha u_\beta\ \partial_\gamma u_\rho + 2k_{\alpha\beta}\ \partial_\gamma u_\rho\ w + k_{\alpha\beta}k_{\gamma\rho}(w)^2\right] + 2F_{\alpha\beta\gamma\rho}\big(\partial_\alpha u_\beta\ \partial_\gamma\phi_\rho + k_{\alpha\beta}\ \partial_\gamma\phi_\rho w\big) + D_{\alpha\beta\gamma\rho}\ \partial_\alpha\phi_\beta\ \partial_\gamma\phi_\rho + C_{\alpha3\beta3}\big(\partial_\alpha w\ \partial_\beta w + 2\phi_\alpha\ \partial_\beta w + \phi_\alpha\phi_\beta\big)\Big\}\,d\Omega \tag{3}$$

$$U^O = \frac{1}{2}\lambda\int N^O_{\alpha\beta}\ \partial_\alpha w\ \partial_\beta w\ d\Omega \tag{4}$$

$$V = \int\left[N_{\alpha\beta}\big(\partial_\alpha u_\beta + k_{\alpha\beta}\ w\big) + M_{\alpha\beta}\ \partial_\alpha\phi_\beta + Q_\alpha\big(\phi_\alpha + \partial_\alpha w\big)\right]d\Omega \tag{5}$$

$$U^c = \frac{1}{2}\int\big(A_{\alpha\beta\gamma\rho}\ N_{\alpha\beta}\ N_{\gamma\rho} + 2B_{\alpha\beta\gamma\rho}\ N_{\alpha\beta}\ M_{\gamma\rho} + G_{\alpha\beta\gamma\rho}\ M_{\alpha\beta}\ M_{\gamma\rho} + A_{\alpha3\beta3}\ Q_\alpha\ Q_\beta\big)d\Omega \tag{6}$$

$$T = \frac{1}{2}\omega^2\int\left[m_0\big(u_\alpha u_\alpha + ww\big) + 2m_1 u_\alpha\phi_\alpha + m_2\phi_\alpha\phi_\alpha\right]d\Omega \tag{7}$$

$$W = \int\big(p_\alpha u_\alpha + pw\big)d\Omega + \int_{c_\sigma}\big(\widetilde{N}_{\alpha\beta}u_\alpha + \widetilde{M}_{\alpha\beta}\phi_\alpha + \widetilde{Q}_\beta w\big)n_\beta dc \tag{8}$$

$$\overline{W} = \int_{c_u}\left[N_{\alpha\beta}\big(-\widetilde{u}_\alpha + u_\alpha\big) + M_{\alpha\beta}\big(-\widetilde{\phi}_\alpha + \phi_\alpha\big) + Q_\beta\big(-\widetilde{w} + w\big)\right]n_\beta dc \tag{9}$$

In equations (3) to (9), $C_{\alpha\beta\gamma\rho}$, $D_{\alpha\beta\gamma\rho}$, and $F_{\alpha\beta\gamma\rho}$ are extensional stiffnesses, bending stiffnesses, and stiffness interaction coefficients of the shell; $C_{\alpha3\beta3}$ are transverse shear

stiffnesses of the shell; $A_{\alpha\beta\gamma\rho}$, $B_{\alpha\beta\gamma\rho}$, $G_{\alpha\beta\gamma\rho}$, and $A_{\alpha 3\beta 3}$ are shell compliance coefficients (see appendix A); $k_{\alpha\beta}$ are the curvature components and twist of the shell surface; $\lambda N^{o}_{\alpha\beta}$ are the initial stress resultants (prestress field) which are proportional to the in-plane load factor λ; p_α and p are the external load components in the orthogonal coordinate directions x_α and x_3, respectively; m_0, m_1, and m_2 are density parameters of the shell defined in appendix B; ω is the circular frequency of vibration of the shell; Ω is the shell domain; c_σ and c_u are portions of the boundary over which tractions and displacements are prescribed; n_α is the unit normal to the boundary; the quantities with a tilde denote prescribed boundary stress resultants and displacements; and $\partial_\alpha \equiv \frac{\partial}{\partial x_\alpha}$.

FINITE-ELEMENT DISCRETIZATION

The shell region is decomposed into finite elements $\Omega^{(e)}$ connected at appropriate nodes, where the superscript e refers to the element. A typical element is isolated from the model and the fundamental unknowns are approximated by expressions of the form:

Displacement models

$$u_\alpha = N^i \psi^i_\alpha \tag{10}$$

$$w = N^i \psi^i_3 \tag{11}$$

$$\phi_\alpha = N^i \psi^i_{3+\alpha} \tag{12}$$

Mixed models

In addition to the approximations of the generalized displacements (eqs. (10) to (12)), the stress resultants are approximated by

$$N_{\alpha\beta} = N^i H^i_{\alpha+\beta-1} \tag{13}$$

$$M_{\alpha\beta} = N^i H^i_{\alpha+\beta+2} \tag{14}$$

$$Q_\alpha = N^i H^i_{\alpha+6} \tag{15}$$

where superscripts identify the location and subscripts designate the ordering of nodal unknowns; N^i are the shape (or interpolation) functions; ψ^i_J (i = 1 to m, J = 1 to 5) are nodal displacement parameters (including, possibly, nodeless variables); $H^i_{\bar{J}}$ (i = 1 to m, $\bar{J}$ = 1 to 8)

are nodal stress-resultant parameters; m equals the number of shape functions in the approximation; Greek indices take the values 1,2; and a repeated lowercase Latin index denotes summation over the range 1 to m.

ELEMENT-BEHAVIOR REPRESENTATION

A number of displacement and mixed finite elements having both triangular and quadrilateral shapes were developed in the present study. All the elements satisfy the continuity conditions required by the variational principles on which they are based. Within each family of elements, different shape (or interpolation) functions are used for approximating the fundamental unknowns. The characteristics and designations of these elements are summarized in table 1 and are referred to frequently in the subsequent sections.

All the triangular elements developed are based on complete polynomial approximations of the fundamental unknowns, thus ensuring that the functional variation is independent of coordinate transformations. Most of the quadrilateral elements considered in the present study are of the serendipity type (refs. 19 and 20), that is, with their nodes located along the element boundaries. The polynomial approximations used in these elements include terms which are of higher order than the complete expansion, and therefore, the functional variation is dependent on coordinate transformation.

In each element, the same set of shape functions is used for approximating all the fundamental unknowns and the nodal parameters are selected to be the values of the fundamental unknowns at the different nodes. However, in one of the elements (SQ8-4 element), polynomials of different degree were used for approximating different sets of fundamental unknowns (lower degree polynomials were used for approximating the rotations); in the SQH element, products of first-order Hermitian polynomials were chosen as shape functions and the nodal parameters consisted of the generalized displacements, their first derivatives, and mixed second derivative with respect to the dimensionless local coordinates ξ_1 and ξ_2. (See appendix C.) Continuity of these derivatives is enforced along the interelement boundaries. Since this is not required by the variational principle, the element is overconforming.

For the two quadrilateral stiffness elements with four and eight nodes, internal degrees of freedom are added through the addition of displacement modes which vanish along the edges of the element. Those modes are usually called bubble functions (ref. 21). The shape functions associated with the internal degrees of freedom are products of the equations of the element boundaries times another polynomial, with the product representing bubble or internal displacement modes (elements SQ5, SQ7, SQ9, and SQ11). The case of one internal mode (SQ5 and SQ9) corresponds to zero degree of the latter polynomial. (See table 1 and appendix C.)

In all the elements developed, the rigid body modes that cause no straining have not been included explicitly in the displacement fields; rather, implicit representation of these modes was made. A quantitative estimate of the accuracy of rigid-body-mode representation was made by evaluating the six lowest eigenvalues of the element stiffness matrix. This is discussed further in connection with the numerical studies.

For modeling shells with curved boundaries, isoparametric elements were used in which the element boundary curves are approximated by the same shape functions used in approximating the behavior functions, that is,

$$x_\alpha = N^i x_\alpha^i \tag{16}$$

where x_α^i are the nodal values of x_α. Numerical results obtained with the use of isoparametric SQ12 elements are presented in the next main section.

FINITE-ELEMENT EQUATIONS

The governing equations for each element are obtained by first replacing the fundamental unknowns by their expressions in terms of the shape functions (eqs. (10) to (15)) in the appropriate functional (action integral for displacement models and Hellinger-Reissner functional for mixed models) and then applying the stationary conditions of that functional. This leads to a set of equations for each element of the following form:

Displacement models

$$\left[K_{IJ}^{ij} + \lambda \bar{K}_{IJ}^{ij}\right] \psi_J^j = P_I^i + \omega^2 M_{IJ}^{ij} \psi_J^j \tag{17}$$

Mixed models

$$\left.\begin{aligned} -S_{I\bar{J}}^{ij} H_{\bar{J}}^j + \bar{S}_{\bar{I}J}^{ij} \psi_J^j &= 0 \\ \text{and} \\ \bar{S}_{I\bar{J}}^{ij} H_{\bar{J}}^j + \lambda \bar{K}_{IJ}^{ij} \psi_J^j &= P_I^i + \omega^2 M_{IJ}^{ij} \psi_J^j \end{aligned}\right\} \tag{18}$$

where K_{IJ}^{ij} and $\bar{K}_{IJ}^{ij}$ are stiffness and geometric, or initial stress, stiffness coefficients; M_{IJ}^{ij} are consistent mass coefficients; $S_{I\bar{J}}^{ij}$ and $\bar{S}_{\bar{I}J}^{ij}$ are "generalized" stiffness coefficients; and P_I^i are consistent load coefficients. The formulas for the aforementioned stiffness, mass,

and load coefficients are given in appendix D. For stress-analysis problems, $\lambda = \omega = 0$; for bifurcation-buckling problems, $\omega = P_I^i = 0$; and for free-vibration problems, $\lambda = P_I^i = 0$.

In equations (17) and (18) the range of the lowercase Latin superscripts is 1 to m; the range of the uppercase Latin subscripts (I,J) and $(\bar{I},\bar{J})$ is 1 to 5 and 1 to 8, respectively. The K, M, and S terms are completely symmetric under the interchange of one pair of indices for another, each pair of indices consisting of a superscript and a subscript just beneath it.

To write equations (17) and (18) in matrix form, the first superscript-subscript pair of each of the K, S, and M terms defines the row number and the second pair defines the column number. For example, in equations (17) the term K_{IJ}^{ij} is located in the $[5(i-1) + I]$th row and the $[5(j-1) + J]$th column of the element stiffness matrix.

In the stress-analysis problems, the internal degrees of freedom (nodal parameters associated with bubble modes) can be eliminated without any loss of accuracy by using the static condensation procedure (ref. 22). In stability and vibration problems, this is not done since it results in approximate elemental matrices.

The integrals in the expressions for the stiffness, mass, and load coefficients (appendix D) are evaluated by means of the numerical quadrature formulas presented in references 20 and 23. In each case, the quadrature formula selected had the least number of points required to ensure exact evaluation of the integrals (depending on the degree of the interpolation polynomials). Exceptions to this are the cases of general quadrilateral or isoparametric elements based on the displacement models in which the stiffness and geometric stiffness coefficients contain fractional rational functions that are approximated by polynomials in the numerical quadrature process. Each entry in the elemental matrices S and $\bar{S}$ of the mixed models (eqs. (18)) contains just a single term. (See appendix D.) In contrast, the entries of the matrix K of the displacement models (eqs. (17)) are linear combinations of at least four terms, as implied by the repeated (dummy) subscripts of the coefficients K in appendix D. In view of this, the formation of the elemental matrices for the mixed models is simpler and was found to be less time consuming than for the displacement models.

BOUNDARY CONDITIONS

In the displacement models, only kinematic (geometric) boundary conditions need to be satisfied. Force (stress) boundary conditions can also be satisfied if displacement derivatives are chosen as nodal parameters (e.g., SQH element). The effect of introducing the stress boundary conditions on the accuracy of solutions is discussed in the examples in the section "Numerical Studies."

In the mixed models, both kinematic and force (stress) boundary conditions must be satisfied. The boundary conditions used in the present study are listed in table 2. The numeral 1 in this table indicates that the nodal parameter is retained and 0 indicates that the nodal parameter is set to zero.

For inclined (or curved) boundaries, it is convenient to use a modified set of nodal parameters including normal and tangential components of displacements and stress resultants at the boundary points, that is, $u_{\alpha'}$, $\phi_{\alpha'}$, $N_{\alpha'\beta'}$, $M_{\alpha'\beta'}$, and $Q_{\alpha'}$ (see fig. 2), where

$$\begin{Bmatrix} u_\alpha \\ \phi_\alpha \end{Bmatrix} = \ell_{\alpha,\alpha'} \begin{Bmatrix} u_{\alpha'} \\ \phi_{\alpha'} \end{Bmatrix} \tag{19}$$

$$\begin{Bmatrix} N_{\alpha\beta} \\ M_{\alpha\beta} \end{Bmatrix} = \ell_{\alpha,\alpha'}\ \ell_{\beta,\beta'} \begin{Bmatrix} N_{\alpha'\beta'} \\ M_{\alpha'\beta'} \end{Bmatrix} \tag{20}$$

$$Q_\alpha = \ell_{\alpha,\alpha'}\ Q_{\alpha'} \tag{21}$$

with $$\ell_{\alpha,\alpha'} = \cos(x_\alpha, x_{\alpha'}) \tag{22}$$

The element equations at that boundary point are modified accordingly. For example, equations (17) are modified as follows:

$$\left[K^{ij}_{I'J'} + \lambda \bar{K}^{ij}_{I'J'}\right] \psi^j_{J'} = P^i_{I'} + \omega^2\ M^{ij}_{I'J'}\ \psi^j_{J'} \tag{23}$$

where the relations between $K^{ij}_{I'J'}$ and K^{ij}_{IJ} are given by

$$K^{ij}_{\alpha'\beta'} = \ell_{\alpha,\alpha'}\ \ell_{\beta,\beta'}\ K^{ij}_{\alpha\beta} \tag{24}$$

$$K^{ij}_{\alpha'3} = \ell_{\alpha,\alpha'}\ K^{ij}_{\alpha3} \tag{25}$$

$$K^{ij}_{\alpha',\beta'+3} = \ell_{\alpha,\alpha'}\ \ell_{\beta,\beta'}\ K^{ij}_{\alpha,\beta+3} \tag{26}$$

$$K^{ij}_{3'3'} = K^{ij}_{33} \tag{27}$$

$$K^{ij}_{3,\alpha'+3} = \ell_{\alpha,\alpha'}\, K^{ij}_{3,\alpha+3} \tag{28}$$

$$K^{ij}_{\alpha'+3,\beta'+3} = \ell_{\alpha,\alpha'}\, \ell_{\beta,\beta'}\, K^{ij}_{\alpha+3,\beta+3} \tag{29}$$

with similar relations for $\bar{K}^{ij}_{I'J'}$ and $M^{ij}_{I'J'}$.

ASSEMBLY AND SOLUTION OF EQUATIONS

If the elemental matrices are assembled and the boundary conditions are incorporated, the resulting finite-element field equations can be represented in the following compact form:

Displacement models

$$\left[\left[K\right] + \lambda\left[\bar{K}\right]\right]\langle\psi\rangle = \langle P\rangle + \omega^2\left[M\right]\langle\psi\rangle \tag{30}$$

Mixed models

$$\begin{bmatrix} -[S] & [\bar{S}] \\ [\bar{S}]^T & \lambda[\bar{K}] \end{bmatrix}\begin{Bmatrix} H \\ \psi \end{Bmatrix} = \begin{Bmatrix} 0 \\ P \end{Bmatrix} + \omega^2 \begin{bmatrix} 0 & 0 \\ 0 & M \end{bmatrix}\begin{Bmatrix} H \\ \psi \end{Bmatrix} \tag{31}$$

where $[K]$, $[\bar{K}]$, $[M]$, and $\langle P\rangle$ contain the stiffness, geometric stiffness, mass, and load distributions; $[S]$ and $[\bar{S}]$ contain the "generalized" stiffness distributions; $\langle\psi\rangle$ and $\langle H\rangle$ are the vectors of nodal unknowns composed of the subvectors ψ^i_J and H^i_J at the various nodes; and the superscript T denotes transposition. Note that in the mixed models (eqs. (31)), the stress resultants are assembled first.

The matrices $[K]$ and $[S]$ are symmetric, positive definite, and can be banded; the matrices $[M]$ and $[\bar{K}]$ are banded symmetric; and the matrix $[\bar{S}]$ is sparse.

For stress-analysis problems, that is, $\lambda = \omega = 0$, the governing equations of the displacement models (eqs. (30)) can be solved by any of the efficient direct techniques published in the literature. (See, e.g., refs. 24 to 26.) On the other hand, the governing equations of the mixed models can best be solved by the hypermatrix Gaussian elimination scheme. (See ref. 27.)

For eigenvalue problems, it is convenient to modify the equations of the mixed models (eqs. (31)) by first eliminating the stress resultants and then rewriting the resulting equations in the following form:

$$\left[\left[\tilde{S}\right] + \lambda\left[\bar{K}\right]\right]\left\{\psi\right\} = \left\{P\right\} + \omega^2\left[M\right]\left\{\psi\right\} \tag{32}$$

where

$$\left[\tilde{S}\right] = \left[\bar{S}\right]^T \left[S\right]^{-1} \left[\bar{S}\right] \tag{33}$$

The matrix $\left[\tilde{S}\right]$ is positive definite.

EIGENVALUE EXTRACTION TECHNIQUES

In the absence of the external load vector $\left\{P\right\}$, equations (30) and (31) define an algebraic eigenvalue problem. For free-vibration problems $\lambda = \left\{P\right\} = 0$, the natural frequencies are obtained by applying the subspace iteration technique presented in reference 28 to the equations of the displacement model.

The technique is based on the use of simultaneous inverse iteration with Gram-Schmidt orthogonalization. The number of vectors used in the iteration process is more than the eigenvectors required, but much less than the dimensions of the matrices considered.

For the mixed models, the natural frequencies are obtained by applying the Sturm sequence technique with iterations to the modified equations (eqs. (32)). In this technique the desired roots are first isolated by Sturm sequence procedure, then the inverse iteration technique is applied for the determination of individual roots along with their eigenvectors. (See ref. 29.)

For bifurcation-buckling problems, where only the minimum buckling load parameter is required, it is more efficient to use the inverse-power method presented in reference 30 for both the displacement and mixed models.

EVALUATION OF STRESS RESULTANTS

In the mixed models, once the problem is solved, all the stress resultants are readily available. On the other hand, in the displacement models the stress resultants are obtained from the nodal displacement parameters by using the following relations:

$$\begin{Bmatrix} N_{\alpha\beta} \\ M_{\alpha\beta} \end{Bmatrix} = \begin{Bmatrix} C_{\alpha\beta\gamma\rho} \\ F_{\alpha\beta\gamma\rho} \end{Bmatrix} \left(\partial_\gamma N^i \psi^i_\rho + k_{\gamma\rho} N^i \psi^i_3\right) + \begin{Bmatrix} F_{\alpha\beta\gamma\rho} \\ D_{\alpha\beta\gamma\rho} \end{Bmatrix} \partial_\gamma N^i \psi^i_{3+\rho} \tag{34}$$

$$Q_\alpha = C_{\alpha 3 \beta 3} \left(\partial_\beta N^i \psi^i_3 + N^i \psi^i_{3+\beta} \right) \tag{35}$$

The stress resultants obtained from equations (34) and (35) generally violate both the interior differential equilibrium and the stress-resultant boundary conditions and generate discontinuities at the element nodes. Therefore, in the present study the customary procedure of averaging contributions of contiguous elements at common nodes is followed. Such averaging is not needed for the SQH element.

Other techniques have been suggested to improve the accuracy of the stress calculations. These include the integral stress technique (ref. 31), which is based on least-squares minimization of the stress error function within each element, and the conjugate stress method (ref. 32), which uses biorthogonal expansion to the displacement approximation. Both these approaches involve additional computational efforts and are not used in the present study.

NUMERICAL STUDIES

To assess the relative merits of the different displacement and mixed finite-element models developed in this study (table 1), a large number of linear stress-analysis, free-vibration, and bifurcation-buckling problems are solved by these finite-element models. Particular emphasis is placed on the effects of shear deformation and anisotropic material behavior on the accuracy and rate of convergence of the different models.

The numerical examples are aimed at clarifying a number of questions concerning each of the following effects on the accuracy and rate of convergence of finite-element solutions: (a) an increase in the order of approximating polynomials, (b) addition of internal degrees of freedom, and (c) use of derivatives of generalized displacements as nodal parameters.

PLATE EVALUATION RESULTS

Four sets of plate problems are solved which contain some of the characteristics typical of practical problems and at the same time are problems for which an essentially exact solution can be obtained. In one of the problems, comparison is made with experimental results. The problems examined are

(a) Stress, free vibration, and bifurcation buckling of laminated orthotropic square plates with simply supported edges

(b) Stress analysis of orthotropic square plates with clamped edges

(c) Stress and bifurcation-buckling analysis of square anisotropic plates with simply supported edges

(d) Stress analysis of cantilevered skew plates

All the models in table 1 are applied to problems (a) and (b). The higher order displacement and mixed elements are applied to problem (c). The higher order quadrilateral displacement models SQH and SQ12 are applied to problem (d). The results of these studies are discussed subsequently.

Square Plates

The first set of problems considered is that of the stress, free vibration, and bifurcation buckling of orthotropic and anisotropic square plates. Most of the results presented in this section are for the symmetrically laminated nine-layered graphite-epoxy plates shown in figure 3. For these plates two fiber orientations are analyzed:

(a) Orthotropic plates with fiber orientation (0/90/0/90/0/90/0/90/0)

(b) Anisotropic plates with fiber orientation $(\theta/-\theta/\theta/-\theta/\theta/-\theta/\theta/-\theta/\theta)$, where $0 < \theta \leqq 45^{\circ}$

For orthotropic plates the total thickness of the 0° and 90° layers is the same, and for anisotropic plates the total thickness of the θ and $-\theta$ layers is the same. Boundary conditions for both simply supported and clamped plates are considered.

Simply Supported Orthotropic Plates

The orthotropic plate problems are selected because an exact (analytic) solution can be obtained, and therefore, a reliable assessment of the accuracy of the different finite-element models can be made. The various solutions obtained are listed first and are discussed subsequently. Since doubly symmetric deformations of the plate are considered, only one-quarter of the plate was analyzed, and the symmetric boundary conditions along the center line are listed in table 2.

For stress-analysis problems, the plates were subjected to uniform loading p_o. In addition to studying the accuracy of the maximum displacements and stress resultants obtained by the various displacement and mixed models, an error index E_f (a function of f) has been introduced to provide a quantitative measure of the relative accuracy of the stress resultants and displacements obtained by the different models. The error index is given by

$$E_f = \frac{1}{\bar{n}} \sqrt{\sum_{i=1}^{\bar{n}} \left(\frac{f_i - \tilde{f}_i}{|f_{max}|} \right)^2} \tag{36}$$

where

f any of the stress resultants or generalized displacements

$f_i, \tilde{f}_i$ exact and approximate values, respectively, of the function at the ith node

$|f_{max}|$ maximum absolute value of the exact function in the domain of interest (one-quarter of the plate)

$\bar{n}$ total number of nodes in one-quarter of the plate

The error index (eq. (36)) is essentially a weighted root-mean-square error. The smaller the error index E_f, the more accurate the approximate solution (obtained by the finite-element model) is.

To study the effect of shear deformation on the performance of the different finite-element models, three values of the thickness ratio h/a of the plate were considered: h/a = 0.1, 0.01, and 0.001. As a quantitative measure of the shear deformation, the ratio of the strain energy due to transverse shears to the total strain energy was computed for the three plates. The results are shown in table 3. As can be seen from this table, the shear deformation is quite important for the first plate and is negligible for the latter. Table 4 gives the values of the error index E_f for each of the stress resultants and generalized displacements obtained by some of the stiffness and mixed finite-element models for two plate thicknesses (h/a = 0.1 and 0.01) and three different grids. An indication of the accuracy and rate of convergence of the solutions obtained by the different models is given in figures 4 and 5, and the effect of h/a on the accuracy of the different models is shown in figure 6.

The doubly symmetric free-vibration modes of the plate are analyzed by the various element models. An indication of the accuracy and rate of convergence of the fundamental frequency obtained by different displacement and mixed models is given in table 5 and figure 7 for plates with thickness ratios h/a of 0.1 and 0.01. Figure 8 shows the effect of addition of internal degrees of freedom on the accuracy and rate of convergence of the four- and eight-node stiffness quadrilateral elements. Table 6 shows the rate of convergence of the three vibration frequencies $\omega_{1,3}$, $\omega_{3,1}$, and $\omega_{3,3}$ obtained by different stiffness models.

To study the effect of the bending-extensional coupling on the accuracy of the higher order models, the SQ12 and SQH elements were applied to the free-vibration problem of two-layered orthotropic plates. Results obtained by these two elements for the two plates with h/a = 0.1 and 0.01 are shown in table 7 along with the exact solutions.

As a quantitative measure of the shear deformation, the exact frequencies obtained by the shear-deformation and classical theories are compared in tables 5, 6, and 7.

Since the accuracy of the different elements for buckling problems is expected to be similar to that for vibration problems, only the SQ12 and SQH elements were applied to the bifurcation buckling of a plate subjected to uniaxial edge compression λN_{11}^o. The results

obtained using a 2 × 2 grid in the plate quarter are given in table 8 along with the exact solutions for the three thickness ratios h/a = 0.1, 0.01, and 0.001.

An examination of the results obtained for simply supported orthotropic plates reveals

(1) Although the convergence of the solutions obtained by all the displacement models is monotonic in character, the convergence of the lower order models is much slower than that of the higher order models. This is particularly true for stress resultants and for thinner plates. (See figs. 4 and 7.)

(2) For the same total number of degrees of freedom, the higher order displacement models (e.g., SQ12 and SQH) lead to considerably more accurate results than the lower order models. This is particularly true for stress resultants and for thinner plates. (See fig. 5.) The same phenomenon is observed for vibration frequencies. As an example of this, for plates with h/a = 0.1, the fundamental frequency obtained by the SQ12 and SQH elements and 2 × 2 grid (corresponding to 99 and 108 degrees of freedom) agrees with the exact frequency to four significant digits. (See table 5.) In contrast, the error in the fundamental frequency obtained by the SQ4 element and 5 × 5 grid (108 degrees of freedom) is approximately 2 percent. For higher frequencies and thinner plates, the accuracy of the SQ4 element deteriorated much more rapidly than that of the higher order models. (See tables 5 and 6.)

(3) The accuracy of the solutions obtained by the lower order displacement models (SQ4 element) is very sensitive to variations in the thickness ratio of the plate. For thinner plates, the accuracy of this element was found to be very poor. (See tables 4, 5, and 6.) This is because the assumed displacement functions require that the element edges remain straight, and the predominant bending deformation in thin plates is therefore poorly represented. This fact has been recognized by previous investigators and improvements have been suggested. (See, e.g., refs. 12, 14, 15, and 33.) However, no procedure exists to improve the accuracy of the element for all ranges of thickness ratio of the plate.

(4) The SQ8-4 element, with different-order polynomial approximations for displacements and rotations, although considerably more accurate than the SQ4 element, is found to be less accurate than the SQ8 element. (See fig. 4.) For thin plates (h/a = 0.001), the performance of the SQ8-4 element was found to be unsatisfactory. (See fig. 6.)

(5) Of all the finite-element models considered, the most accurate results for a given total number of degrees of freedom were obtained with the SQH element. (See fig. 5 and tables 5 and 6.) The SQH element has the added advantage that the stress resultants are continuous along the interelement boundaries and no averaging is needed in their evaluation. However, in the presence of concentrated loads or discontinuities in the geometric or material characteristics, some of the nodal parameters are discontinuous and a special treatment is needed. (See, e.g., ref. 34.)

(6) Bending-extensional coupling does not appear to have any adverse effect on the accuracy of the higher order displacement models. (See table 7.)

(7) The addition of internal degrees of freedom (bubble modes) to the displacement models results, in general, in improving the performance of the element. (See tables 4, 5, and 6 and fig. 8.) In stress-analysis problems where the internal degrees of freedom can be eliminated by static condensation techniques, this is an effective way of improving the accuracy of the element, without affecting the accuracy of the solution. For free-vibration problems, the addition of internal degrees of freedom is less effective than the addition of nodes to the element. An exception to this is the case of the SQ8 element when applied to the analysis of higher vibration modes of plates. In this case addition of higher order polynomial terms associated with internal degrees of freedom has a more pronounced effect on the accuracy than the addition of nodes. (Compare the frequencies obtained by SQ9 and SQ12 elements for the case $m = 3$, $n = 3$ in table 6.)

(8) Whereas for the SQ4 element addition of a single internal degree of freedom results in considerable improvement in accuracy, for the SQ8 element three internal degrees of freedom have to be added before a pronounced effect on accuracy can be observed. (See fig. 8.) An exception to this is the case of higher vibration modes, where the addition of a single internal degree of freedom improves the accuracy of the SQ8 element substantially. (See table 6.)

(9) The solutions obtained by the mixed models are more accurate and less sensitive to variations in the thickness ratio of the plate than those obtained by the displacement models based on the same shape functions. (See tables 4 and 5 and figs. 4, 5, and 6.) However, the convergence of the solutions obtained by the lower order mixed models (MT3 and MQ4) is slow and oscillatory in character. Also, for a given number of degrees of freedom, the accuracy of the solutions obtained by mixed models is lower than that obtained by higher order displacement models (SQH, ST10, and SQ12). (See fig. 5.)

Two other conclusions were found but the solutions on which they are based are not reported herein. These are

(10) The accuracy of the solutions obtained by the triangular elements was found to be sensitive to the choice of their orientation. The best accuracy was obtained when the displacement models (ST6 and ST10) had opposite orientation to that of the mixed models (MT3 and MT6). (See fig. 4.) The results shown in tables 4, 5, and 6 and in figures 4, 5, 6, and 7 were obtained for the aforementioned choice.

(11) The effect of satisfying the force boundary conditions for the SQH element (in addition to the kinematic conditions) was found to be insignificant. Differences occurred only in the fourth significant digit.

Before closing this section, a comparison of the elements developed in the present study with those previously reported in the literature is in order. Since most of the latter elements do not include shear deformation, the problem of an isotropic square plate with $h/a = 0.01$, for which the shear deformation is negligible, was selected. The plate had simply supported edges and was subjected to uniform loading p_o. The convergence of solutions obtained by several classical plate elements was reported in reference 11. Figure 9(a), which is reproduced from reference 11, is contrasted with figures 9(b), (c), and (d), which show the convergence of the center displacement w, center bending moment M_{11}, and strain energy U obtained by a number of displacement and mixed shear-flexible elements. Except for very coarse grids (2×2 or less in the plate quarter), the higher order elements developed in the present study are competitive with the refined elements previously reported in the literature. The problem of the thin isotropic plate represents a rather severe test for the accuracy of the shear-flexible elements, since the accuracy of such elements reduces with the diminishing of shear deformation.

Clamped Plates

To study the effect of clamped edges as boundary conditions on the accuracy of the different stiffness models, the edges of the orthotropic plates considered in the previous subsection were assumed to be totally clamped and the plates were analyzed by the different stiffness and mixed models. The plates were subjected to uniform loading of intensity p_o. The standard of comparison was taken to be the solution obtained by the SQH element and a 6×6 grid in the plate quarter for $h/a = 0.1$, and an 8×8 grid for $h/a = 0.01$ and 0.001. An indication of the accuracy and rate of convergence of displacements and stress resultants obtained by the different models is given in figure 10 for three plate thicknesses, namely, $h/a = 0.1$, 0.01, and 0.001. Also, figure 11 shows the distribution of the transverse displacement w and the bending moment M_{11} for the thinner plates (with $h/a = 0.01$ and 0.001) obtained by the higher order displacement models SQ12 and SQH and the mixed model MQ8 with a 2×2 grid in the plate quarter. As can be seen from figure 10, the solutions obtained by the different displacement and mixed models were, in general, less accurate than those for simply supported edges (fig. 6). This is particularly true for thinner plates. An exception to this is the SQH element, which exhibited very high accuracy and fast convergence for all thickness ratios. Also, the remarks made in the previous subsection regarding the effect of h/a on the accuracy and convergence of the solutions obtained by different models were found to apply in this case, as well.

Anisotropic Plates

To study the effect of anisotropy on the performance of the higher order displacement models, the fiber orientations of the graphite-epoxy plate shown in figure 3 were chosen to be $(\theta/-\theta/\theta/-\theta/\theta/-\theta/\theta/-\theta/\theta)$ with $0 < \theta \leqq 45^{\circ}$. The plate had simply supported edges and was subjected to uniform loading of intensity p_o.

Before the numerical studies were conducted, the effects of variations of θ on the response of the plate were studied. Also, an attempt was made to introduce a quantitative measure of the degree of anisotropy of the plate. Since the elastic coefficients $C_{\alpha 3 \beta 3}$ (with $\alpha \neq \beta$) and $C_{\alpha\beta\gamma\rho}$, $F_{\alpha\beta\gamma\rho}$, and $D_{\alpha\beta\gamma\rho}$ (with either $\alpha = \beta$ and $\gamma \neq \rho$ or $\alpha \neq \beta$ and $\gamma = \rho$) vanish for orthotropic (and isotropic) plates and are nonzero only for anisotropic plates, it seems reasonable to take their contribution to the total strain energy of the plate as a quantitative estimate of its degree of anisotropy. Henceforth, the contributions of the anisotropic coefficients to the total strain energy will be referred to as U_a.

Figure 12 shows the effect of variations in θ on the values of the displacement w and the bending-moment resultant M_{11} at the center of the plate as well as on the strain energies U, U_a, and U_{sh}. An examination of figure 12(c) reveals that the case $\theta = 45^o$ leads to the highest degree of anisotropy and the maximum value of the shear deformation. Therefore, the anisotropic plate with $\theta = 45^o$ was adopted for the convergence studies.

An indication of the accuracy and convergence of the higher order displacement models ST10, SQ12, and SQH and the mixed model MQ8 is given in figure 13 for the plate thicknesses h/a = 0.1, 0.01, and 0.001. The standard of comparison (converged solution) was taken to be the solution obtained by the SQH element and an 8 × 8 grid in the whole plate. Figure 14 shows the distribution of the transverse displacement w and the stress resultant M_{11} for the thinner plates (h/a = 0.01 and 0.001) obtained by the SQ12 and SQH elements with a 4 × 4 grid, along with the converged solutions. As in the cases of simply supported and clamped orthotropic plates, the fastest convergence was obtained by using the SQH elements. The only adverse effect of the anisotropy on the performance of the elements is in the nonmonotonic character of the convergence of stress resultants. (See fig. 13(b).)

As a further check on the accuracy of the SQH elements in the case of anisotropic plates, the bifurcation-buckling problem of the eight-layered anisotropic plate shown in figure 15 was analyzed. The plate is subjected to combined compressive and shear edge loading. The same plate was analyzed in reference 35 using Galerkin's method. The results obtained using three grid sizes of SQH elements (in the whole plate) are given in table 9 along with those of reference 35. Also, the buckling mode shapes are shown in figure 15.

Skew Plates

The next problem considered is that of the stress analysis of an isotropic skew plate subjected to uniform transverse loading (fig. 16). The problem was selected because it includes a more complex set of boundary conditions and stress patterns than the ones previously considered.

For this plate and these boundary conditions, an unbounded bending moment and a stress singularity occur at point B. (See ref. 36.) The nature of the singularity remains unaltered even when the shear-deformation theory (ref. 37) is used.

Analytical and experimental studies of this problem were reported in reference 38. The analytic solution was obtained by applying the mixed Hellinger-Reissner formulation in conjunction with direct variational methods to the classical plate theory (with shear deformation neglected).

The plate was analyzed with both the SQ12 and SQH elements. An indication of the accuracy and convergence of solutions obtained by both elements is given in figures 16(a) and (b). Shown in figures 16(c) and (d) are the experimental and analytical solutions of reference 38 compared with the present solutions.

An examination of figures 16(c) and (d) reveals that the solutions obtained by both the SQH and SQ12 elements, in addition to having fast monotonic convergence, exhibit clearly the sharp gradient (singularity) of the bending-moment resultant M_{22} at point B. Of the two finite-element solutions, the SQH solution has a faster convergence and appears to be more accurate. Moreover, for a 4 × 4 or finer grid, the total number of degrees of freedom in the SQH solution is less than those in the corresponding SQ12 solution.

SHELL EVALUATION RESULTS

Five sets of shell problems are solved by the displacement models developed in the present study. Comparison is made with exact and other approximate solutions whenever available. These problems are

(a) Stress and free-vibration analysis of orthotropic shallow spherical segments

(b) Stress analysis of anisotropic shallow spherical segments

(c) Stress analysis of an isotropic cylindrical shell with a circular cutout

(d) Free vibrations of an orthotropic cylindrical shell

(e) Free vibrations of an anisotropic cylindrical shell

All the displacement models listed in table 1 are applied to problem (a). Only the higher order models are applied to problem (b). The isoparametric SQ12 element is applied to problem (c), and the SQH element is applied to problems (d) and (e). The results of these studies are discussed subsequently.

Shallow Spherical Shells

As a first application to a shallow-shell problem, consider the stress and free-vibration analyses of simply supported, nine-layered, graphite-epoxy spherical segments. The geometric and material characteristics of the shell are shown in figure 17. As for the laminated plates examined in the previous subsections, shallow shells with two fiber orientations have been analyzed:

(a) Orthotropic shells with fiber orientation (0/90/0/90/0/90/0/90/0)

(b) Anisotropic shells with fiber orientation $(\theta/-\theta/\theta/-\theta/\theta/-\theta/\theta/-\theta/\theta)$, with $0 < \theta \leqq 45^{o}$

Orthotropic Shallow Shells

For the orthotropic shells considered, analytic solutions were obtained and used as a standard for comparing the different finite-element solutions. Doubly symmetric deformations of the shell were considered, and therefore, only one-quarter of the shell was analyzed.

For stress-analysis problems, the shells were subjected to uniform loading p_o. The different displacement models were used to obtain solutions for three thickness ratios of the shell (h/a = 0.1, 0.01, and 0.001). As a quantitative measure for the shear deformation, the ratios of the strain energy due to transverse shear to the total strain energy of the shell were computed for the three shells. Results are given in table 10, and as for orthotropic plates, the shear deformation is quite important for the thickest shell and is negligible for the two thinner shells.

An indication of the accuracy and rate of convergence of the solutions obtained by the different models is given in figure 18 for the shell with h/a = 0.1. The effect of h/a on the accuracy of the different finite-element solutions is shown in figure 19. The distributions of the transverse displacement w and the stress resultants N_{22} and M_{11} obtained by the higher order elements SQ12 and SQH with a 2 × 2 grid in the shell quarter are shown in figure 20 along with the exact solutions for the two thinner shells (h/a = 0.01 and 0.001).

The first four doubly symmetric vibration frequencies obtained by the different displacement models are listed in table 11 along with the exact frequencies for two thickness ratios (h/a = 0.1 and h/a = 0.01). The solutions obtained using the SQ4 element were, in general, far removed from the exact solutions and are not reported herein.

The orientation of the ST6 and ST10 elements, for optimum accuracy, was found to be the same as that for orthotropic plate problems. (See fig. 4.)

An examination of figures 18, 19, and 20 and table 11 reveals that the remarks made in connection with the orthotropic-plate problems regarding the effectiveness of the higher order models (ST10, SQ12, and SQH elements) and the effect of internal degrees of freedom, apply in this case as well. The apparent poor performance of the different models for the case of very thin shells (with h/a = 0.001) is due to the boundary-layer effects exhibited by the stress resultants (see fig. 20), hence the difficulties (and nonmonotonicity) in convergence observed in figure 19. The convergence of the total energy obtained by the higher order models was fast and monotonic, even for the very thin shell. (See fig. 19(d).)

Anisotropic Shallow Shells

For anisotropic shells the fiber orientations were chosen to be $(\theta/-\theta/\theta/-\theta/\theta/-\theta/\theta/-\theta/\theta)$ with $0 < \theta \leqq 45^{o}$. The shells were subjected to uniform loading of intensity p_o. The quantitative measures for the degree of anisotropy and amount of shear deformation introduced for anisotropic plates were used for the anisotropic shallow shells as well.

Figure 21 shows the effect of variations in θ on the values of the center displacement w and the center stress resultants N_{22} and M_{11} for two thickness ratios of the shell (h/a = 0.1 and 0.01). Also shown (fig. 21(d)) are the strain energies U, U_a, and U_{sh}. The maximum values of U_{sh}/U and U_a/U occur at different values of θ. This is to be contrasted with the anisotropic plates, for which the maximum values occurred at $\theta = 45^{o}$.

The accuracy and convergence studies were conducted for shells with $\theta = 45^{o}$. Figure 22 gives an indication of the accuracy and convergence of the center displacement w and the strain energy U obtained by the higher order displacement models (ST10, SQ12, and SQH) for the three thickness ratios h/a = 0.1, 0.01, and 0.001. The standards of comparison (converged solutions) were taken to be the solutions obtained by the SQH elements. An 8×8 grid was used for shells with h/a = 0.1 and 0.01, and a 10×10 grid was used for shells with h/a = 0.001. The distributions of the normal displacement w and the stress resultants N_{22} and M_{11} obtained by the SQ12 and SQH elements with a 4×4 grid for the thinner shells (with h/a = 0.01 and 0.001) are shown in figure 23 along with the converged solutions. As in all the previous problems, the SQH solutions had the fastest convergence. The degradation of accuracy due to anisotropy for very thin shells, though not pronounced for higher order displacement models, can be clearly seen by comparing the results in figures 20 and 23.

Rigid Body Modes

For shallow shells, the rigid body modes are trigonometric in character and therefore are only approximated by the polynomial shape functions used in the present study. To assess the accuracy of the approximation, the eigenvalues of the stiffness matrices of the various displacement models were computed for the three anisotropic shallow shells with h/a = 0.1, 0.01, and 0.001. The lowest six eigenvalues correspond to rigid body modes; the higher modes are straining modes. Table 12 summarizes the lowest seven eigenvalues, the maximum eigenvalues, and the traces of the stiffness matrices for the various models. In all cases the ratio $\bar{\beta}_7/\bar{\beta}_6$ was greater than 10^5, which indicates that the rigid body modes are satisfactorily represented in these models.

Cylindrical Shells

Isotropic Cylinder With a Circular Cutout

Consider the stress analysis of an isotropic cylindrical shell with a circular cutout subjected to a uniform axial tensile stress at its free ends. The geometric characteristics of the shell and loading are shown in figure 24. The problem was selected to assess the accuracy of the isoparametric SQ12 elements in situations where high stress gradients and curved boundaries occur. The shell and loading are doubly symmetric, and therefore, only one-quarter of the shell was analyzed.

An approximate analytic solution for the problem, assuming the cylinder to be of infinite length, was given in reference 39, where it was shown that for this shell, the shallow-shell approximation is valid. Therefore, the use of the SQ12 elements, with local element coordinates coinciding with global shell coordinates, is justified. A difference-based variational solution was given in reference 40. Finite-element solutions using higher order triangular elements were reported in reference 41. All the aforementioned solutions were based on the classical shell theory (with shear deformation neglected). Solution to a similar cylinder problem using a refined grid of shear-flexible quadrilateral elements was reported in reference 42.

Four graded networks with 4 × 4, 5 × 4, 5 × 6, and 8 × 6 SQ12 elements were used to analyze the shell. (See fig. 25.) In an attempt to make a rational choice for the variation of the grid size in both the x_1- and x_2-directions, a variable grid parameter ζ was introduced (ref. 43 and fig. 26):

$$\zeta_r = \frac{n}{L}\left(\eta_{r+1} - \eta_r\right) \tag{37}$$

where ζ_r is the relative size of the rth element, η refers to each of the x_1- and x_2-coordinates, η_r and η_{r+1} are the coordinates of the ends of the element, and n is the number of elements in the η-direction. A second-degree polynomial variation of ζ_r was chosen, that is,

$$\zeta_r = a + br + cr^2 \tag{38}$$

where r is the element number $1 \leqq r \leqq n$. The coefficients a, b, and c of the polynomial are determined by specifying the relative sizes of the first and last elements ζ_1 and ζ_n, and using the following three equations:

$$\frac{1}{n}\sum_{r=1}^{n} \zeta_r = 1.0 \tag{39}$$

$$\zeta_1 = a + b + c \tag{40}$$

$$\zeta_n = a + bn + cn^2 \tag{41}$$

The characteristics of the grids used in the present study are shown in figure 26.

The maximum stress concentrations σ_{11}/σ_o and strain energies obtained by the four grids are given in table 13 along with results of previous investigators. Membrane stress distributions obtained by the 4 × 4 and 8 × 6 grids are shown in figure 27. The high accuracy and rapid convergence of the solutions obtained by the isoparametric SQ12 elements are clearly demonstrated by this example.

Orthotropic Cylinders

The natural frequencies and mode shapes of orthotropic, two-layered, simply supported circular cylinders without axial restraint are studied. The problems are selected to assess the accuracy of the SQH elements when applied to laminated closed cylinders with high bending-extensional coupling. The geometric characteristics of the shells studied are shown in figure 28. Shells with fiber orientation (90/0) are analyzed.

For these cylinders an analytic solution is obtained and is used as a basis for comparison of the finite-element solutions. It is found that for this shell, the shallow-shell (Donnell's) theory approximation is valid. The doubly symmetric vibration modes of the cylinders are analyzed and the symmetric boundary conditions along three of the edges are applied. This eliminates the axial rigid body mode of the cylinder and allows obtaining the vibration modes having odd values of m (axial direction) and even values of n (circumferential direction). Initially a uniform grid with 2 × 2 SQH elements was used to model one octant of the cylinder (grid 1, fig. 29); however, this resulted in poor accuracy for the frequencies and mode shapes with $n \geq 4$. Subsequently, the 2 × 2 grid was modified to cover only one-eighth of the circumference (grid 2, fig. 29). This resulted in considerable improvement in the accuracy of the frequencies for $n = 4$. The frequencies obtained by the two grids are given in table 14 along with the analytic solutions obtained by both the shear-deformation and classical shallow-shell theories. This table shows the decrease in accuracy as the element size-to-wavelength ratio increases in the circumferential direction, as indicated by the increase of n. Numerically, the error increases from less than 0.5 percent for $m = 1$, $n = 2$ to approximately 25 percent for $m = 1$, $n = 4$. The increased stiffness of the finite-element model due to the larger element size-to-wavelength ratio has caused a greater increase in the error of the finite-element analysis between the two modes. The present example shows that the SQH elements lead to very accurate frequencies provided the element size is less than half the wavelength of the vibration mode.

Anisotropic Cylinders

As a final example, consider the free-vibration analysis of anisotropic two-layered circular cylinders. The shells have the same characteristics as those for the orthotropic cylinders discussed in the preceding subsection, except for the fiber orientation, which is chosen to be (45/–45).

Solutions are obtained using three grids with 2 × 4, 4 × 8, and 6 × 12 SQH elements in the whole cylinder. (See fig. 30.) In order to eliminate the axial rigid body mode of the cylinder, u_1 is set equal to zero at the center of each grid. The fundamental frequency and associated mode shapes are shown in figure 31. The rapid convergence of the solutions obtained by the SQH elements is clearly demonstrated by this example.

CONCLUDING REMARKS

Several shear-flexible finite-element models are applied to the linear static, stability, and vibration problems of plates and shells. The study is based on the shallow-shell theory with effects of shear deformation, anisotropic material behavior, and bending-extensional coupling included. Both stiffness (displacement) and mixed finite-element models are considered. All the elements examined are conforming, satisfactorily represent the rigid body modes, and exhibit uniform convergence for stress-analysis, free-vibration, and buckling problems. Primary attention in this study is given to the effects of shear deformation and anisotropic material behavior on the accuracy and convergence of different finite-element models.

On the basis of the present study, the following conclusions seem to be justified:

1. Higher order displacement models (with cubic or bicubic interpolation polynomials) have the following advantages over lower order models:

   (a) The total number of unknowns required for a prescribed level of accuracy is less in the higher order than in the lower order models. This is particularly true for stress resultants and for thinner plates (with negligible shear deformation).

   (b) The performance of the higher order models is considerably less sensitive to variations in the thickness ratio and shear deformation than that of the lower order models.

2. The use of derivatives of displacements as nodal parameters (SQH element) has the obvious advantage that the stress resultants are defined directly at the nodes and no averaging is needed. In addition, this results in improving the performance of the element. However, in the presence of concentrated loads or discontinuities in the geometric or elastic characteristics of the shell, some of the parameters will be discontinuous and a special treatment is needed.

3. The addition of internal degrees of freedom (bubble modes) to displacement models results, in most cases, in improving the performance of the element. In stress-analysis problems where the internal degrees of freedom can be eliminated by static condensation techniques, this is an effective way of improving the accuracy of plate and shell elements without affecting the accuracy of the solution. For free-vibration (and buckling) problems, the addition of internal degrees of freedom is less effective than the addition of nodes to the element. An exception to this is the case of the eight-node quadrilateral element when applied to the analysis of higher vibration modes. In this case, addition of internal degrees of freedom has a much more pronounced effect on the accuracy than the addition of nodes.

4. If mixed models are contrasted with displacement models, the following can be noted:

(a) The development of mixed models involves considerably less algebra than the development of displacement models.

(b) The performance of mixed models is, in general, insensitive to variations in the thickness ratio and shear deformation.

(c) Use of lower order interpolation functions (linear or bilinear) leads to a mediocre type of performance. Considerable improvement in the performance is achieved by using quadratic shape functions.

(d) For a given number of degrees of freedom, the higher order displacement models (with cubic or bicubic interpolation polynomials) lead to higher accuracy than the mixed models with quadratic shape functions. The effective use of mixed models requires the development of efficient equation-handling techniques (e.g., based on hypermatrix storage schemes).

5. Whereas material anisotropy was shown to have an adverse effect on the performance of different displacement and mixed elements, the bending-extensional coupling does not seem to have any pronounced effect on the accuracy and convergence of these elements.

Langley Research Center
National Aeronautics and Space Administration
Hampton, Va. 23665
November 10, 1975

APPENDIX A

FUNDAMENTAL EQUATIONS OF SHEAR-DEFORMATION SHALLOW-SHELL THEORY

The fundamental equations of the shallow-shell theory are given in this appendix.

STRAIN-DISPLACEMENT RELATIONSHIPS

The relationships between strain and displacement are

$$\epsilon_{\alpha\beta} = \frac{1}{2}(\partial_\alpha u_\beta + \partial_\beta u_\alpha) + k_{\alpha\beta}\, w$$

$$\chi_{\alpha\beta} = \frac{1}{2}(\partial_\alpha \phi_\beta + \partial_\beta \phi_\alpha)$$

$$2\epsilon_{\alpha 3} = \partial_\alpha w + \phi_\alpha$$

where $\epsilon_{\alpha\beta}$ are the extensional strains of the reference surface of the shell; $\chi_{\alpha\beta}$ are the curvature changes and twist; and $2\epsilon_{\alpha 3}$ are the transverse shearing strain components.

CONSTITUTIVE RELATIONS OF THE SHELL

The relations between the stress resultants and strain components of the shell are

$$N_{\alpha\beta} = C_{\alpha\beta\gamma\rho}\, \epsilon_{\gamma\rho} + F_{\alpha\beta\gamma\rho}\, \chi_{\gamma\rho}$$

$$M_{\alpha\beta} = F_{\alpha\beta\gamma\rho}\, \epsilon_{\gamma\rho} + D_{\alpha\beta\gamma\rho}\, \chi_{\gamma\rho}$$

$$Q_\alpha = C_{\alpha 3\beta 3}\, 2\epsilon_{\beta 3}$$

The inverse relations are given by

$$\epsilon_{\alpha\beta} = A_{\alpha\beta\gamma\rho}\, N_{\gamma\rho} + B_{\alpha\beta\gamma\rho}\, M_{\gamma\rho}$$

$$\chi_{\alpha\beta} = B_{\alpha\beta\gamma\rho}\ N_{\gamma\rho} + G_{\alpha\beta\gamma\rho}\ M_{\gamma\rho}$$

$$2\epsilon_{\alpha 3} = A_{\alpha 3\beta 3}\ Q_{\beta}$$

The C, F, and D coefficients are shell stiffnesses and the A, B, and G coefficients are shell compliances defined in appendix B.

APPENDIX B

ELASTIC COEFFICIENTS OF LAMINATED SHELLS

ELASTIC STIFFNESSES OF THE LAYERS

The nonzero stiffness coefficients $c^{(k)}_{\alpha\beta\gamma\rho}$ and $c^{(k)}_{\alpha 3\beta 3}$ of the kth orthotropic layer of the shell referred to the directions of principal elasticity are given by

$$c^{(k)}_{1111} = E^{(k)}_L \Big/ \bar{\lambda}^{(k)}$$

$$c^{(k)}_{1122} = \nu^{(k)}_{LT}\, E^{(k)}_T \Big/ \bar{\lambda}^{(k)}$$

$$c^{(k)}_{2222} = E^{(k)}_T \Big/ \bar{\lambda}^{(k)}$$

$$c^{(k)}_{1212} = G^{(k)}_{LT}$$

and

$$c^{(k)}_{1313} = G^{(k)}_{LT}$$

$$c^{(k)}_{2323} = G^{(k)}_{TT}$$

where the subscripts L and T denote the direction of fibers and the transverse direction, ν_{LT} is Poisson's ratio measuring the strain in the T-direction due to a uniaxial normal stress in the L-direction:

$$\nu_{TL}\, E_L = \nu_{LT}\, E_T$$

$$\bar{\lambda} = 1 - \nu_{LT}\, \nu_{TL}$$

and the superscript k refers to the kth layer.

APPENDIX B

The stiffness coefficients $c_{\alpha\beta\gamma\rho}$ and $c_{\alpha 3\beta 3}$ satisfy the following symmetry relationships:

$$c_{\alpha\beta\gamma\rho} = c_{\gamma\rho\alpha\beta} = c_{\beta\alpha\gamma\rho} = c_{\alpha\beta\rho\gamma}$$

and

$$c_{\alpha 3\beta 3} = c_{\beta 3\alpha 3} = c_{3\alpha\beta 3} = c_{\alpha 33\beta}$$

If the coordinates x_α are rotated, the elastic coefficients $c_{\alpha\beta\gamma\rho}$ and $c_{\alpha 3\beta 3}$ transform as components of fourth- and second-order tensors, respectively. The transformation law of these coefficients is expressed as follows:

$$c_{\alpha'\beta'\gamma'\rho'} = c_{\alpha\beta\gamma\rho}\, \ell_{\alpha,\alpha'}\, \ell_{\beta,\beta'}\, \ell_{\gamma,\gamma'}\, \ell_{\rho,\rho'}$$

and

$$c_{\alpha' 3\beta' 3} = c_{\alpha 3\beta 3}\, \ell_{\alpha,\alpha'}\, \ell_{\beta,\beta'}$$

where $c_{\alpha'\beta'\gamma'\rho'}$ and $c_{\alpha' 3\beta' 3}$ are the stiffness-coefficients referred to the new coordinate system $x_{\alpha'}$ and

$$\ell_{\alpha,\alpha'} = \cos(x_\alpha, x_{\alpha'})$$

ELASTIC COEFFICIENTS OF THE SHELL

The equivalent elastic stiffnesses of the shell are given by

$$\left[C_{\alpha\beta\gamma\rho},\ F_{\alpha\beta\gamma\rho},\ D_{\alpha\beta\gamma\rho}\right] = \sum_{k=1}^{NL} \int_{h_{k-1}}^{h_k} c^{(k)}_{\alpha\beta\gamma\rho} \left[1,\ x_3,\ x_3^2\right] dx_3$$

and

$$C_{\alpha 3\beta 3} = \sum_{k=1}^{NL} \int_{h_{k-1}}^{h_k} c^{(k)}_{\alpha 3\beta 3}\, dx_3$$

where NL is the total number of layers of the shell and h_k and h_{k-1} are the distances from the reference surface to the top and bottom surfaces of the kth layer, respectively. The elastic compliances of the shell $A_{\alpha\beta\gamma\rho}$, $B_{\alpha\beta\gamma\rho}$, $G_{\alpha\beta\gamma\rho}$, and $A_{\alpha 3\beta 3}$ are obtained by inversion of the matrix of the elastic stiffnesses. (See ref. 18.)

APPENDIX B

The shell stiffnesses and compliance coefficients satisfy symmetry and transformation relations similar to those of the stiffness coefficients of individual layers.

The density parameters of the shell are given by

$$\left[m_0,\ m_1,\ m_2\right] = \sum_{k=1}^{NL} \int_{h_{k-1}}^{h_k} \rho_s^{(k)} \left[1,\ x_3,\ x_3^2\right] dx_3$$

where $\rho_s^{(k)}$ is the mass density of the kth layer of the shell.

APPENDIX C

SHAPE FUNCTIONS USED IN PRESENT STUDY

QUADRILATERAL ELEMENTS

The expressions of the shape functions for the different elements developed in this study in terms of the quadrilateral coordinates ξ_1,ξ_2 (ref. 44) are given in this appendix.

Bilinear Shape Functions

The shape functions for the bilinear approximations (elements SQ4 and MQ4, see sketch (a)) are given by

$$N^j = \frac{1}{4}\left(1 + \xi_1\xi_1^{(j)}\right)\left(1 + \xi_2\xi_2^{(j)}\right)$$

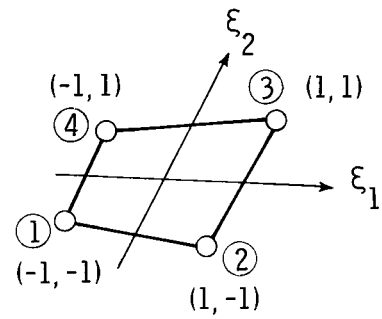

Sketch (a)

where $\xi_\alpha^{(j)}$ (with α = 1,2) are the quadrilateral coordinates of node j.

Quadratic Shape Functions

The shape functions for the quadratic approximations (elements SQ8 and MQ8, see sketch (b)) are given by

Corner nodes

$$N^j = \frac{1}{4}\left(1 + \xi_1\xi_1^{(j)}\right)\left(1 + \xi_2\xi_2^{(j)}\right)\left(\xi_1\xi_1^{(j)} + \xi_2\xi_2^{(j)} - 1\right) \qquad (j = 1,3,5,7)$$

Midside nodes

$$N^j = \frac{1}{2}\left(1 - \xi_1^{\,2}\right)\left(1 + \xi_2\xi_2^{(j)}\right) \qquad (j = 2,6)$$

$$N^j = \frac{1}{2}\left(1 + \xi_1\xi_1^{(j)}\right)\left(1 - \xi_2^{\,2}\right) \qquad (j = 4,8)$$

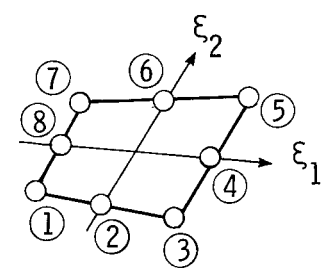

Sketch (b)

APPENDIX C

Cubic Shape Functions

The shape functions for the cubic approximations (element SQ12, see sketch (c)) are given by

Corner nodes

$$N^j = \frac{1}{32}\left(1 + \xi_1\xi_1^{(j)}\right)\left(1 + \xi_2\xi_2^{(j)}\right)\left[9\left(\xi_1^{\,2} + \xi_2^{\,2}\right) - 10\right] \qquad (j = 1,4,7,10)$$

Other nodes

$$N^j = \frac{9}{32}\left(1 - \xi_1^{\,2}\right)\left(1 + 9\xi_1\xi_1^{(j)}\right)\left(1 + \xi_2\xi_2^{(j)}\right) \qquad (j = 2,3,8,9)$$

$$N^j = \frac{9}{32}\left(1 + \xi_1\xi_1^{(j)}\right)\left(1 + 9\xi_2\xi_2^{(j)}\right)\left(1 - \xi_2^{\,2}\right) \qquad (j = 5,6,11,12)$$

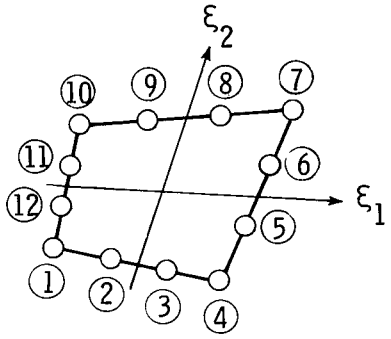

Sketch (c)

Hermitian Shape Functions

The Hermitian shape functions (element SQH, sketch (d)) used in the present study were products of the following set of first-order Hermite polynomials (sketch (e)):

$$f_1(\zeta) = \frac{1}{4}\left(\zeta^3 - 3\zeta + 2\right)$$

$$f_2(\zeta) = \frac{1}{4}\left(\zeta^3 - \zeta^2 - \zeta + 1\right)$$

$$f_3(\zeta) = -\frac{1}{4}\left(\zeta^3 - 3\zeta - 2\right)$$

$$f_4(\zeta) = \frac{1}{4}\left(\zeta^3 + \zeta^2 - \zeta - 1\right)$$

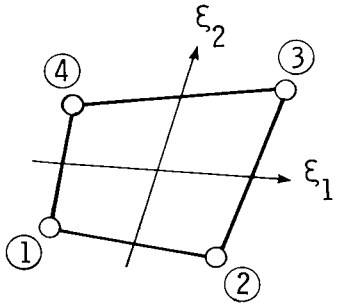

Sketch (d)

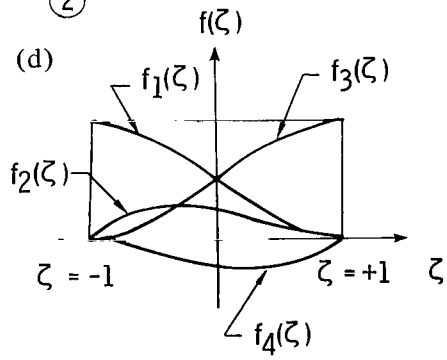

Sketch (e)

APPENDIX C

If the order of the nodal parameters at each node is chosen to be v, $\frac{\partial v}{\partial \xi_1}$, $\frac{\partial v}{\partial \xi_2}$, and $\frac{\partial^2 v}{\partial \xi_1 \partial \xi_2}$, where v denotes any of the fundamental unknowns, then the shape functions are given by

$$N^j = f_i(\xi_1) f_\ell(\xi_2)$$

$$N^{j+1} = f_{i+1}(\xi_1) f_\ell(\xi_2)$$

$$N^{j+2} = f_i(\xi_1) f_{\ell+1}(\xi_2)$$

$$N^{j+3} = f_{i+1}(\xi_1) f_{\ell+1}(\xi_2)$$

where the subscripts i and ℓ are functions of j as follows:

j	i	ℓ
1	1	1
5	3	1
9	3	3
13	1	3

Shape Functions Associated With Nodeless Variables (Bubble Modes)

Elements SQ5 and SQ9

These elements have one bubble mode given by

$$N^j = (1 - \xi_1^2)(1 - \xi_2^2) \qquad \begin{pmatrix} j = 5 & \text{for SQ5} \\ j = 9 & \text{for SQ9} \end{pmatrix}$$

APPENDIX C

Elements SQ7 and SQ11

These elements have three bubble modes given by

$$N^{j} = (1 - \xi_1^2)(1 - \xi_2^2)$$

$$N^{j+1} = \xi_1(1 - \xi_1^2)(1 - \xi_2^2)$$

$$N^{j+2} = \xi_2(1 - \xi_1^2)(1 - \xi_2^2)$$

(j = 5 for SQ7; j = 9 for SQ11)

TRIANGULAR ELEMENTS

The expressions of the shape functions for the different elements developed in this study in terms of the triangular (or area) coordinates ξ_1, ξ_2, ξ_3 (ref. 44) are given in the following sections.

Linear Shape Functions

The shape functions for the linear approximations (element MT3, sketch (f)) in terms of triangular coordinates are given by

$$N^{j} = \xi_j \qquad (j = 1 \text{ to } 3)$$

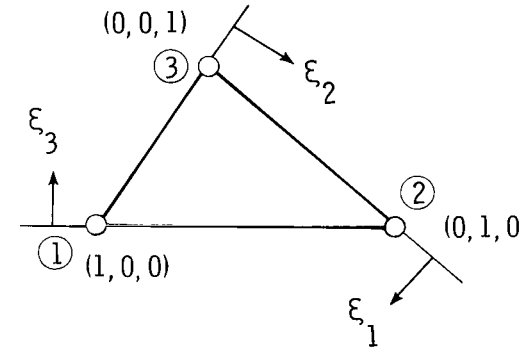

Sketch (f)

Quadratic Shape Functions

The shape functions for the quadratic approximations (elements ST6 and MT6, sketch (g)) in triangular coordinates are

Corner nodes

$$N^{j} = \xi_i(2\xi_i - 1) \qquad (j = 2i - 1;\ i = 1 \text{ to } 3 \text{ and is not summed})$$

APPENDIX C

Midside nodes

$$N^j = 4\xi_i\,\xi_{i+1} \qquad (j = 2i;\ i = 1 \text{ to } 3 \text{ and is not summed};\ \xi_4 = \xi_1)$$

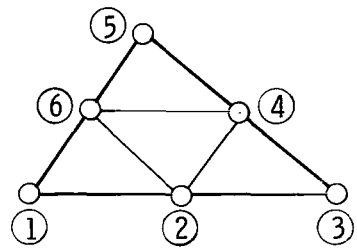

Sketch (g)

Cubic Shape Functions

The shape functions for the cubic approximations (element ST10, sketch (h)) in triangular coordinates are given by

Corner nodes (nodes 1, 4, 7)

$$N^j = \frac{1}{2}(3\xi_i - 1)(3\xi_i - 2)\xi_i \qquad (j = 3i - 2;\ i = 1 \text{ to } 3 \text{ and is not summed})$$

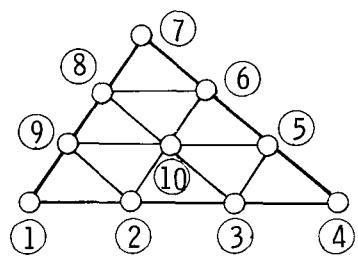

Sketch (h)

Boundary nodes

$$N^j = \frac{9}{2}\,\xi_i\,\xi_{i+1}(3\xi_i - 1) \quad (j = 3i - 1;\ \text{nodes } 2, 5, 8)$$

$$N^j = \frac{9}{2}\,\xi_i\,\xi_{i+1}(3\xi_{i+1} - 1) \quad (j = 3i;\ \text{nodes } 3, 6, 9)$$

$$\Big\} \quad (i = 1 \text{ to } 3 \text{ and is not summed};\ \xi_4 = \xi_1)$$

Interior node (node 10)

$$N^j = 27\xi_1\xi_2\xi_3$$

APPENDIX D

FORMULAS FOR COEFFICIENTS IN GOVERNING EQUATIONS FOR INDIVIDUAL ELEMENTS

The expressions for the independent stiffness coefficients in equations (17) are given by

$$K^{ij}_{\alpha\beta} = \int_{\Omega(e)} C_{\alpha\gamma\beta\rho}\ \partial_\gamma N^i\ \partial_\rho N^j\ d\Omega$$

$$K^{ij}_{\alpha 3} = \int_{\Omega(e)} C_{\alpha\gamma\beta\rho}\ k_{\beta\rho}\ \partial_\gamma N^i\ N^j\ d\Omega$$

$$K^{ij}_{\alpha,\beta+3} = \int_{\Omega(e)} F_{\alpha\gamma\beta\rho}\ \partial_\gamma N^i\ \partial_\rho N^j\ d\Omega$$

$$K^{ij}_{33} = \int_{\Omega(e)} \left[C_{\alpha\gamma\beta\rho}\ k_{\alpha\gamma}\ k_{\beta\rho}\ N^i\ N^j + C_{\alpha 3\beta 3}\ \partial_\alpha N^i\ \partial_\beta N^j\right] d\Omega$$

$$K^{ij}_{\alpha+3,3} = \int_{\Omega(e)} \left[F_{\alpha\gamma\beta\rho}\ k_{\beta\rho}\ \partial_\gamma N^i\ N^j + C_{\alpha 3\beta 3}\ N^i\ \partial_\beta N^j\right] d\Omega$$

$$K^{ij}_{\alpha+3,\beta+3} = \int_{\Omega(e)} \left[D_{\alpha\gamma\beta\rho}\ \partial_\gamma N^i\ \partial_\rho N^j + C_{\alpha 3\beta 3}\ N^i\ N^j\right] d\Omega$$

The independent nonzero geometric stiffness coefficients are given by

$$\bar{K}^{ij}_{33} = \int_{\Omega(e)} N^o_{\alpha\beta}\ \partial_\alpha N^i\ \partial_\beta N^j\ d\Omega$$

The independent nonzero consistent mass coefficients are given by

$$M^{ij}_{\alpha\beta} = \int_{\Omega(e)} m_0\ \delta_{\alpha\beta}\ N^i\ N^j\ d\Omega$$

$$M^{ij}_{\alpha,\beta+3} = \int_{\Omega(e)} m_1\ \delta_{\alpha\beta}\ N^i\ N^j\ d\Omega$$

$$M^{ij}_{33} = \int_{\Omega(e)} m_0\ N^i\ N^j\ d\Omega$$

$$M^{ij}_{\alpha+3,\beta+3} = \int_{\Omega(e)} m_2 \ \delta_{\alpha\beta} \ N^i \ N^j \ d\Omega$$

where $\delta_{\alpha\beta}$ is the Kronecker delta on α and β.

The expressions for the "generalized" stiffness coefficients in equations (18) are given by

$$S^{ij}_{\alpha+\beta-1,\gamma+\rho-1} = \int_{\Omega(e)} A_{\alpha\beta\gamma\rho} \ N^i \ N^j \ d\Omega$$

$$S^{ij}_{\alpha+\beta-1,\gamma+\rho+2} = \int_{\Omega(e)} B_{\alpha\beta\gamma\rho} \ N^i \ N^j \ d\Omega$$

$$S^{ij}_{\alpha+\beta+2,\gamma+\rho+2} = \int_{\Omega(e)} G_{\alpha\beta\gamma\rho} \ N^i \ N^j \ d\Omega$$

$$S^{ij}_{\alpha+6,\beta+6} = \int_{\Omega(e)} A_{\alpha3\beta3} \ N^i \ N^j \ d\Omega$$

$$\bar{S}^{ij}_{\alpha+\beta-1,\gamma} = \kappa \int_{\Omega(e)} \left(\delta_{\beta\gamma} N^i \ \partial_\alpha N^j + \delta_{\alpha\gamma} N^i \ \partial_\beta N^j\right) d\Omega$$

$$\bar{S}^{ij}_{\alpha+\beta-1,3} = \int_{\Omega(e)} k_{\alpha\beta} \ N^i \ N^j \ d\Omega$$

$$\bar{S}^{ij}_{\alpha+\beta+2,\gamma+3} = \kappa \int_{\Omega(e)} \left(\delta_{\beta\gamma} N^i \ \partial_\alpha N^j + \delta_{\alpha\gamma} N^i \ \partial_\beta N^j\right) d\Omega$$

$$\bar{S}^{ij}_{\alpha+6,3} = \int_{\Omega(e)} N^i \ \partial_\alpha N^j \ d\Omega$$

$$\bar{S}^{ij}_{\alpha+6,\beta+3} = \delta_{\alpha\beta} \int_{\Omega(e)} N^i \ N^j \ d\Omega$$

The consistent nodal load coefficients are given by

$$P^i_\alpha = \int_{\Omega(e)} N^i \ N^j \ p^j_\alpha \ d\Omega$$

$$P^i_3 = \int_{\Omega(e)} N^i \ N^j \ p^j \ d\Omega$$

In the above equations the contributions of the line integrals have been neglected for simplicity; κ is a constant equal to 1 when $\alpha \neq \beta$ and 1/2 when $\alpha = \beta$; the range of the lowercase Latin indices is 1 to m, where m is the number of shape functions; the range of the Greek indices is 1,2; and a repeated index denotes summation over the full range of the index.

It should be mentioned that for elements with internal degrees of freedom (SQ5, SQ7, SQ9, and SQ11), the indices i,j in the expressions for P^i_α and P^i_3 were assumed to have a range equal to the number of nodes in the element (i.e., 4 for SQ5 and SQ7 elements, and 8 for SQ9 and SQ11 elements). This means that the loading was distributed on the nodes of these elements and no loading was associated with internal degrees of freedom.

REFERENCES

1. Whitney, J. M.; and Pagano, N. J.: Shear Deformation in Heterogeneous Anisotropic Plates. Trans. ASME, Ser. E: J. Appl. Mech., vol. 37, no. 4, Dec. 1970, pp. 1031-1036.
2. Srinivas, S.; and Rao, A. K.: Bending, Vibration and Buckling of Simply Supported Thick Orthotropic Rectangular Plates and Laminates. Int. J. Solids & Struct., vol. 6, no. 11, Nov. 1970, pp. 1463-1481.
3. Pagano, N. J.; and Hatfield, Sharon J.: Elastic Behavior of Multilayered Bidirectional Composites. AIAA J., vol. 10, no. 7, July 1972, pp. 931-933.
4. Noor, Ahmed K.: Free Vibrations of Multilayered Composite Plates. AIAA J., vol. 11, no. 7, July 1973, pp. 1038-1039.
5. Noor, Ahmed K.; and Rarig, Pamela L.: Three-Dimensional Solutions of Laminated Cylinders. Comput. Methods Appl. Mech. & Eng., vol. 3, no. 3, May 1974, pp. 319-334.
6. Barker, Richard M.; Lin, Fu-Tien; and Dana, Jon R.: Three-Dimensional Finite-Element Analysis of Laminated Composites. Comput. & Struct., vol. 2, nos. 5/6, Dec. 1972, pp. 1013-1029.
7. Mau, S. T.; Tong, P.; and Pian, T. H. H.: Finite Element Solutions for Laminated Thick Plates. J. Compos. Mater., vol. 6, Apr. 1972, pp. 304-311.
8. Argyris, J. H.; and Scharpf, D. W.: Finite Element Theory of Plates and Shells Including Shear Strain Effects. High Speed Computing of Elastic Structures, Volume 61, B. Fraeijs de Veubeke, ed., Univ. de Liège, 1971, pp. 253-292.
9. Key, Samuel W.; and Beisinger, Zelma E.: The Analysis of Thin Shells With Transverse Shear Strains by the Finite Element Method. Proceedings of the Second Conference on Matrix Methods in Structural Mechanics, AFFDL-TR-68-150, U.S. Air Force, Dec. 1969, pp. 667-710.
10. Irons, Bruce M.; and Razzaque, Abdur: Introduction of Shear Deformations Into a Thin Plate Displacement Formulation. AIAA J., vol. 11, no. 10, Oct. 1973, pp. 1438-1439.
11. Narayanaswami, R.: New Triangular and Quadrilateral Plate-Bending Finite Elements. NASA TN D-7407, 1974.
12. Zienkiewicz, O. C.; Taylor, R. L.; and Too, J. M.: Reduced Integration Technique in General Analysis of Plates and Shells. Int. J. Numerical Methods Eng., vol. 3, no. 2, Apr.-June 1971, pp. 275-290.
13. Fried, Isaac: Shear in C^0 and C^1 Bending Finite Elements. Int. J. Solids & Struct., vol. 9, no. 4, Apr. 1973, pp. 449-460.
14. Fried, Isaac: Residual Energy Balancing Technique in the Generation of Plate Bending Finite Elements. Comput. & Struct., vol. 4, no. 4, Aug. 1974, pp. 771-778.

15. Wempner, Gerald A.; Oden, J. Tinsley; and Kross, Dennis A.: Finite-Element Analysis of Thin Shells. J. Eng. Mech. Div., American Soc. Civil Eng., vol. 94, no. EM6, Dec. 1968, pp. 1273-1294.

16. Dhatt, G. S.: Numerical Analysis of Thin Shells by Curved Triangular Elements Based on Discrete-Kirchhoff Hypothesis. Application of Finite Element Methods in Civil Engineering, William H. Rowan, Jr., and Robert M. Hackett, eds., American Soc. Civil Eng., Nov. 1969, pp. 255-278.

17. Pawsey, Stuart F.; and Clough, Ray W.: Improved Numerical Integration of Thick Shell Finite Elements. Int. J. Numerical Methods Eng., vol. 3, no. 4, Oct.-Dec. 1971, pp. 575-586.

18. Ambartsumyan, S. A.: Theory of Anisotropic Shells. NASA TT F-118, 1964.

19. Taylor, Robert L.: On Completeness of Shape Functions for Finite Element Analysis. Int. J. Numerical Methods Eng., vol. 4, no. 1, 1972, pp. 17-22.

20. Zienkiewicz, O. C.: The Finite Element Method in Engineering Science. McGraw-Hill Pub. Co., Ltd., c.1971.

21. Sander, G.; and Beckers, P.: Improvements of Finite Element Solutions for Structural and Nonstructural Applications. AFFDL-TR-72-94, U.S. Air Force, Dec. 1972. (Available from DDC as AD 762 947.)

22. Wilson, Edward L.: The Static Condensation Algorithm. Int. J. Numerical Methods Eng., vol. 8, no. 1, 1974, pp. 198-203.

23. Cowper, G. R.: Gaussian Quadrature Formulas for Triangles. Int. J. Numerical Methods Eng., vol. 7, no. 3, 1973, pp. 405-408.

24. Cantin, Gilles: An Equation Solver of Very Large Capacity. Int. J. Numerical Methods Eng., vol. 3, no. 3, July-Sept. 1971, pp. 379-388.

25. Wilson, Edward L.; Bathe, Klaus-Jürgen; and Doherty, William P.: Direct Solution of Large Systems of Linear Equations. Comput. & Struct., vol. 4, no. 2, Mar. 1974, pp. 363-372.

26. Irons, Bruce M.: A Frontal Solution Program for Finite Element Analysis. Int. J. Numerical Methods Eng., vol. 2, no. 1, Jan.-Mar. 1970, pp. 5-32.

27. Johnson, Th. Lunde: Note on Symmetric Decomposition of Some Special Symmetric Matrices. Comput. Methods Appl. Mech. & Eng., vol. 1, no. 3, 1972, pp. 301-306.

28. Bathe, Klaus-Jürgen: Solution Methods for Large Generalized Eigenvalue Problems in Structural Engineering. SESM UC SESM 71-20, Univ. of California, Nov. 1971.

29. Gupta, K. K.: Eigenproblem Solution by a Combined Sturm Sequence and Inverse Iteration Technique. Int. J. Numerical Methods Eng., vol. 7, no. 1, 1973, pp. 17-42.

30. Anderson, M. S.; Fulton, R. E.; Heard, W. L., Jr.; and Walz, J. E.: Stress, Buckling, and Vibration Analysis of Shells of Revolution. Comput. & Struct., vol. 1, nos. 1/2, Aug. 1971, pp. 157-192.

31. Argyris, J. H.; and Willam, K. J.: Some Considerations for the Evaluation of Finite Element Models. Nucl. Eng. & Des., vol. 28, no. 1, 1974, pp. 76-96.

32. Oden, J. T.; and Brauchli, H. J.: On the Calculation of Consistent Stress Distributions in Finite Element Approximations. Int. J. Numerical Methods Eng., vol. 6, 1971, pp. 317-325.

33. Wilson, E. L.; Taylor, R. L.; Doherty, W.; and Ghaboussi, J.: Incompatible Displacement Models. Numerical and Computer Methods in Structural Mechanics, Steven J. Fenves, Nicholas Perrone, Arthur R. Robinson, and William C. Schnobrich, eds., Academic Press, Inc., 1973, pp. 43-57.

34. Bell, Kalbein: On the Quintic Triangular Plate Bending Element. Div. Struct. Mech., Norwegian Inst. Technol., Univ. of Trondheim, Norway, June 1972.

35. Chamis, Christos C.: Buckling of Anisotropic Composite Plates. J. Struct. Div., American Soc. Civil Eng., vol. 95, no. ST10, Oct. 1969, pp. 2119-2139.

36. Morley, L. S. D.: Skew Plates and Structures. Macmillan Co., 1963.

37. Williams, M. L.: Surface Stress Singularities Resulting From Various Boundary Conditions in Angular Corners of Plates Under Bending. GALCIT Publ. No. 330, [1954]. (Reprinted from ASME Proceedings of the First National Congress of Applied Mechanics.)

38. Plass, H. J., Jr.; Gaines, J. H.; and Newsom, C. D.: Application of Reissner's Variational Principle to Cantilever Plate Deflection and Vibration Problems. J. Appl. Mech., vol. 29, Mar. 1962, pp. 127-135.

39. Eringen, A. C.; Naghdi, A. K.; and Thiel, C. C.: State of Stress in a Circular Cylindrical Shell With a Circular Hole. Tech. Rep. No. 3-6 (Contract NObs-78866), General Technology Corp., Aug. 1964.

40. Johnson, Donald E.: A Difference-Based Variational Method for Shells. Int. J. Solids & Struct., vol. 6, no. 6, June 1970, pp. 699-724.

41. Lindberg, Garry M.; and Olson, Mervyn D.: A High-Precision Triangular Cylindrical Shell Finite Element. AIAA J., vol. 9, no. 3, Mar. 1971, pp. 530-532.

42. Key, Samuel W.: The Analysis of Thin Shells With a Doubly Curved Arbitrary Quadrilateral Finite Element. Comput. & Struct., vol. 2, no. 4, Sept. 1972, pp. 637-673.

43. Noor, A. K.; and Khandelwal, V. K.: Improved Finite-Difference Variant for the Bending Analysis of Arbitrary Cylindrical Shells. UNICIV Rep. No. R-58, Univ. of New South Wales, Dec. 1969.

44. Desai, Chandrakant S.; and Abel, John F.: Introduction to the Finite Element Method. Van Nostrand Reinhold Co., c.1972.

TABLE 1.- CHARACTERISTICS OF SHEAR-FLEXIBLE FINITE-ELEMENT MODELS USED IN PRESENT STUDY

Formulation	Element shape	Number of nodes	Approximation	Internal D.O.F.[a] per unknown	Total number of D.O.F.[a]		Designation	
					Shell	Plate[b]	Name	Symbol
Displacement (stiffness)	Quadrilateral	4	Bilinear	None	20	12	SQ4	△
		4		1	25	15	SQ5	⏃
		4		3	35	21	SQ7	✳
		8	Quadratic	None	40	24	SQ8	□
		8		1	45	27	SQ9	⊡
		8		3	55	33	SQ11	⊠
		12	Cubic	None	60	36	SQ12	○
		4	Product of first-order Hermitian polynomials	None	80	48	SQH	▷
		8 for u_α,w 4 for ϕ_α	Quadratic Bilinear	None	32	16	SQ8-4	◺
	Triangular	6	Quadratic	None	30	18	ST6	◇
		10	Cubic		50	30	ST10	▽
Mixed	Quadrilateral	4	Bilinear	None	52	32	MQ4	■
		8	Quadratic	None	104	64	MQ8	◆
	Triangular	3	Linear	None	39	24	MT3	▲
		6	Quadratic		78	48	MT6	●

[a]Degrees of freedom.

[b]Degenerate case of symmetrically laminated plates.

TABLE 2.- BOUNDARY CONDITIONS USED IN PRESENT STUDY

[0 denotes suppressed degree of freedom; 1, free (unrestrained)]

(a) Kinematic boundary conditions

Boundary x_α = Const	u_α	$u_{3-\alpha}$	w	ϕ_α	$\phi_{3-\alpha}$
Simple support	1	0	0	1	0
Clamped	0	0	0	0	0
Line of symmetry	0	1	1	0	1

(b) Force boundary conditions

Boundary x_α = Const	$N_{\alpha,\alpha}$	$N_{3-\alpha,3-\alpha}$	N_{12}	$M_{\alpha,\alpha}$	$M_{3-\alpha,3-\alpha}$	M_{12}	Q_α	$Q_{3-\alpha}$
Simple support	0	${}^a\kappa_a$	1	0	${}^a\kappa_a$	1	1	${}^a\kappa_a$
Clamped	1	1	1	1	1	1	1	${}^a\kappa_a$
Free	0	1	0	0	1	0	0	1
Line of symmetry	1	1	0	1	1	0	0	1

${}^a\kappa_a$ = 1 for anisotropic shells and 0 for isotropic or orthotropic shells.

TABLE 2.- Concluded

(c) Boundary conditions for SQH element along edge x_α = Const

Displacement	Simple support				Clamped				Line of symmetry			
	f [a]	$\partial_\alpha f$	$\partial_{3-\alpha} f$	$\partial_1\partial_2 f$	f	$\partial_\alpha f$	$\partial_{3-\alpha} f$	$\partial_1\partial_2 f$	f	$\partial_\alpha f$	$\partial_{3-\alpha} f$	$\partial_1\partial_2 f$
u_α	1	b_κ	1	b_κ	0	1	0	1	0	1	0	1
$u_{3-\alpha}$	0	1	0	1	0	1	0	1	1	0	1	0
w	0	1	0	1	0	1	0	1	1	0	1	0
ϕ_α	1	b_κ	1	b_κ	0	1	0	1	0	1	0	1
$\phi_{3-\alpha}$	0	1	0	1	0	1	0	1	1	0	1	0

[a] f stands for any of the generalized displacements u_α, w, ϕ_α.

b_κ = 0 if force boundary conditions are imposed and 1 otherwise.

TABLE 3.- EFFECT OF THICKNESS RATIO h/a ON TOTAL AND TRANSVERSE SHEAR-STRAIN ENERGIES OF PLATES

[Simply supported, nine-layered, square orthotropic plate subjected to uniform pressure loading p_o; U denotes total strain energy of plate and U_{sh} denotes shear-strain energy of plate]

h/a	$UE_T h/p_o{}^2 a^4$	$\frac{U_{sh}}{U} \times 100$
0.1	0.1256	26.055
.01	9.2980	.3577
.001	926.5123	.0036

TABLE 4.- ERROR INDEX FOR GENERALIZED DISPLACEMENTS AND STRESS RESULTANTS OBTAINED BY DIFFERENT STIFFNESS AND MIXED MODELS

[Simply supported, nine–layered, square orthotropic plate subjected to uniform loading;

$$E_f = \frac{1}{\bar{n}} \sqrt{\sum_{i=1}^{\bar{n}} \left(\frac{f_i - \tilde{f}_i}{|f_{max}|} \right)^2}$$

]

(a) $\frac{h}{a} = 0.1$

Grid size (quarter plate)	Values of $E_f \times 10^4$ for									
	SQ4	SQ5	SQ7	ST6	SQ8	SQ12	SQH	MT3	MQ4	MT6
					f = w					
2 X 2	212.75	36.37	28.64	8.73	2.19	1.62	0.84	274.91	179.87	23.23
3 X 3	76.74	9.65	8.51	1.49	.37	.27	.13	69.89	75.51	6.42
4 X 4	35.60	3.98	3.69	.46	.38	.08	.04	33.83	27.66	
					$f = \phi_1$					
2 X 2	242.91	74.48	70.82	17.94	2.13	1.74	0.40	347.48	213.04	16.71
3 X 3	85.58	21.36	20.82	4.13	.37	.27	.05	116.89	77.46	6.94
4 X 4	39.20	8.90	8.76	1.57	.90	.07	.03	44.90	30.65	
					$f = \phi_2$					
2 X 2	241.23	80.42	77.81	16.53	2.35	1.97	0.34	347.00	223.64	16.77
3 X 3	84.65	23.33	22.95	3.61	.41	.31	.10	118.69	80.82	6.72
4 X 4	38.65	9.72	9.62	1.19	.25	.08	.03	45.22	32.41	
					$f = M_{11}$					
2 X 2	612.41	581.50	581.40	928.74	69.26	11.08	0.90	219.86	210.60	12.62
3 X 3	289.46	277.50	277.48	586.61	22.53	2.43	.27	78.74	95.72	8.01
4 X 4	162.51	157.00	156.99	422.01	10.01	.82	.11	36.60	36.24	

TABLE 4.- Continued

(a) Concluded

Grid size (quarter plate)	Values of $E_f \times 10^4$ for -									
	SQ4	SQ5	SQ7	ST6	SQ8	SQ12	SQH	MT3	MQ4	MT6
					$f = M_{22}$					
2 X 2	623.40	598.13	598.21	1032.73	82.22	12.03	2.49	249.57	244.63	14.92
3 X 3	303.48	293.98	293.98	713.88	27.20	2.78	.59	92.22	111.02	9.51
4 X 4	173.43	168.99	168.99	543.92	12.09	.97	.21	42.99	43.97	
					$f = Q_1$					
2 X 2	1333.68	1399.47	1399.36	1724.02	89.53	39.78	19.71	93.06	67.58	28.57
3 X 3	602.92	608.81	608.47	1183.26	29.53	11.48	7.83	68.81	36.45	19.44
4 X 4	326.58	325.75	325.62	891.00	13.50	5.03	4.76	32.07	16.32	
					$f = Q_2$					
2 X 2	1647.63	1741.03	1739.31	2800.71	110.86	49.43	30.08	81.32	52.87	34.66
3 X 3	745.45	755.56	754.88	1879.48	37.57	14.36	11.23	65.77	33.04	25.30
4 X 4	403.70	403.65	403.45	1394.23	17.40	6.33	6.48	37.87	16.92	

TABLE 4.- Continued

(b) $\frac{h}{a} = 0.01$

Grid size (quarter plate)	Values of $E_f \times 10^4$ for –									
	SQ4	SQ5	SQ7	ST6	SQ8	SQ12	SQH	MT3	MQ4	MT6
					f = w					
2 X 2				121.58	51.11	9.06	1.03	319.96	172.69	27.40
3 X 3				39.58	10.51	.54	.19	75.00	66.33	5.25
4 X 4	806.46	416.11	406.94	14.22	3.37	.08	.05	37.48	25.62	
					$f = \phi_1$					
2 X 2				125.18	38.25	9.83	0.97	346.35	209.19	17.08
3 X 3				42.43	8.37	.76	.78	108.31	73.64	5.67
4 X 4	790.37	407.96	402.06	15.60	2.92	.13	.17	43.18	29.71	
					$f = \phi_2$					
2 X 2				124.82	38.48	10.27	2.21	365.39	227.74	18.37
3 X 3				42.45	8.97	.83	1.51	112.04	78.84	5.87
4 X 4	781.46	404.68	399.41	15.60	3.07	.15	.35	44.46	32.41	
					$f = M_{11}$					
2 X 2				895.04	260.91	26.30	66.51	224.72	204.93	28.52
3 X 3				558.53	89.56	5.83	17.91	75.99	91.84	20.42
4 X 4	840.00	450.88	445.94	403.17	36.95	1.76	6.50	44.41	35.08	

TABLE 4.- Concluded

(b) Concluded

Grid size (quarter plate)	Values of $E_f \times 10^4$ for -									
	SQ4	SQ5	SQ7	ST6	SQ8	SQ12	SQH	MT3	MQ4	MT6
					$f = M_{22}$					
2 X 2				965.52	309.37	37.40	76.21	279.10	258.03	33.35
3 X 3				689.66	117.78	9.40	22.58	99.72	114.38	26.88
4 X 4	859.45	462.04	457.63	531.80	52.16	3.00	8.83	52.92	46.04	
					$f = Q_1$					
2 X 2				106803.72	3674.66	1812.85	838.56	100.53	57.10	60.86
3 X 3				77899.77	1514.72	329.35	227.36	80.35	37.56	62.63
4 X 4	4989.61	14280.28	14225.74	60490.19	853.06	97.98	84.28	49.29	16.92	
					$f = Q_2$					
2 X 2				180688.96	4254.03	2366.80	1387.85	97.70	27.27	68.30
3 X 3				128160.13	1638.37	432.93	390.99	94.43	38.84	78.48
4 X 4	6515.33	18870.15	18704.66	97935.41	962.99	130.24	148.25	59.50	19.41	

TABLE 5.- CONVERGENCE OF MINIMUM NONDIMENSIONAL FREQUENCIES $\bar{\lambda}$ OBTAINED BY DIFFERENT FINITE-ELEMENT MODELS

[Simply supported, nine-layered, square orthotropic plate; $\bar{\lambda} = \omega \sqrt{\rho a^2 / E_T}$]

Grid size (quarter plate)	Values of $\bar{\lambda} \frac{a}{h} \times 10^{-1}$ for –											Analytic solution (a)
	SQ4	ST6	SQ8	SQ9	SQ11	ST10	SQ12	SQH	MT3	MQ4	MT6	
						$\frac{h}{a} = 0.1$						
2 X 2	1.827	1.633	1.627	1.627	1.626	1.625	1.625	1.625	1.587	1.619	1.625	1.62500
3 X 3	1.714	1.627	1.625	1.625	1.625				1.620	1.624		(1.88913)
4 X 4	1.675	1.626							1.623	1.625		
5 X 5	1.657											
						$\frac{h}{a} = 0.01$						
2 X 2		2.010	1.932	1.921	1.905	1.892	1.896	1.886	1.836	1.877	1.887	1.88576
3 X 3		1.939	1.899	1.898	1.891	1.887	1.887		1.879	1.884		(1.88913)
4 X 4	4.232	1.910	1.891	1.891					1.884	1.885		
5 X 5	3.558		1.888									

[a]Numbers in parentheses refer to classical-theory solutions (with both shear deformation and rotary inertia neglected).

TABLE 6.- CONVERGENCE OF NONDIMENSIONAL FREQUENCIES $\bar{\lambda}_{m,n}$ OBTAINED BY DIFFERENT STIFFNESS MODELS

[Simply supported, nine–layered, square orthotropic plate; $\bar{\lambda}_{m,n} = \omega_{m,n}\sqrt{\rho a^2/E_T}$]

(a) $\frac{h}{a} = 0.1$

Grid size (quarter plate)	Values of $\bar{\lambda}_{m,n}$ for –								Analytic soultion (a)
	SQ4	ST6	SQ8	SQ9	SQ11	ST10	SQ12	SQH	
m = 1, n = 3									
2 X 2	8.111	6.100	6.094	6.088	5.971	5.937	5.933	5.930	5.92149
3 X 3	6.989	5.972	5.959	5.959	5.931	5.923	5.922		(10.500)
4 X 4	6.519	5.939	5.934	5.934					
m = 3, n = 1									
2 X 2	8.191	6.404	6.393	6.388	6.280	6.249	6.245	6.242	6.23387
3 X 3	7.208	6.281	6.269	6.267	6.242	6.235	6.235		(12.9354)
4 X 4	6.781	6.250	6.245	6.245					
m = 3, n = 3									
2 X 2	11.380	9.197	9.052	8.694	8.559	8.595	8.768	8.478	8.46619
3 X 3	9.901	8.710	8.542	8.517	8.484	8.479	8.488		(17.0022)
4 X 4		8.558	8.487	8.483					

[a]Numbers in parentheses refer to classical-theory solutions (with both shear deformation and rotary inertia neglected).

TABLE 6.- Concluded

(b) $\frac{h}{a} = 0.01$

Grid size (quarter plate)	Values of $\bar{\lambda}_{m,n}$ for –								Analytic solution (a)
	SQ4	ST6	SQ8	SQ9	SQ11	ST10	SQ12	SQH	
				m = 1, n = 3					
2 X 2		1.324	1.278	1.239	1.159	1.070	1.075	1.060	1.03849
3 X 3		1.150	1.112	1.110	1.072	1.043	1.042		(1.0500)
4 X 4	2.885	1.087	1.070	1.070					
				m = 3, n = 1					
2 X 2		1.638	1.530	1.499	1.390	1.303	1.305	1.292	1.27201
3 X 3		1.383	1.349	1.347	1.303	1.276	1.275		(1.29354)
4 X 4	2.985	1.318	1.303	1.303					
				m = 3, n = 3					
2 X 2		2.942	3.856	1.975	1.825	1.902	2.297	1.703	1.67351
3 X 3		2.242	1.926	1.775	1.718	1.709	1.782		(1.70022)
4 X 4	4.146	1.935	1.734	1.716					

[a]Numbers in parentheses refer to classical–theory solutions (with both shear deformation and rotary inertia neglected).

TABLE 7.- ACCURACY OF VIBRATION FREQUENCIES OBTAINED BY SQ12 AND SQH ELEMENTS

[Simply supported, two-layered orthotropic plate; 2 × 2 grid;

$$\bar{\lambda}_{m,n} = \omega_{m,n}\sqrt{\rho a^2/E_T}$$

]

m,n	Values of $[\bar{\lambda}_{m,n}(a/h)^2] \times 10^{-1}$ for –			
	SQ12	SQH	Analytic solution (a)	
	h/a = 0.1			
1,1	1.0580	1.0578	1.0578	(1.1244)
1,3	4.8447	4.8405	4.8305	(6.5730)
3,1				
3,3	7.3000	6.8895	6.8757	(9.6664)
	h/a = 0.01			
1,1	1.1463	1.1303	1.1300	(1.1308)
1,3	7.1596	6.9498	6.7319	(6.7644)
3,1				
3,3	15.7435	10.4152	10.1118	(10.1725)

[a]Numbers in parentheses refer to classical-theory solutions (with both shear deformation and rotary inertia neglected).

TABLE 8.- ACCURACY OF BUCKLING LOAD PARAMETER λ OBTAINED BY SQH AND SQ12 ELEMENTS

[Simply supported, nine-layered, square orthotropic plate subjected to uniaxial edge compression; $N^{o}_{11} = -1$; 2 X 2 grid in one-quarter of plate]

$\frac{h}{a}$	Values of $\lambda a^2/E_T h^3$ for –		
	SQH	SQ12	Analytic solution (a)
0.1	27.012	27.014	27.0069 (36.1597)
.01	36.051	36.419	36.0365 (36.1597)
.001	36.177	69.060	36.1585 (36.1597)

[a]Numbers in parentheses refer to classical-theory solutions (with shear deformation neglected).

TABLE 9.- CONVERGENCE OF BUCKLING LOAD PARAMETER λ OBTAINED BY SQH ELEMENTS

[Simply supported, eight-layered, anisotropic plate with fiber orientation (90/0/-45/45/45/-45/0/90) subjected to combined compressive and shear edge loadings; $\frac{h}{a} = 0.0072$; $N^o_{11} = 0$; $N^o_{12} = 1$; $N^o_{22} = -1$]

Grid size (full plate)	Values of $\lambda a^2/E_T h^3$ for –	
	SQH element	Galerkin's method (ref. 35)[a]
2 X 2	19.745	19.590
3 X 3	19.194	
4 X 4	19.046	

[a]Based on classical theory (with shear deformation neglected).

TABLE 10.- EFFECT OF THICKNESS RATIO h/a ON TOTAL AND TRANSVERSE SHEAR-STRAIN ENERGIES OF SHELLS

[Simply supported, nine-layered, orthotropic shallow spherical shells (R/a = 10, f/a = 0.0125) subjected to uniform pressure loading p_o; U denotes total strain energy and U_{sh} denotes shear-strain energy]

h/a	$UE_T h/(p_o{}^2 a^4)$	$\frac{U_{sh}}{U} \times 100$
0.1	0.1246	25.8512
.01	5.6983	.2353
.001	15.6305	.0014

TABLE 11.- CONVERGENCE OF NONDIMENSIONAL FREQUENCIES $\bar{\lambda}_{m,n}$ OBTAINED BY DIFFERENT STIFFNESS MODELS

[Simply supported, nine-layered, orthotropic shallow spherical shell ($\frac{R}{a} = 10$, $\frac{f}{a} = 0.0125$); $\bar{\lambda}_{m,n} = \omega_{m,n}\sqrt{\rho h^2/E_T}$]

(a) $\frac{h}{a} = 0.1$

Grid size (quarter shell)	Values of $\bar{\lambda}_{m,n} \times 10$ for							Analytic solution (a)
	ST6	SQ8	SQ9	SQ11	ST10	SQ12	SQH	
				m = 1, n = 1				
2 X 2	1.639	1.633	1.632	1.631	1.631	1.631	1.630	1.630
3 X 3	1.632	1.631	1.631					
4 X 4		1.630						(1.893)
				m = 1, n = 3				
2 X 2	6.104	6.096	6.091	5.973	5.939	5.935	5.932	5.924
3 X 3	5.974	5.961	5.961					
4 X 4		5.936						(10.496)
				m = 3, n = 1				
2 X 2	6.408	6.395	6.390	6.282	6.251	6.246	6.244	6.236
3 X 3	6.283	6.271	6.270					
4 X 4		6.247						(12.926)
				m = 3, n = 3				
2 X 2	9.201	9.055	8.695	8.560	8.595	8.770	8.478	8.467
3 X 3	8.711	8.543	8.518					
4 X 4		8.487						(17.001)

[a]Numbers in parentheses refer to classical-theory solution (with shear deformation and rotary inertia neglected).

TABLE 11.- Concluded

(b) $\frac{h}{a} = 0.01$

Grid size (quarter shell)	Values of $\bar{\lambda}_{m,n} \times 10^2$ for –							Analytic solution (a)
	ST6	SQ8	SQ9	SQ11	ST10	SQ12	SQH	
m = 1, n = 1								
2 X 2	0.2538	0.2452	0.2443	0.2428	0.2417	0.2419	0.2412	0.2411
3 X 3	.2459	.2422	.2422					
4 X 4		.2416						(0.2414)
m = 1, n = 3								
2 X 2	1.350	1.303	1.265	1.182	1.094	1.099	1.084	1.063
3 X 3	1.173	1.136	1.134					
4 X 4		1.094						(1.074)
m = 3, n = 1								
2 X 2	1.661	1.551	1.520	1.409	1.323	1.325	1.312	1.292
3 X 3	1.403	1.368	1.367					
4 X 4		1.323						(1.313)
m = 3, n = 3								
2 X 2	2.955	3.862	1.986	1.833	1.909	2.303	1.709	1.680
3 X 3	2.250	1.933	1.783					
4 X 4		1.741						(1.707)

[a]Numbers in parentheses refer to classical-theory solution (with shear deformation and rotary inertia neglected).

TABLE 12.- EIGENVALUES $\bar{\beta}$ OF THE STIFFNESS MATRICES FOR VARIOUS DISPLACEMENT MODELS

[Nine-layered, anisotropic shallow spherical shell with fiber orientation (45/-45/45/-45/45/-45/45/-45/45); R/a = 10; f/a = 0.0125; side length of element in coordinate directions is 0.25a; $\bar{\beta} = \beta a^2/E_T$]

Mode	Eigenvalue	Values of $\bar{\beta}$ for –						
		ST6	SQ8	SQ9	SQ11	ST10	SQ12	SQH
		$\frac{h}{a} = 0.1$						
Rigid body	$\bar{\beta}_1$	-1.581×10^{-14}	-3.862×10^{-14}	-4.548×10^{-14}	-4.979×10^{-14}	-2.076×10^{-14}	-5.413×10^{-14}	-2.026×10^{-15}
	$\bar{\beta}_2$	-1.164×10^{-14}	-2.518×10^{-14}	-2.449×10^{-14}	-2.859×10^{-14}	-8.472×10^{-15}	-3.981×10^{-14}	-6.663×10^{-16}
	$\bar{\beta}_3$	-2.831×10^{-15}	-3.585×10^{-15}	-2.388×10^{-14}	-1.734×10^{-14}	-6.781×10^{-15}	-1.550×10^{-14}	4.817×10^{-16}
	$\bar{\beta}_4$	-1.458×10^{-15}	2.821×10^{-15}	-4.073×10^{-16}	-1.166×10^{-14}	7.991×10^{-15}	1.081×10^{-15}	1.217×10^{-15}
	$\bar{\beta}_5$	5.417×10^{-15}	5.748×10^{-15}	4.218×10^{-15}	1.309×10^{-15}	1.349×10^{-14}	6.649×10^{-15}	2.373×10^{-15}
	$\bar{\beta}_6$	1.132×10^{-14}	1.251×10^{-14}	1.338×10^{-14}	5.165×10^{-15}	1.681×10^{-14}	1.250×10^{-14}	5.094×10^{-15}
Straining	$\bar{\beta}_7$	4.278×10^{-5}	5.890×10^{-5}	5.890×10^{-5}	5.183×10^{-5}	1.549×10^{-5}	3.969×10^{-5}	7.870×10^{-7}
	$\bar{\beta}_{max}$	9.389	6.276	1.175×10^{1}	1.175×10^{1}	2.047×10^{1}	1.232×10^{1}	2.679
	Trace	2.170×10^{1}	3.010×10^{1}	4.245×10^{1}	5.162×10^{1}	6.522×10^{1}	8.614×10^{1}	1.233×10^{1}

TABLE 12.- Concluded

Mode	Eigenvalue	Values of $\bar{\beta}$ for –						
		ST6	SQ8	SQ9	SQ11	ST10	SQ12	SQH
		$\frac{h}{a} = 0.01$						
Rigid body	$\bar{\beta}_1$	-6.576×10^{-16}	-1.195×10^{-15}	-3.381×10^{-15}	-9.607×10^{-16}	-2.140×10^{-15}	-2.429×10^{-15}	-5.789×10^{-16}
	$\bar{\beta}_2$	-3.674×10^{-16}	-3.290×10^{-16}	6.559×10^{-17}	-5.841×10^{-16}	-1.312×10^{-15}	-3.426×10^{-17}	-1.665×10^{-16}
	$\bar{\beta}_3$	-1.789×10^{-16}	2.230×10^{-16}	2.532×10^{-16}	1.327×10^{-16}	-7.098×10^{-16}	1.631×10^{-15}	-5.191×10^{-17}
	$\bar{\beta}_4$	2.865×10^{-16}	3.447×10^{-16}	6.021×10^{-16}	4.776×10^{-16}	-8.412×10^{-18}	5.699×10^{-15}	7.140×10^{-17}
	$\bar{\beta}_5$	7.590×10^{-16}	2.430×10^{-15}	1.652×10^{-15}	1.852×10^{-15}	6.582×10^{-16}	7.642×10^{-15}	2.271×10^{-16}
	$\bar{\beta}_6$	1.396×10^{-15}	3.844×10^{-15}	3.718×10^{-15}	6.166×10^{-15}	1.817×10^{-15}	1.080×10^{-14}	9.589×10^{-16}
Straining	$\bar{\beta}_7$	6.455×10^{-8}	6.711×10^{-8}	6.711×10^{-8}	6.651×10^{-8}	4.364×10^{-8}	4.719×10^{-8}	2.091×10^{-9}
	$\bar{\beta}_{max}$	9.389×10^{-1}	6.276×10^{-1}	1.175	1.175	2.047	1.232	2.678×10^{-1}
	Trace	2.169	3.007	4.241	5.158	6.516	8.608	1.232
		$\frac{h}{a} = 0.001$						
Rigid body	$\bar{\beta}_1$	-1.125×10^{-16}	-1.663×10^{-16}	-6.682×10^{-17}	-1.006×10^{-16}	-3.035×10^{-16}	-3.940×10^{-16}	-2.079×10^{-16}
	$\bar{\beta}_2$	-5.080×10^{-17}	-3.068×10^{-17}	-9.103×10^{-19}	-5.557×10^{-17}	-2.039×10^{-16}	-2.291×10^{-16}	-1.714×10^{-16}
	$\bar{\beta}_3$	-1.616×10^{-17}	-1.111×10^{-17}	2.524×10^{-17}	-9.370×10^{-18}	-2.289×10^{-17}	-3.775×10^{-17}	-3.932×10^{-17}
	$\bar{\beta}_4$	-5.074×10^{-18}	1.869×10^{-17}	1.317×10^{-16}	1.233×10^{-17}	-1.784×10^{-17}	3.885×10^{-18}	-1.529×10^{-18}
	$\bar{\beta}_5$	6.254×10^{-17}	9.108×10^{-17}	3.705×10^{-16}	1.326×10^{-16}	2.690×10^{-18}	7.217×10^{-17}	9.669×10^{-18}
	$\bar{\beta}_6$	1.757×10^{-16}	2.191×10^{-16}	3.847×10^{-16}	4.226×10^{-16}	1.089×10^{-16}	1.327×10^{-16}	1.986×10^{-17}
Straining	$\bar{\beta}_7$	5.995×10^{-10}	1.485×10^{-10}	1.485×10^{-10}	9.349×10^{-11}	4.437×10^{-11}	4.730×10^{-11}	7.273×10^{-12}
	$\bar{\beta}_{max}$	9.389×10^{-2}	6.276×10^{-2}	1.175×10^{-1}	1.175×10^{-1}	2.047×10^{-1}	1.232×10^{-1}	2.679×10^{-2}
	Trace	2.167×10^{-1}	3.007×10^{-1}	4.241×10^{-1}	5.158×10^{-1}	6.516×10^{-1}	8.608×10^{-1}	1.232×10^{-1}

TABLE 13.- COMPARISON OF SOLUTIONS OBTAINED BY ISOPARAMETRIC SQ12 ELEMENTS WITH THOSE OF PREVIOUS INVESTIGATORS

[Circular cylindrical shell with a circular cutout loaded in tension]

Grid	Number of degrees of freedom	σ_{11}/σ_o		$\left[UE/(\sigma_o{}^2h^3)\right] \times 10^{-4}$ (b)
		Membrane	Membrane + bending	
4 X 4	525	3.643	4.268	4.734951
5 X 4	640	3.691	4.252	4.735373
5 X 6	920	3.712	4.257	4.711623
8 X 6	1415	3.666	4.223	4.724903
Finite differences (ref. 40)[a]	753	3.603	4.096	
Finite elements (ref. 41)[a]	367	3.690	4.249	4.729269
Analytic solution (ref. 39)[a]		3.658	4.180	

[a]Based on the classical theory (with shear deformation neglected).

[b]Strain energy in one-quarter of the shell.

TABLE 14.- ACCURACY OF VIBRATION FREQUENCIES OBTAINED BY SQH ELEMENTS

[Simply supported, two-layered, orthotropic circular cylinder with $h/R = 0.05$, $R/L_1 = 0.5$; $\bar{\lambda}_{m,n} = \omega_{m,n}\sqrt{\rho R^2/E_T}$]

m,n	Values of $\bar{\lambda}_{m,n}$ for –			
	SQH element		Analytic solution (c)	
	Grid 1[a]	Grid 2[b]		
1,2	0.5512	- - - -	0.5487	(0.5494)
1,4	.7932	0.6396	.6356	(.6473)
3,2	1.7173	- - - -	1.7121	(1.7237)
3,4	1.4143	1.3390	1.3317	(1.3581)

[a]Grid 1: 2 X 2 in shell octant.

[b]Grid 2: 2 X 2 (2 elements in one-eighth of the circumference).

[c]Numbers in parentheses refer to classical-theory solution (with both shear deformation and rotary inertia neglected).

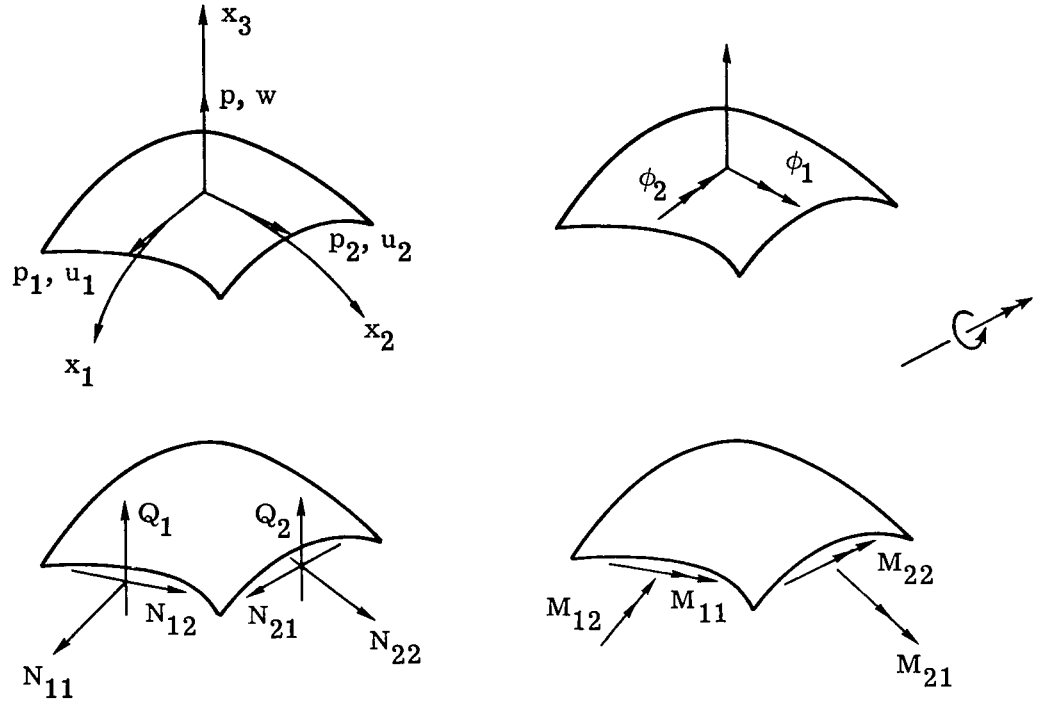

Figure 1.- Shell element and sign convention.

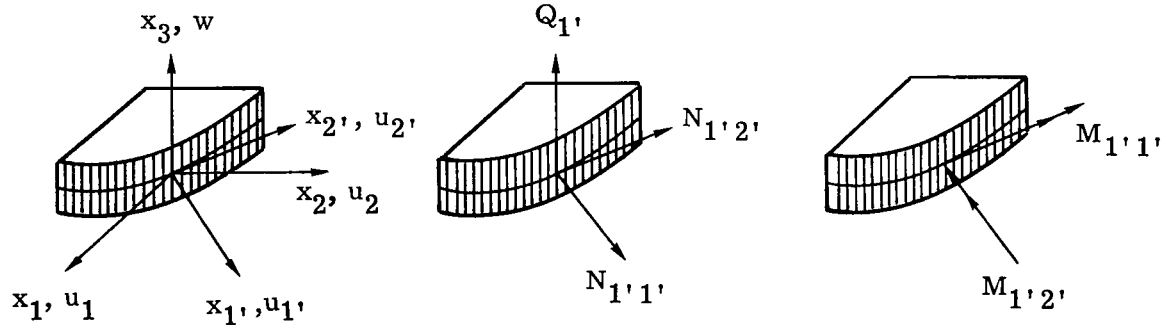

Figure 2.- Stress resultants and displacements at a curved boundary.

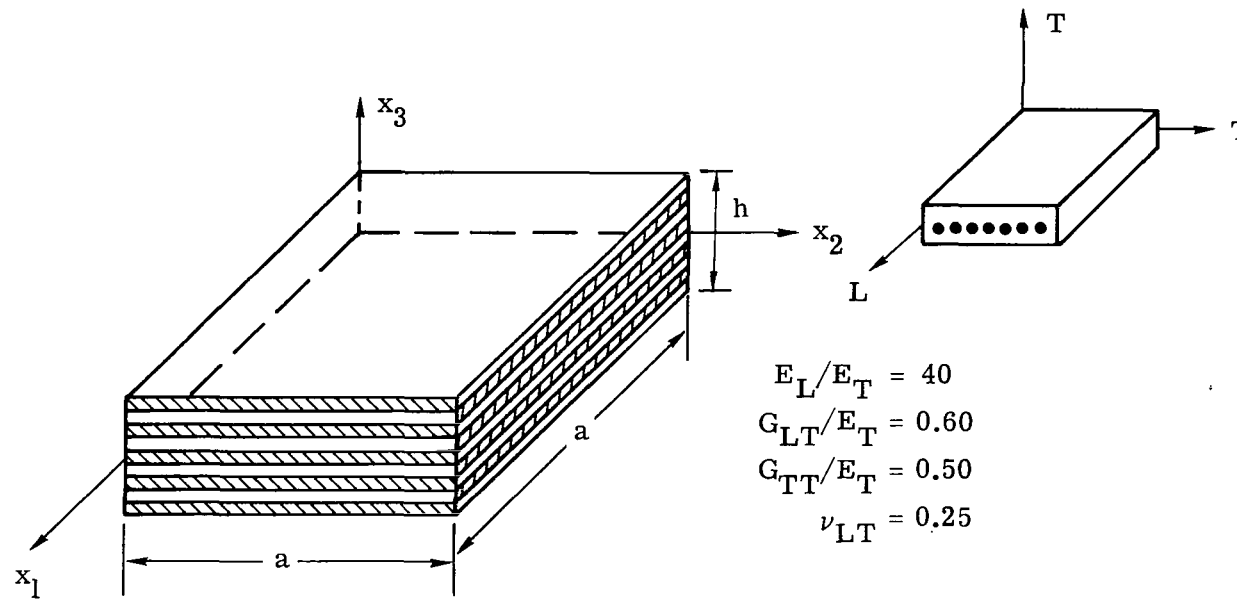

Figure 3.- Characteristics of laminated graphite-epoxy plates used in present study.

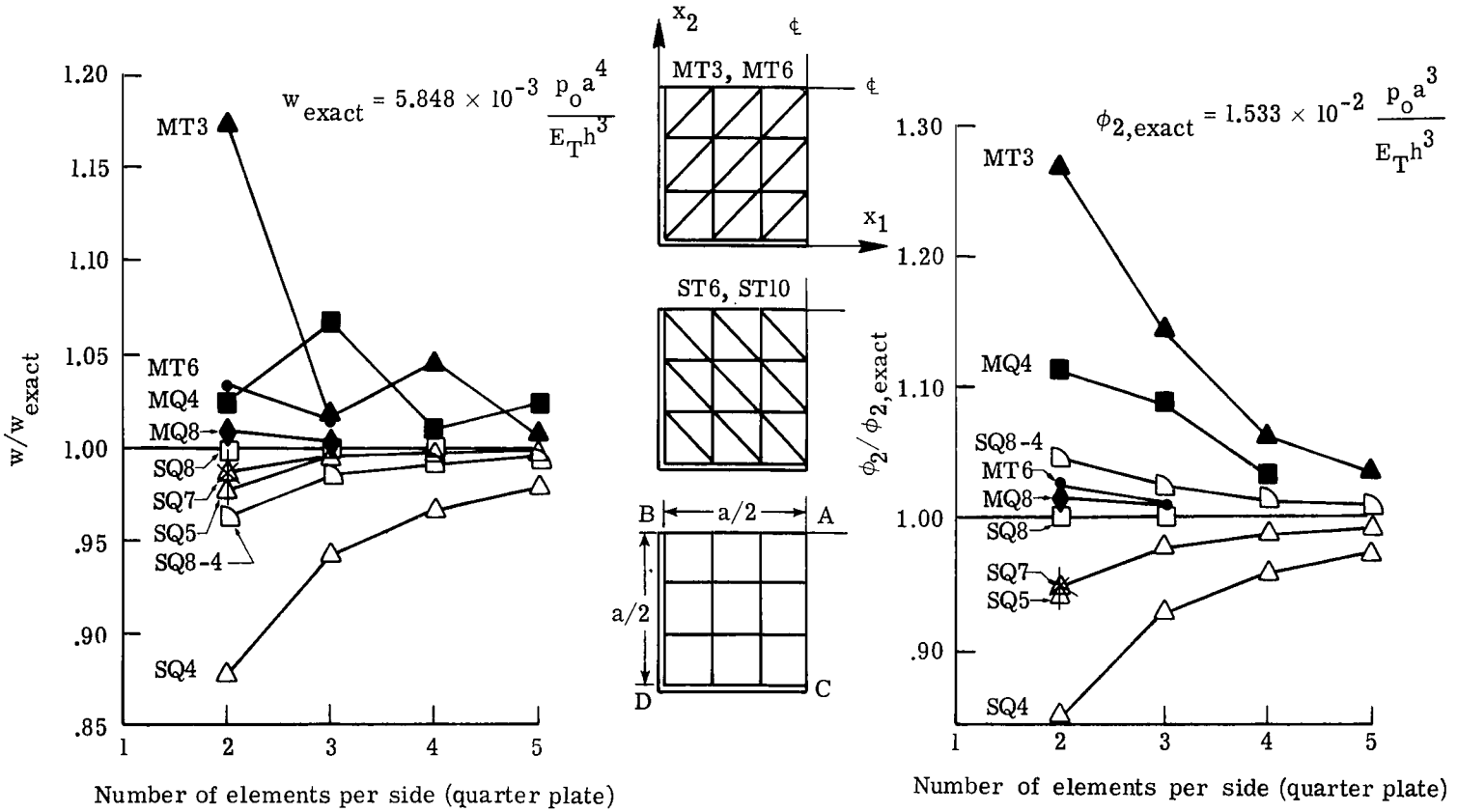

(a) w at point A.

(b) ϕ_2 at point B.

Figure 4.- Convergence of stress resultants and generalized displacements with grid refinement. Simply supported, nine-layered, orthotropic square plate with $\frac{h}{a} = 0.1$.

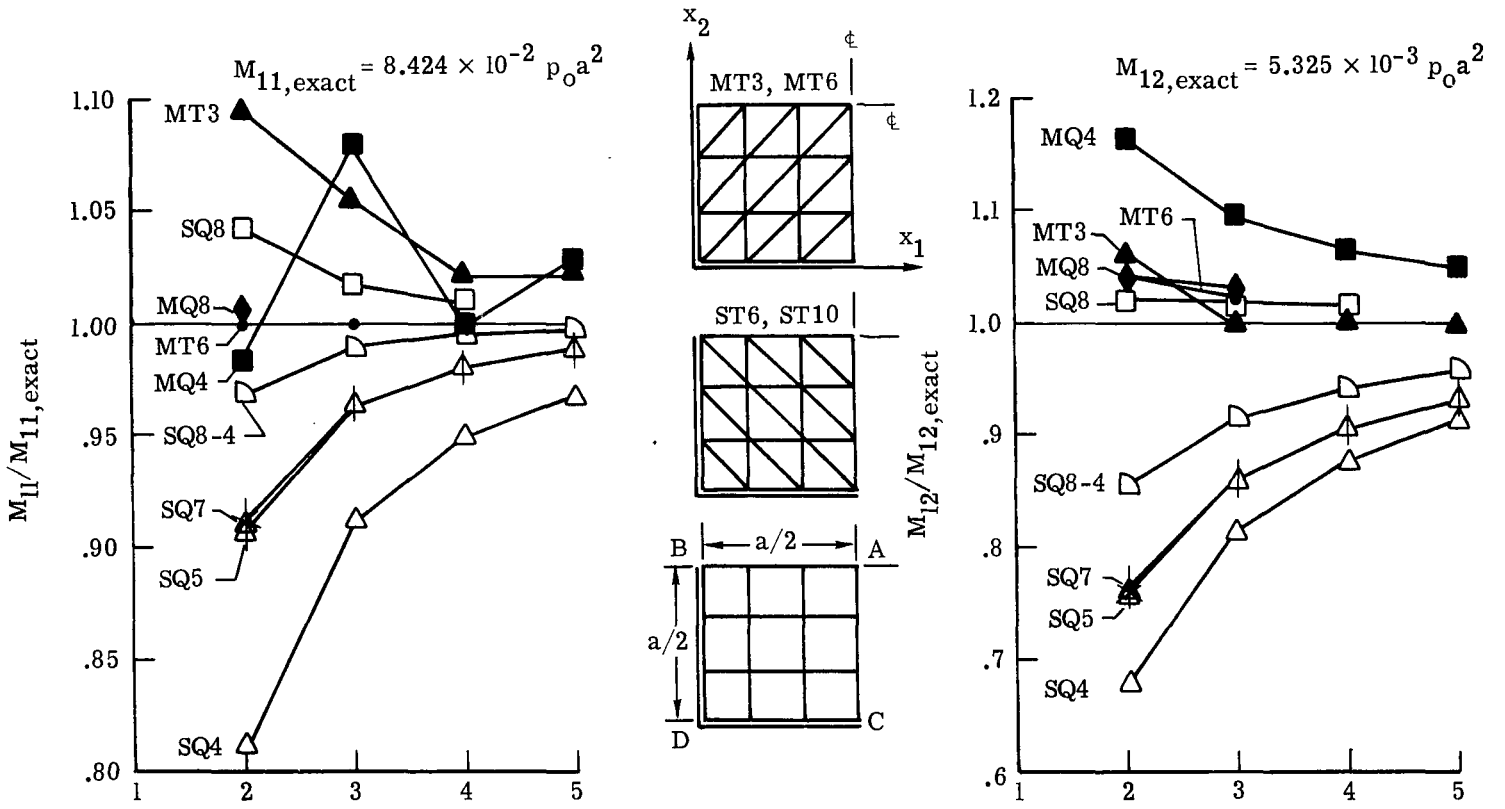

(c) M_{11} at point A.

(d) M_{12} at point D.

Figure 4.- Concluded.

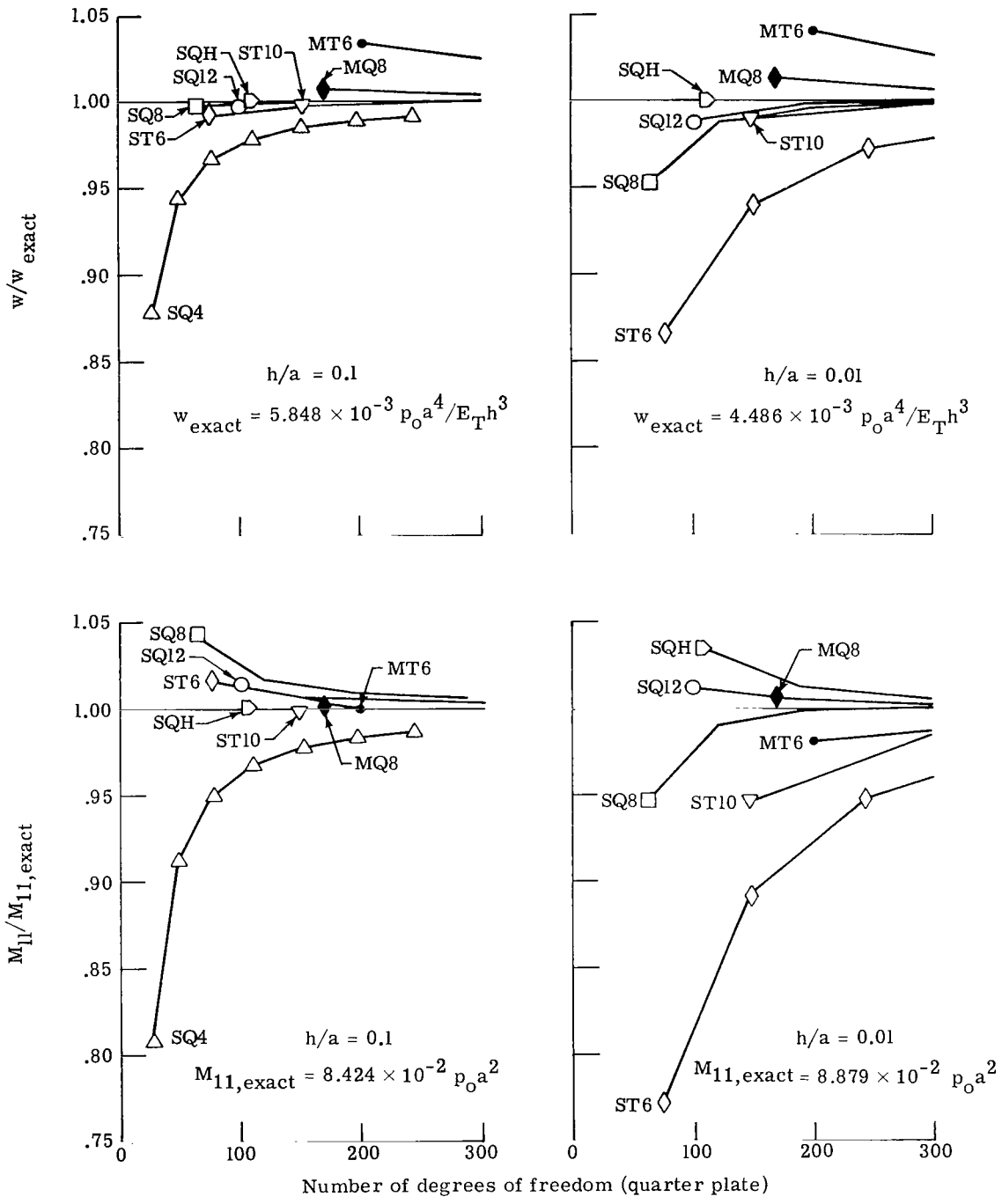

Figure 5.- Convergence of w and M_{11} obtained by different stiffness and mixed models with increasing number of degrees of freedom. Simply supported, nine-layered, orthotropic square plate with $\frac{h}{a}$ = 0.1 and 0.01.

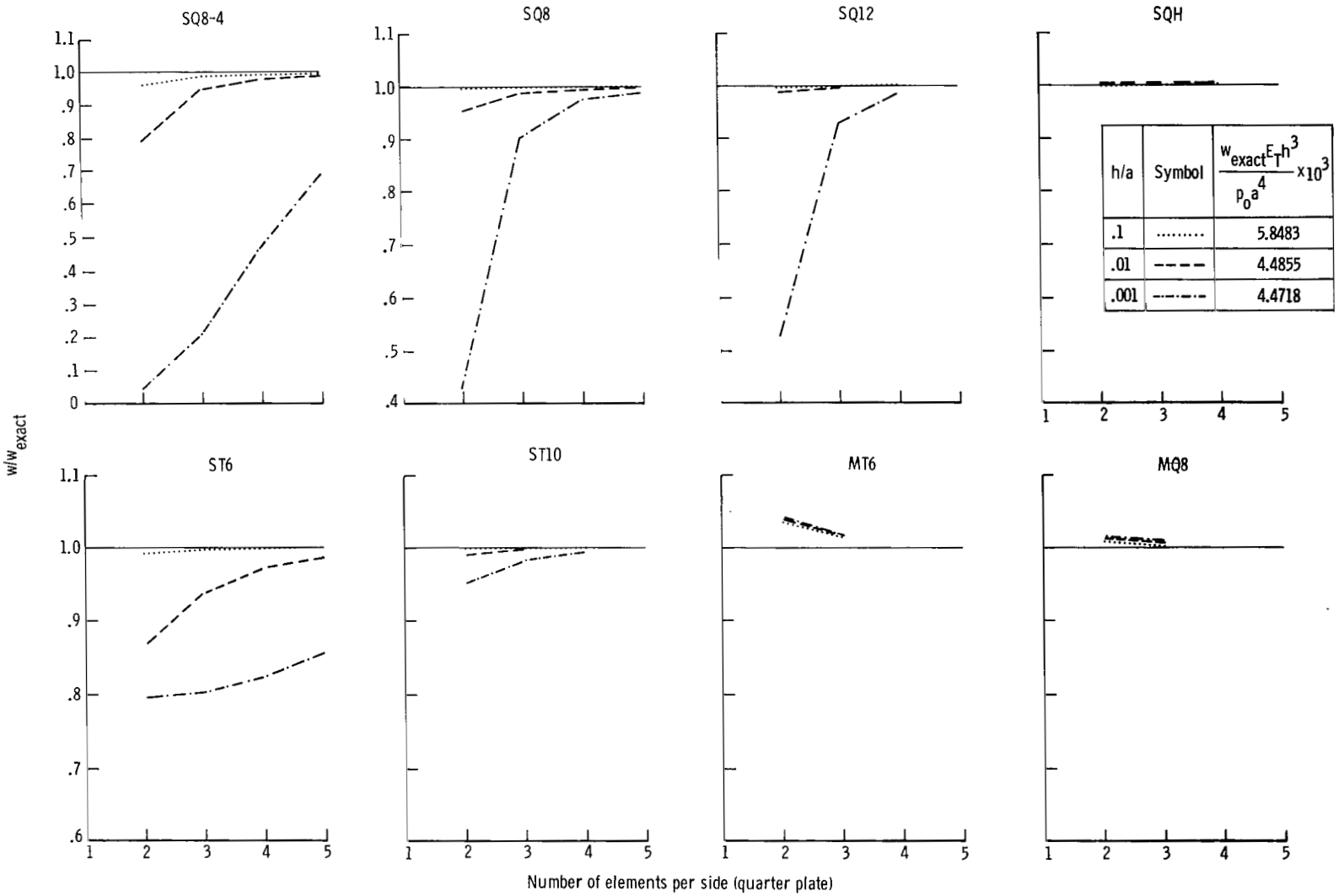

(a) Transverse displacement w at center.

Figure 6.- Effect of h/a on convergence of bending-moment resultant M_{11} and transverse displacement w obtained by different stiffness and mixed models. Simply supported, nine-layered, orthotropic square plate.

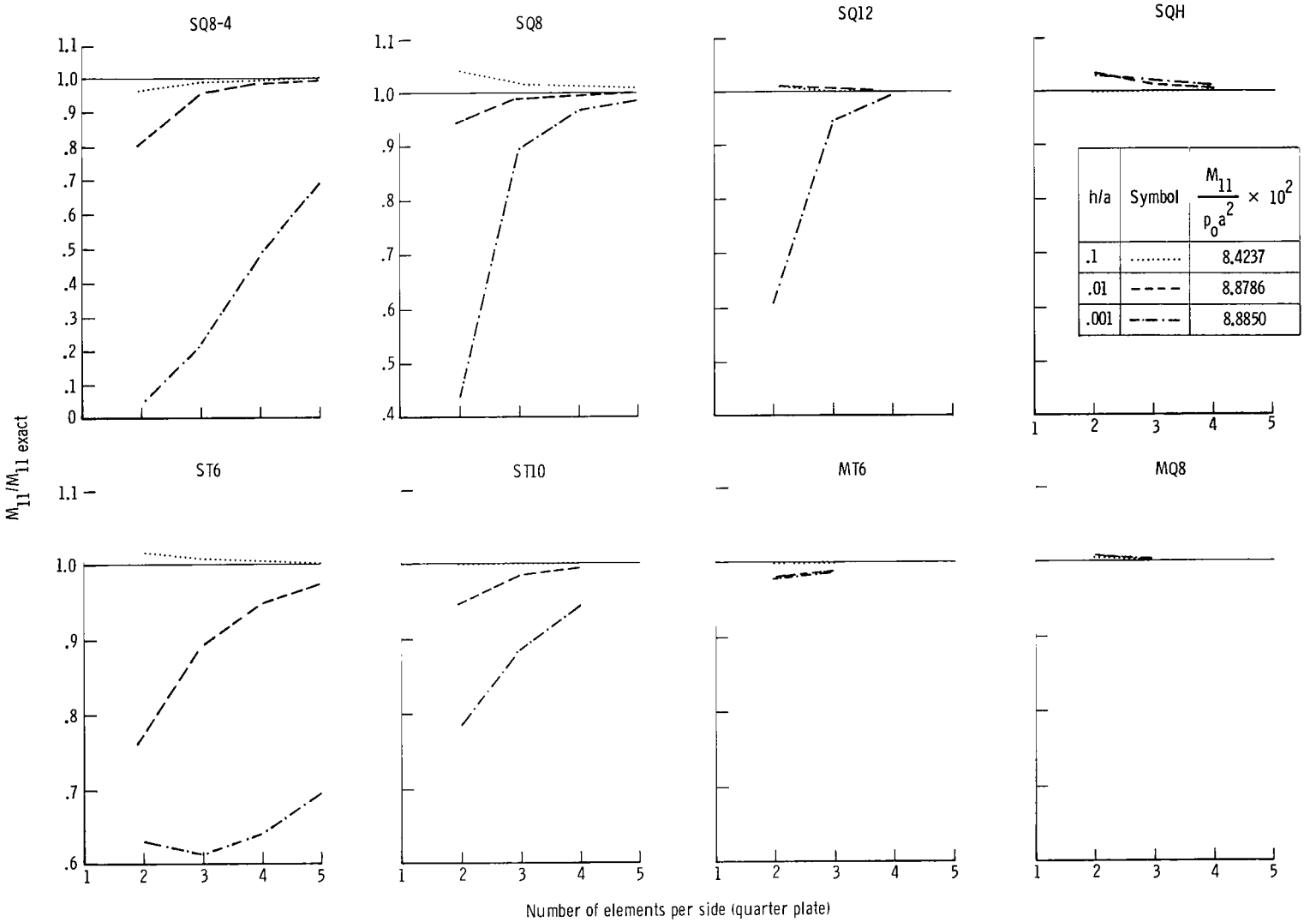

(b) Maximum bending-moment resultant M_{11} at center.

Figure 6.- Concluded.

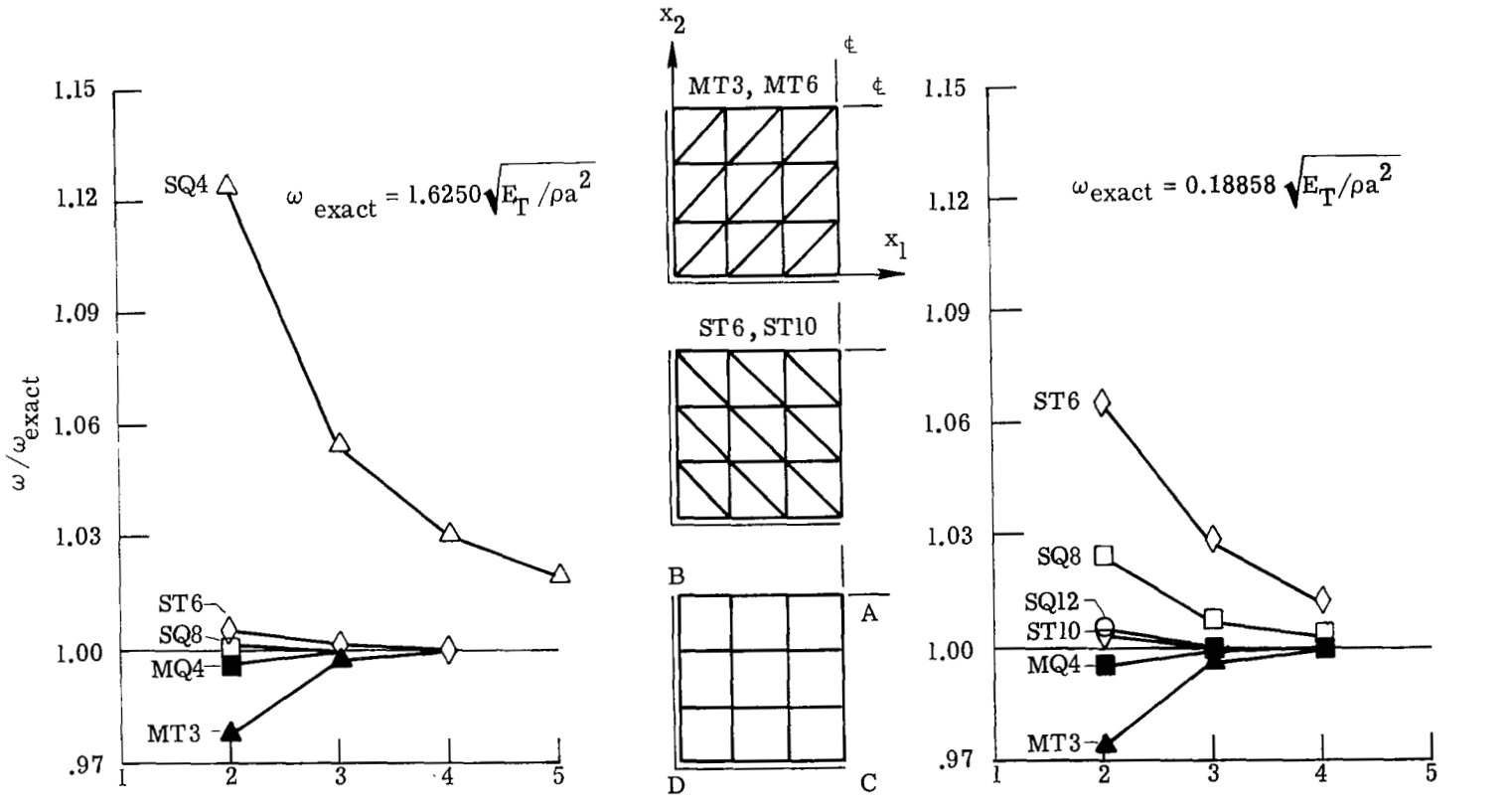

(a) $\frac{h}{a} = 0.1$.

(b) $\frac{h}{a} = 0.01$.

Figure 7.- Convergence of fundamental frequency obtained by different stiffness and mixed models with grid refinement. Simply supported, nine-layered, orthotropic square plate.

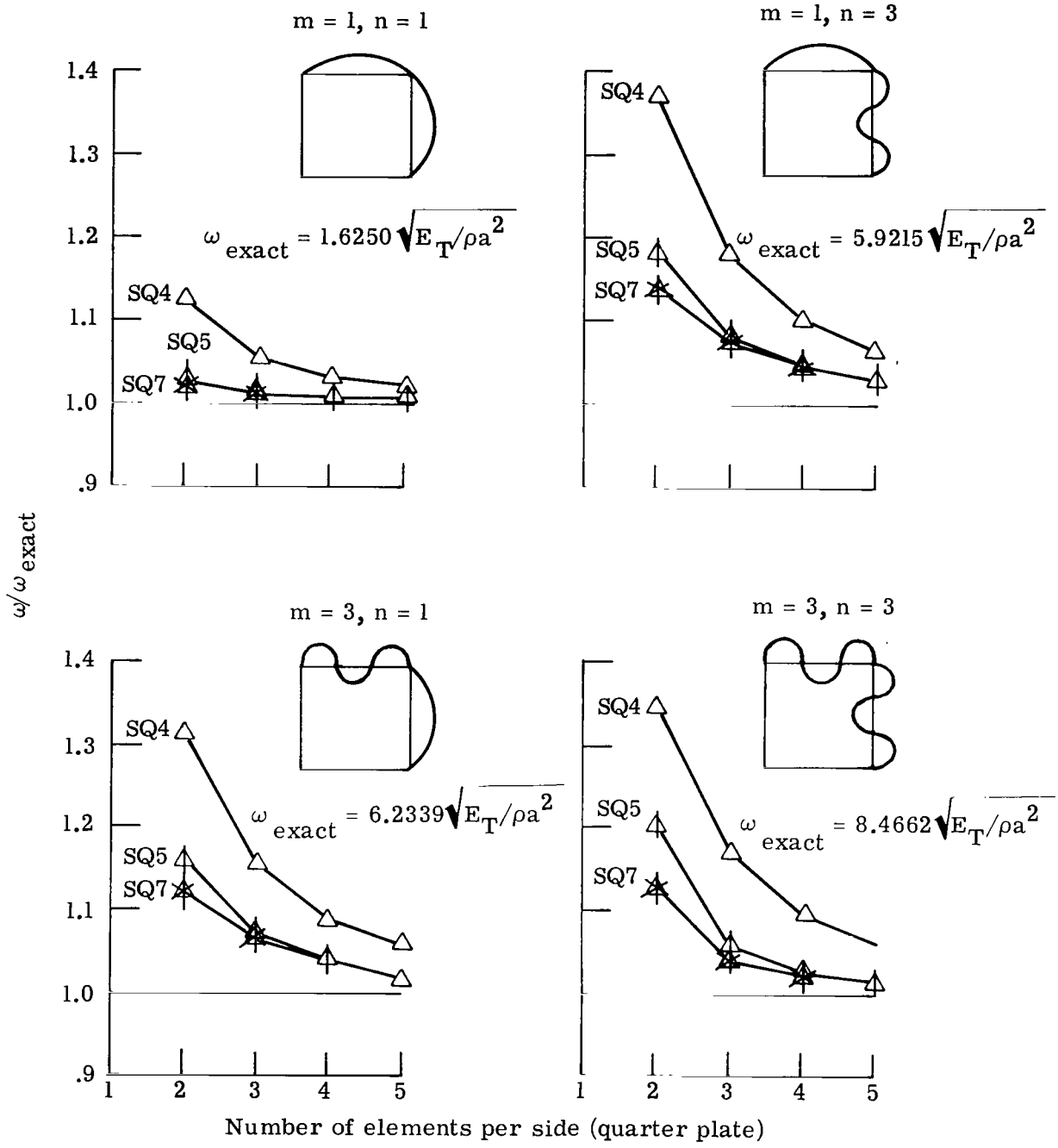

(a) $\frac{h}{a} = 0.1$; four-node quadrilaterals.

Figure 8.- Effect of internal degrees of freedom on accuracy and convergence of vibration frequencies. Simply supported, nine-layered, orthotropic square plate.

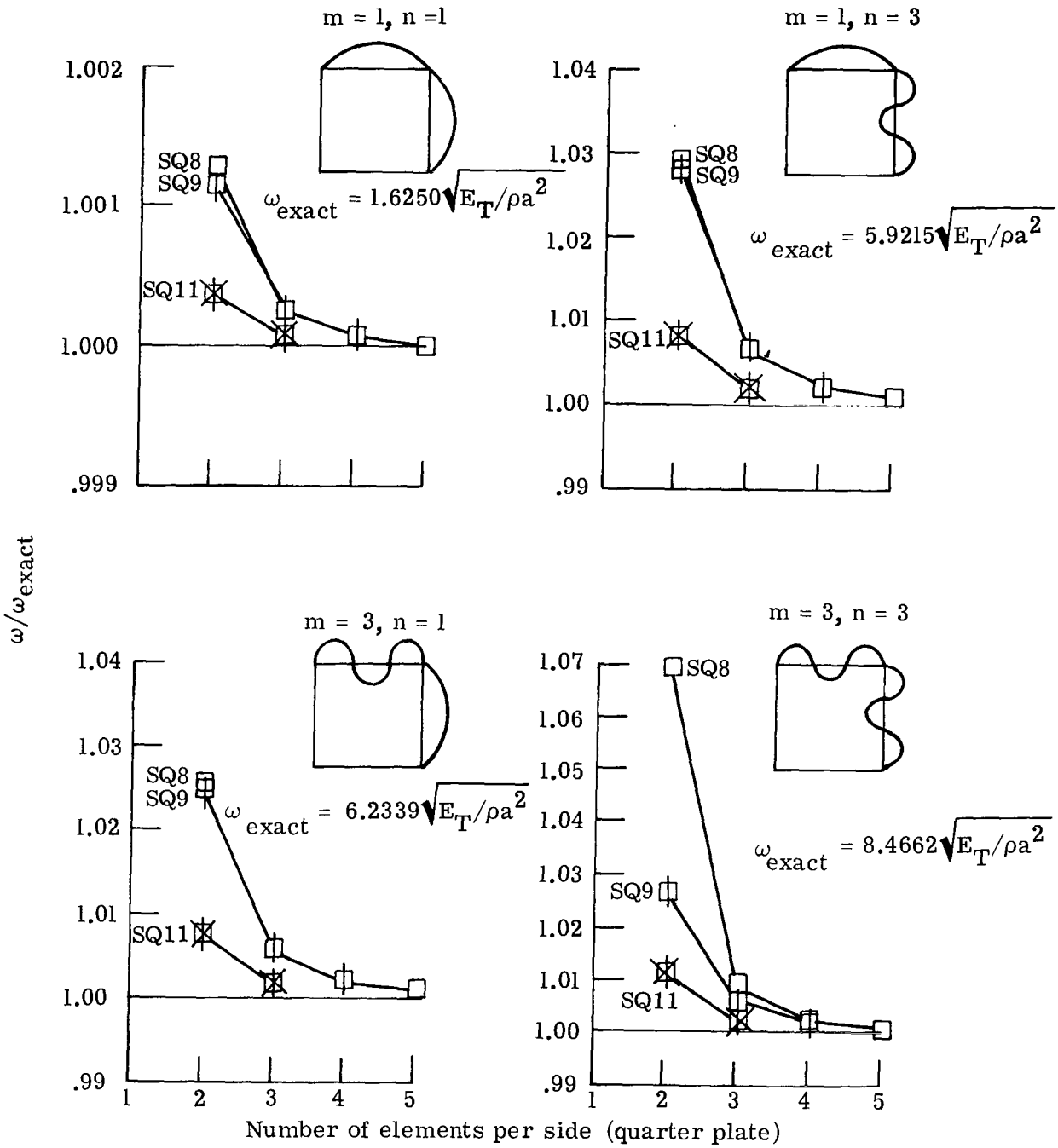

(b) $\frac{h}{a} = 0.1$; eight-node quadrilaterals.

Figure 8.- Continued.

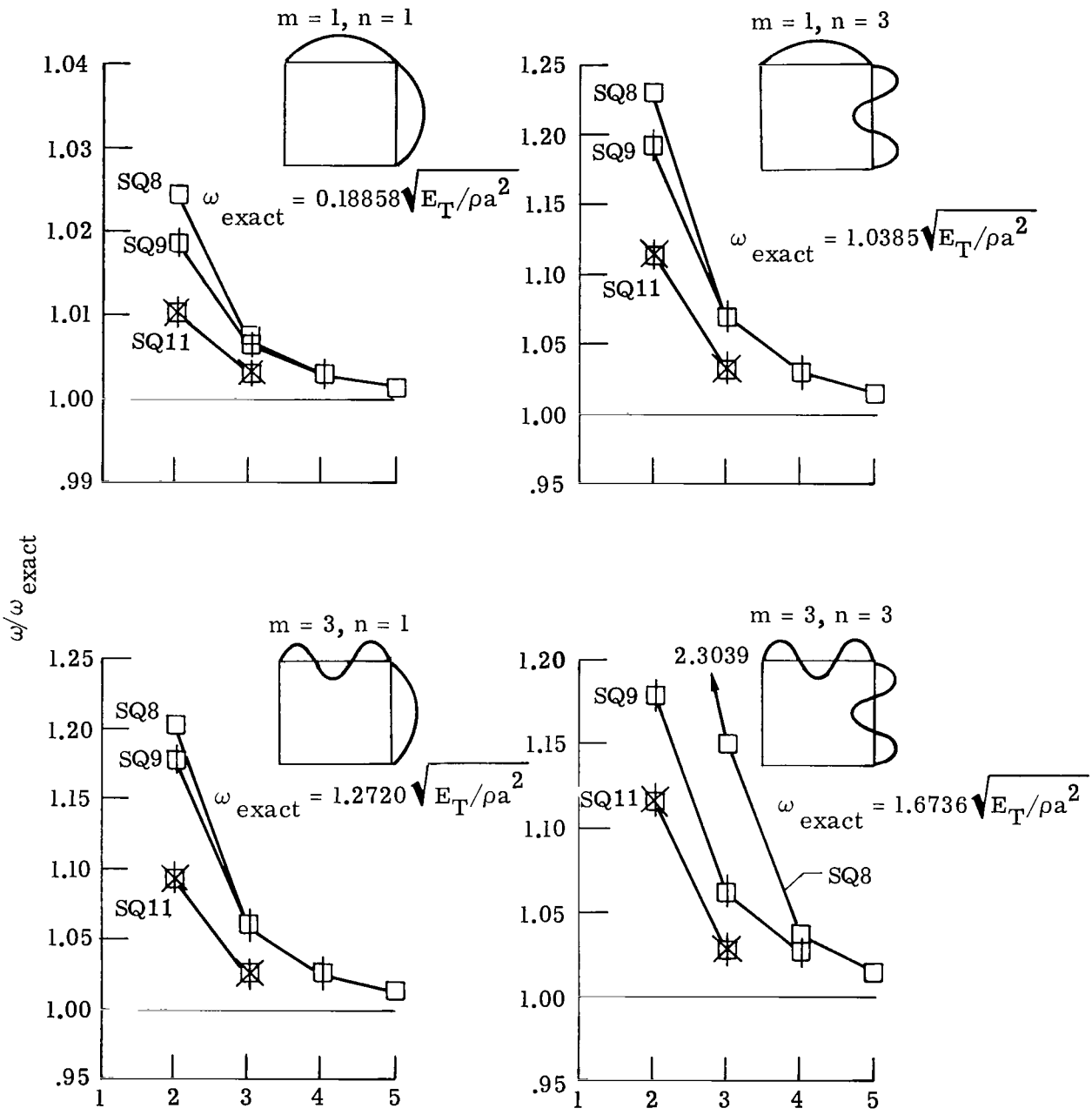

(c) $\frac{h}{a} = 0.01$; eight-node quadrilaterals.

Figure 8.- Concluded.

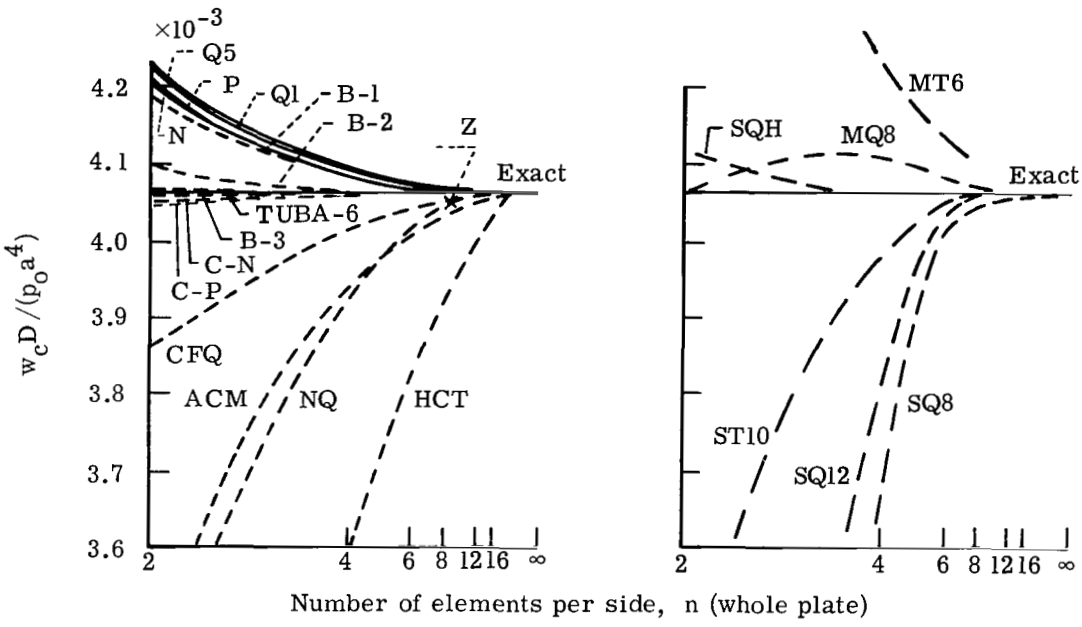

Number of elements per side, n (whole plate)

(a) w at center for previously developed classical-theory elements (ref. 11).

(b) w at center for present shear-flexible elements.

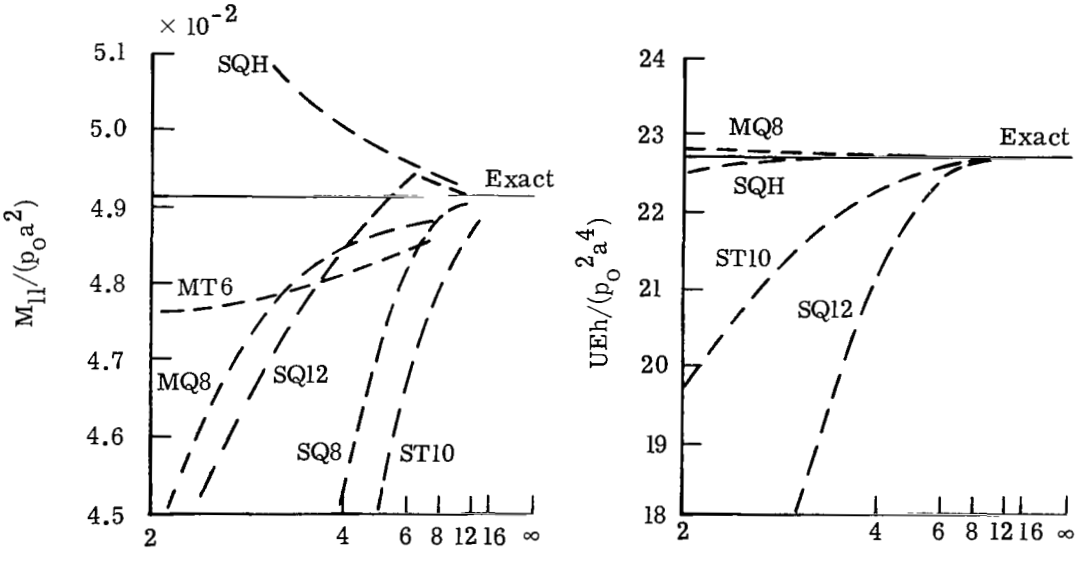

Number of elements per side, n (whole plate)

(c) M_{11} at center for present elements.

(d) Strain energy for present elements.

Figure 9.- Convergence of w, M_{11}, and U with grid size for shear-flexible elements of present study and some previously developed classical-theory elements (ref. 11).

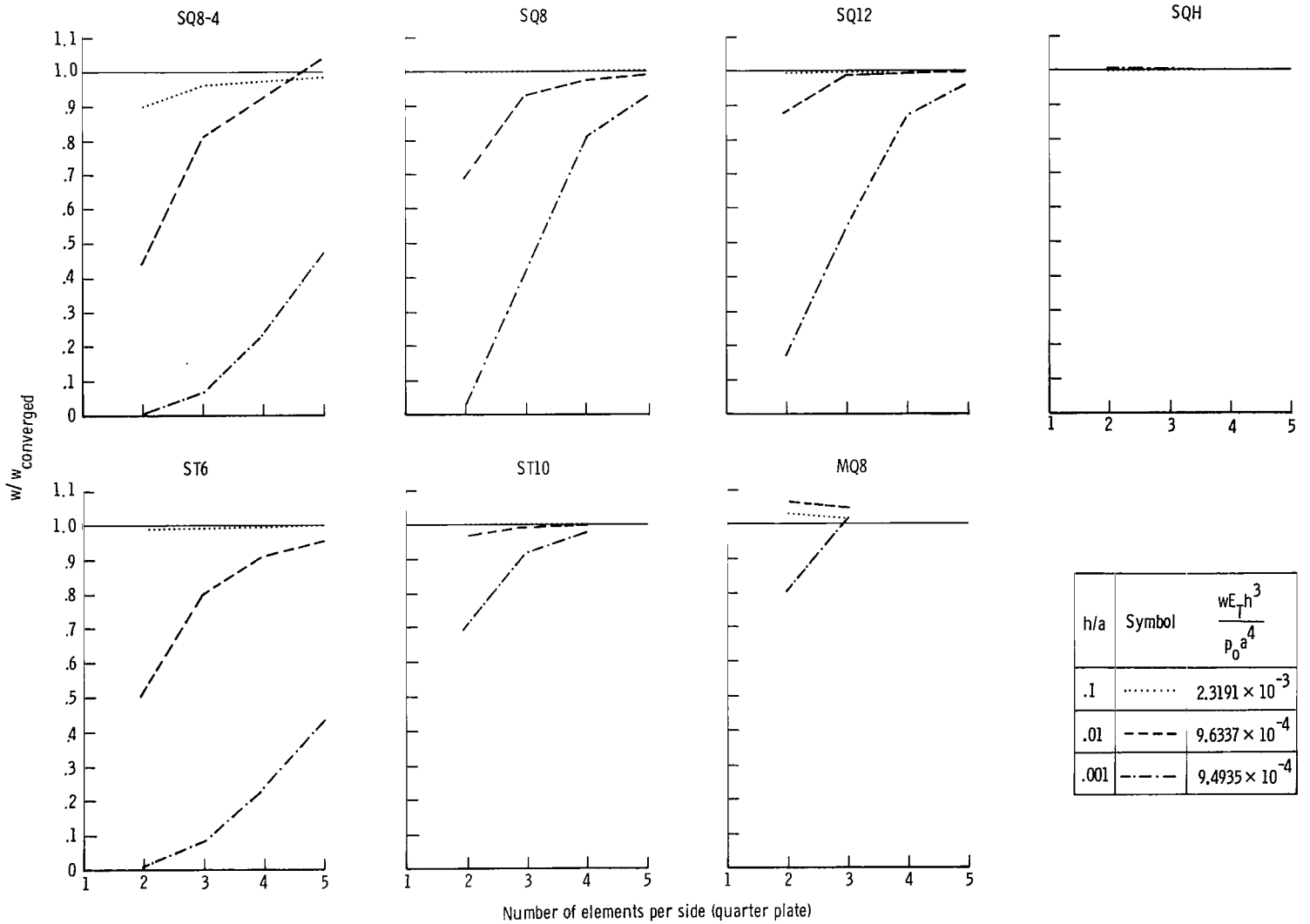

(a) Transverse displacement w at center.

Figure 10.- Effect of h/a on convergence of bending-moment resultant M_{11} and transverse displacement w obtained by different stiffness and mixed models. Clamped, nine-layered, orthotropic square plate.

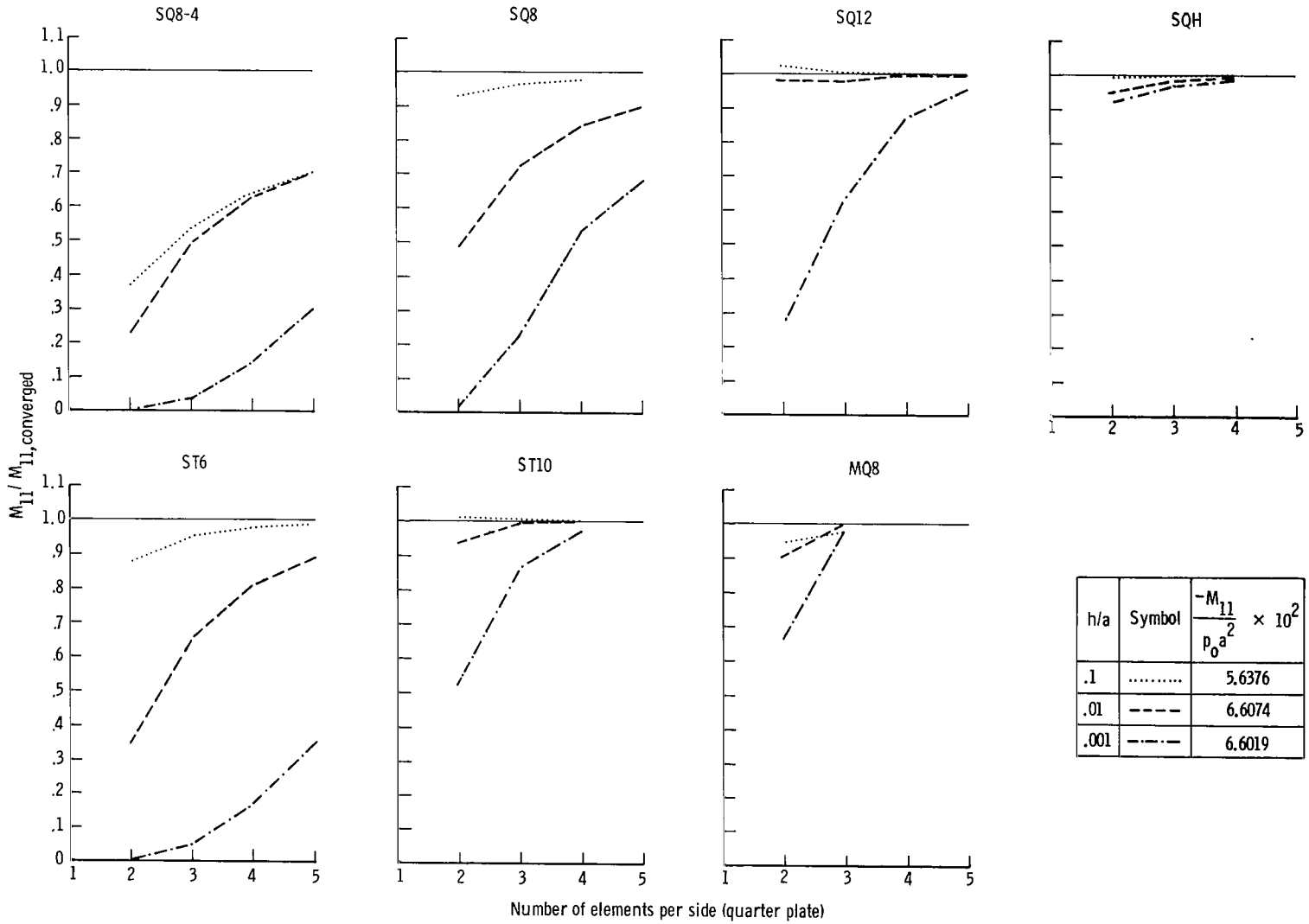

(b) Maximum bending-moment resultant M_{11} at edge.

Figure 10.- Concluded.

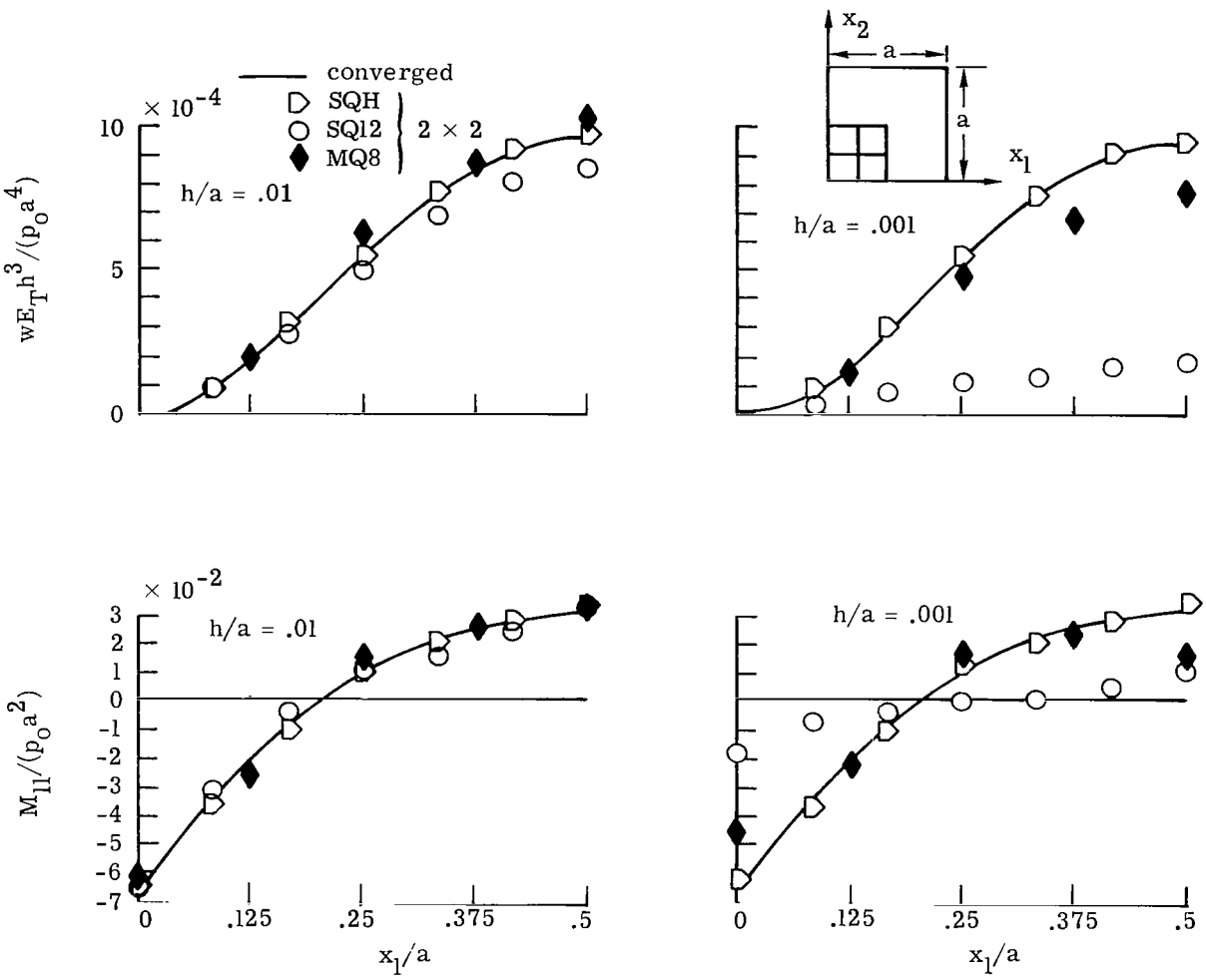

Figure 11.- Distribution of transverse displacement w and bending-moment resultant M_{11} along $x_2 = \frac{a}{2}$. Clamped, nine-layered, orthotropic square plate. $\frac{h}{a} = 0.01$ and 0.001.

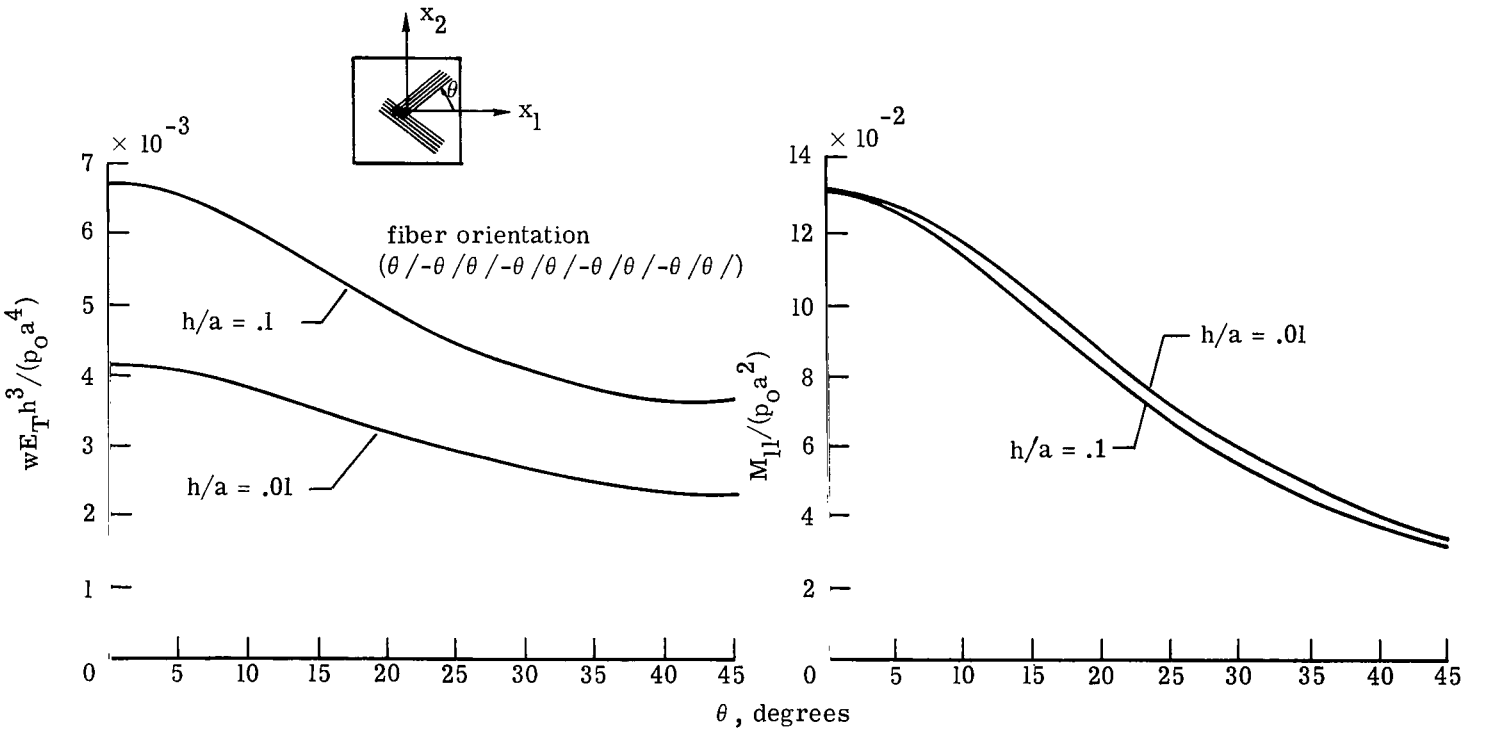

(a) Transverse displacement w at center of plate.

(b) Bending-moment resultant M_{11} at center of plate.

Figure 12.- Effect of fiber orientation on response of simply supported, nine-layered, square anisotropic plate subjected to uniform normal pressure loading.

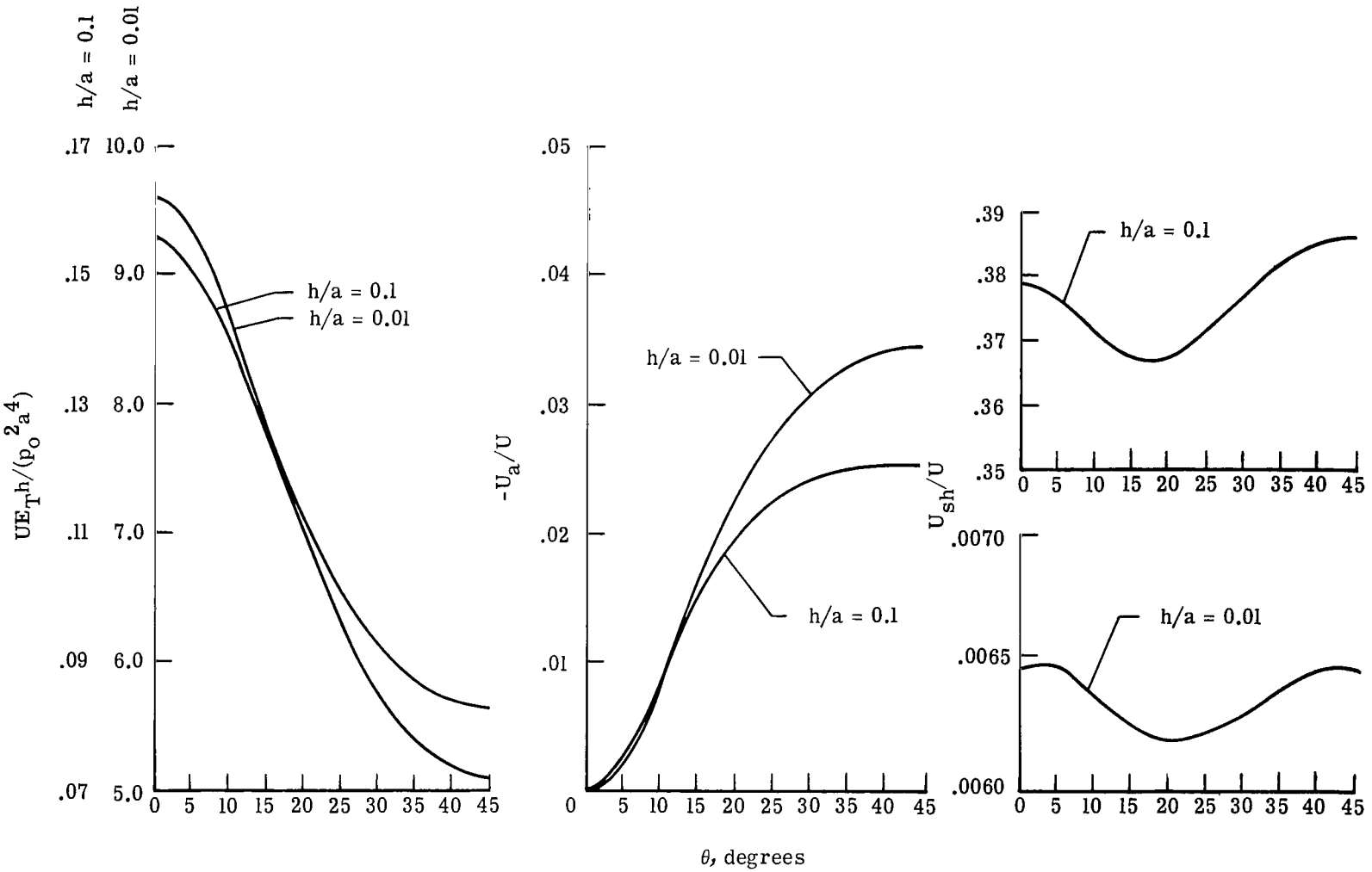

(c) Strain energy and measures of shear deformation and degree of anisotropy in plate as a function of fiber orientation.

Figure 12.- Concluded.

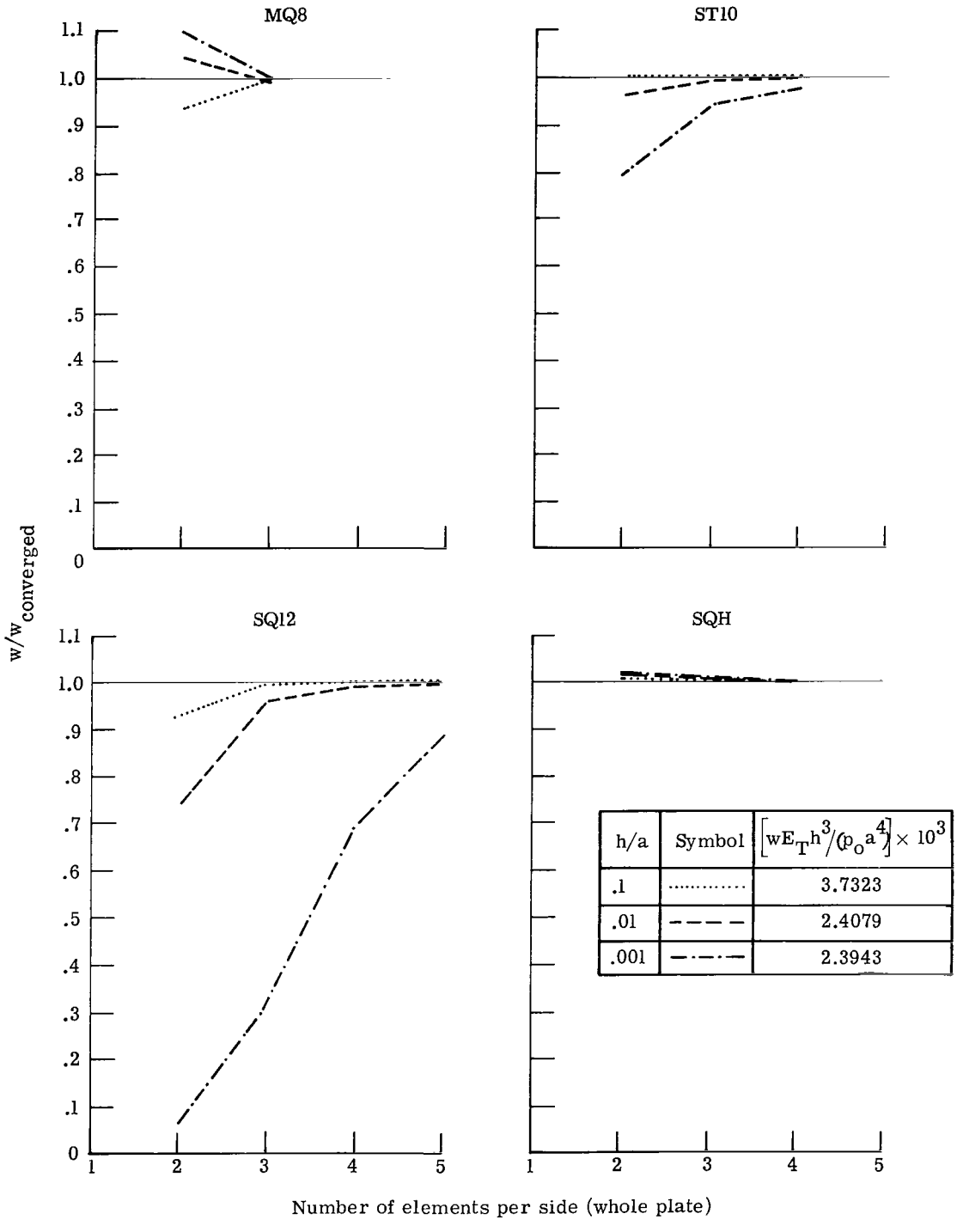

(a) Transverse displacement w at center.

Figure 13.- Effect of h/a on convergence of bending-moment resultant M_{11}, transverse displacement w, and strain energy U obtained by higher order stiffness and mixed models. Simply supported, nine-layered, anisotropic square plate (45/-45/45/-45/45/-45/45/-45/45).

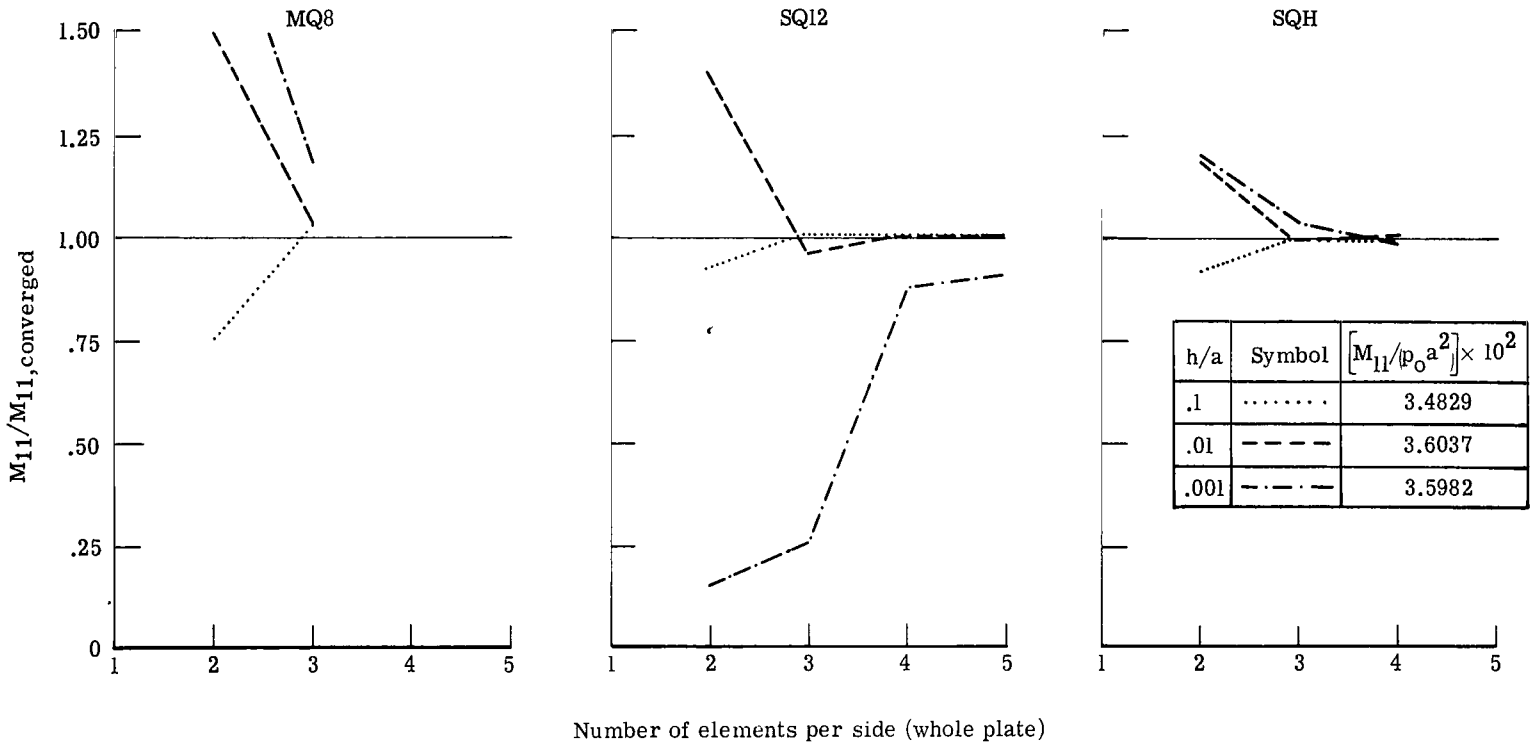

(b) Bending-moment resultant M_{11} at center.

Figure 13.- Continued.

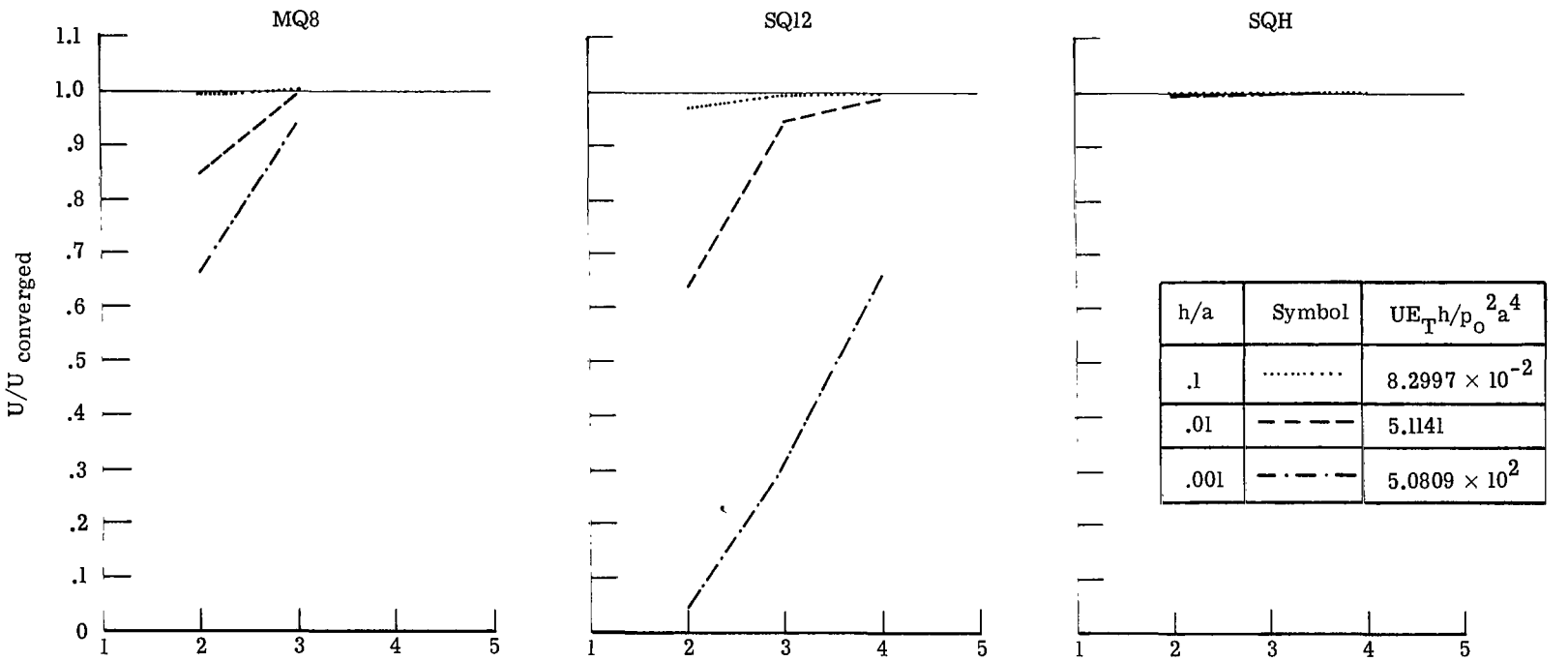

(c) Strain energy U in plate.

Figure 13.- Concluded.

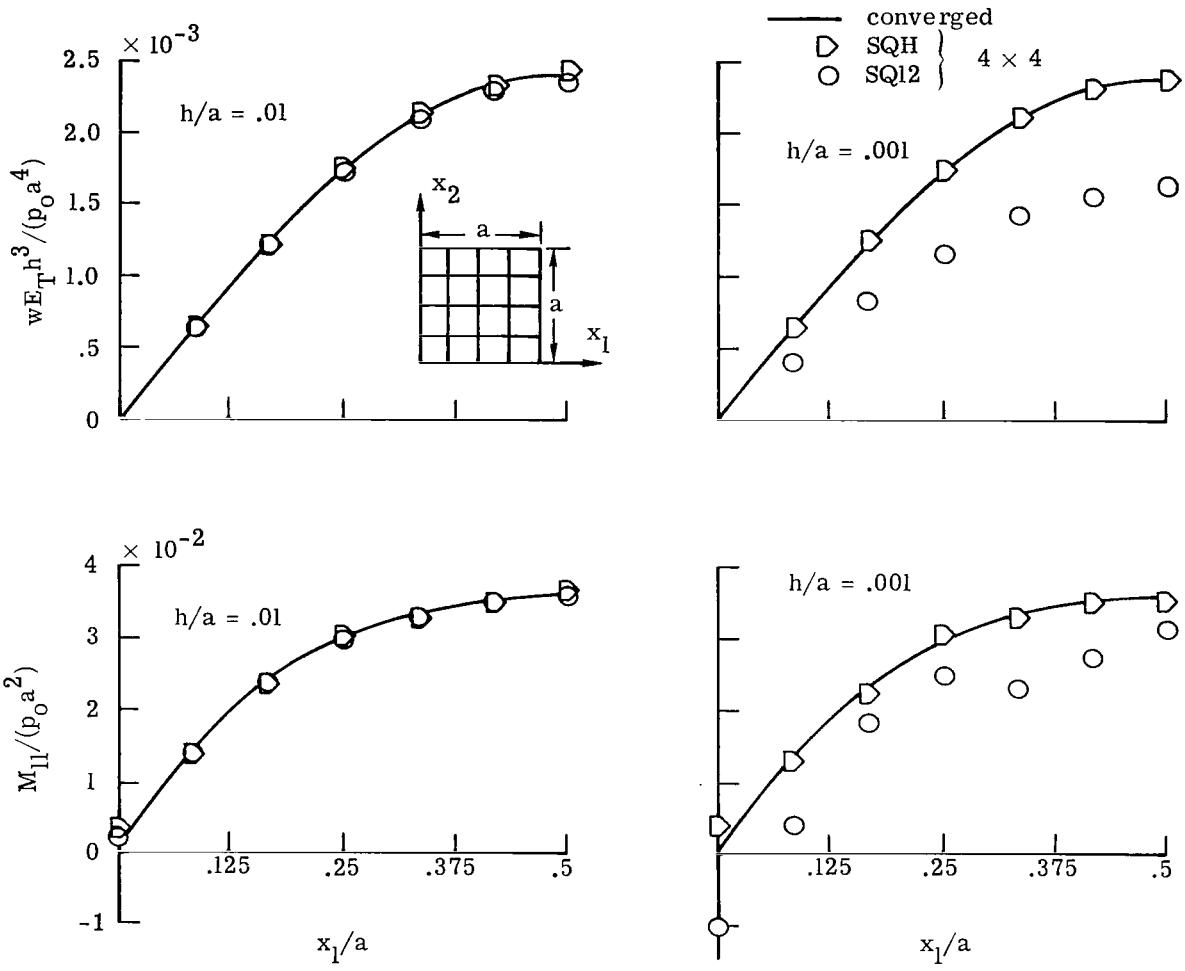

Figure 14.- Distribution of transverse displacement w and bending-moment resultant M_{11} along $x_2 = \frac{a}{2}$. Simply supported, nine-layered, anisotropic square plate. $\frac{h}{a} = 0.01$ and 0.001.

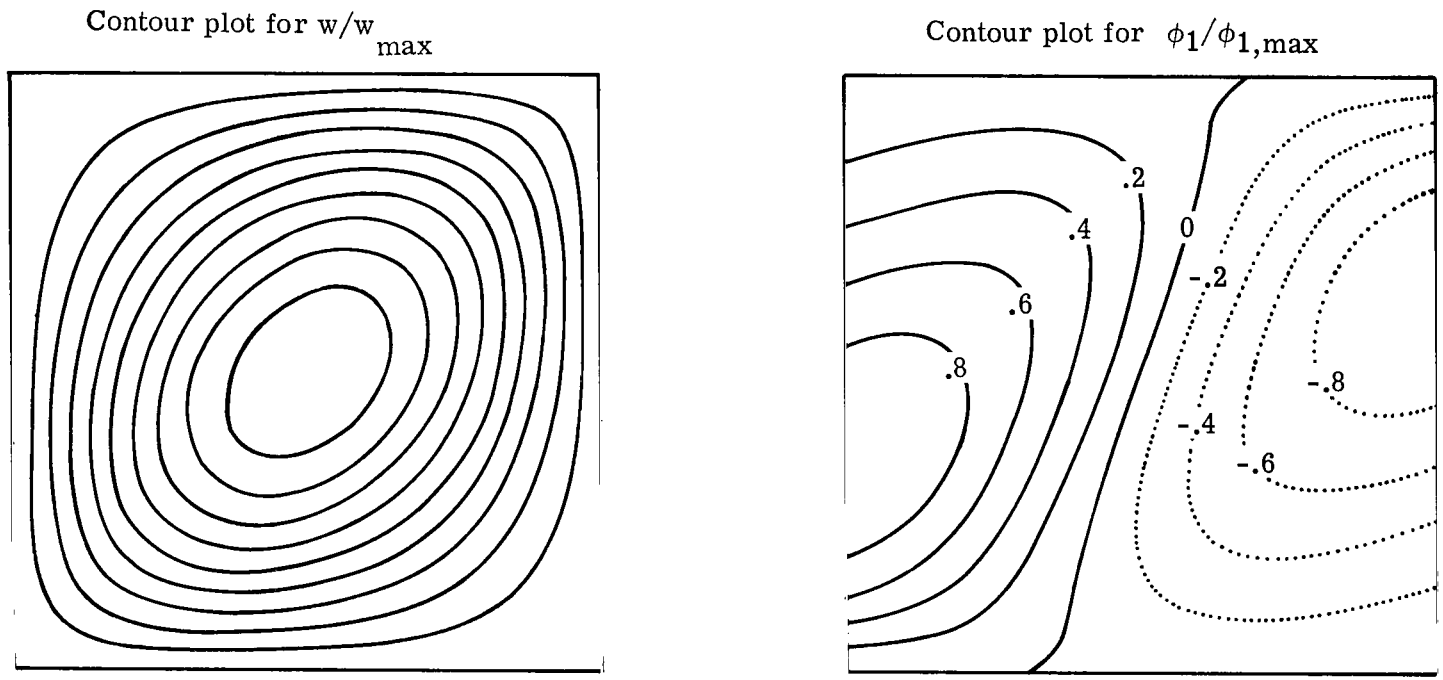

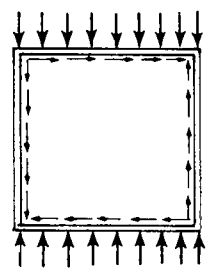

Fiber orientation (90/0/-45/45/45/-45/0/90)

E_L/E_T= 21.77

ν_{LT} = .25

G_{LT}/E_T= .63

G_{TT}/E_T = .49

Figure 15.- Buckling mode shapes for laminated anisotropic plate subjected to combined compressive and shear edge loadings.

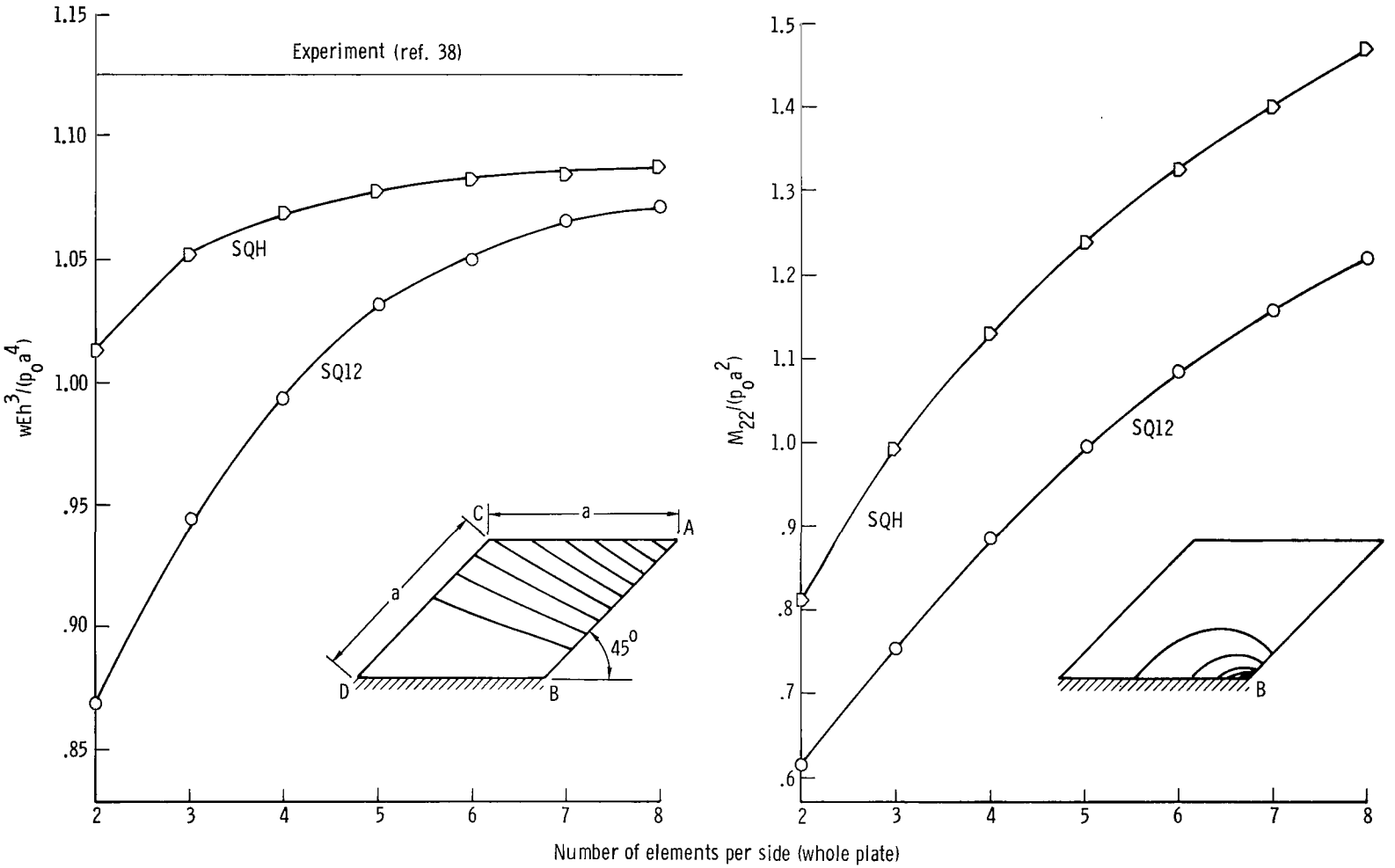

(a) Transverse displacement w at point A.

(b) Bending-moment resultant M_{22} at point B.

Figure 16.- Convergence of maximum transverse displacement w and bending-moment resultant M_{22} obtained by higher order stiffness models. Cantilevered isotropic skew plate under uniform loading.

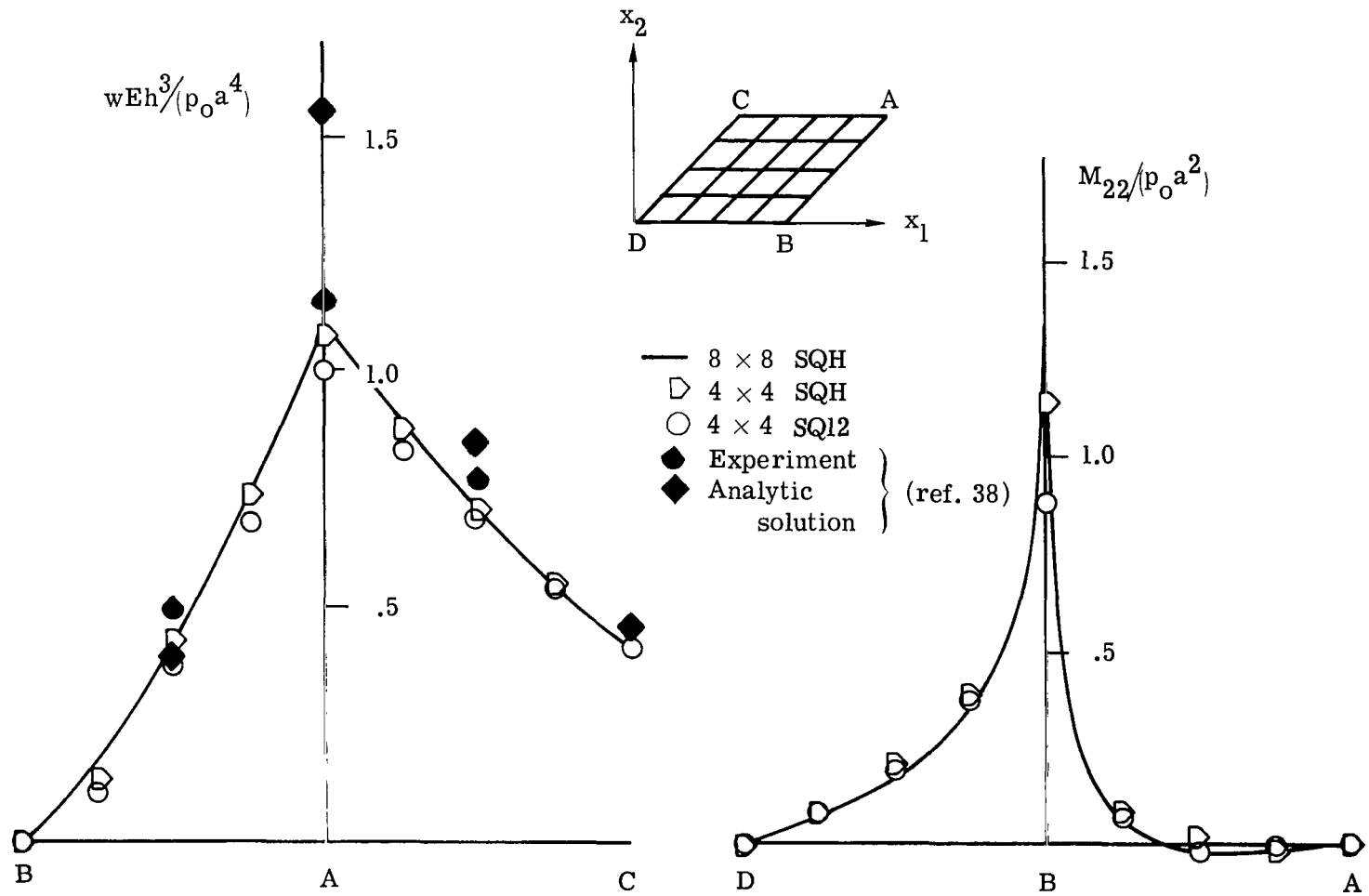

(c) Distribution of w along BAC.

(d) Distribution of M_{22} along DBA.

Figure 16.- Concluded.

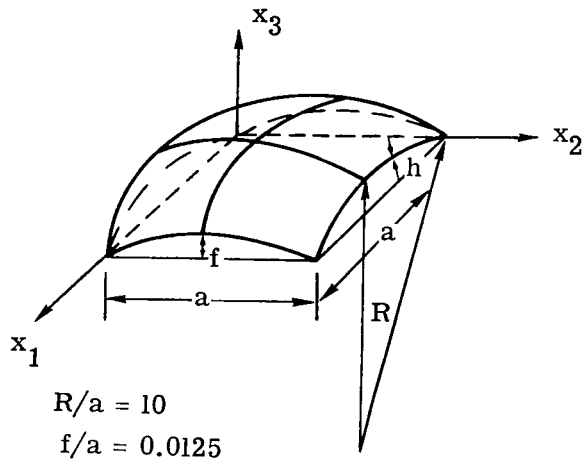

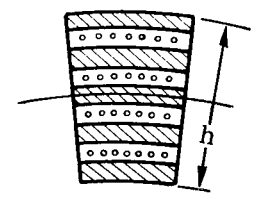

$E_L/E_T = 40$

$G_{LT}/E_T = 0.60$

$G_{TT}/E_T = 0.50$

$\nu_{LT} = 0.25$

Figure 17.- Characteristics of laminated graphite-epoxy shallow shells used in present study.

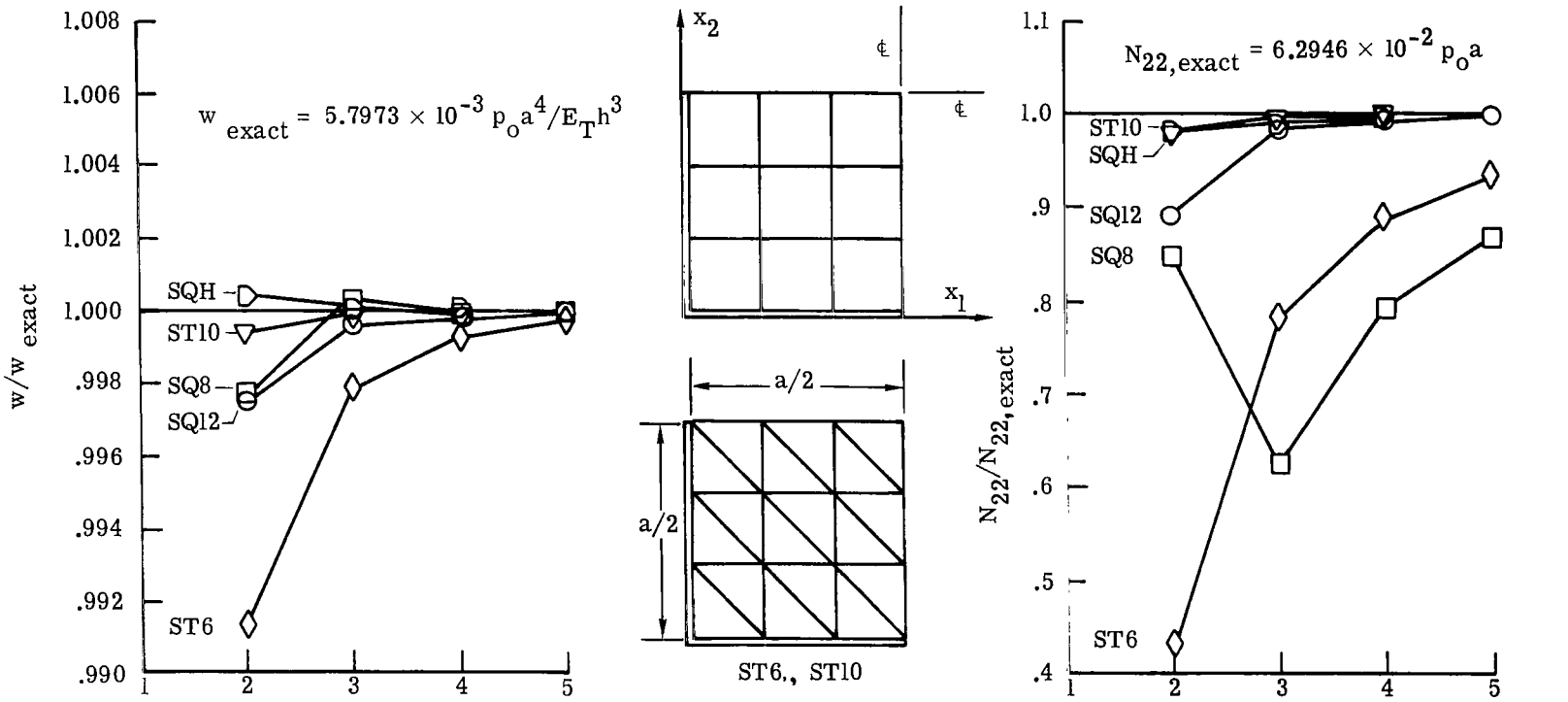

(a) w at center.

(b) N_{22} at center.

Figure 18.- Convergence of stress resultants, transverse displacement and strain energy with grid refinement. Simply supported, nine-layered, orthotropic shallow spherical segment subjected to uniform loading. $\frac{h}{a} = 0.1$.

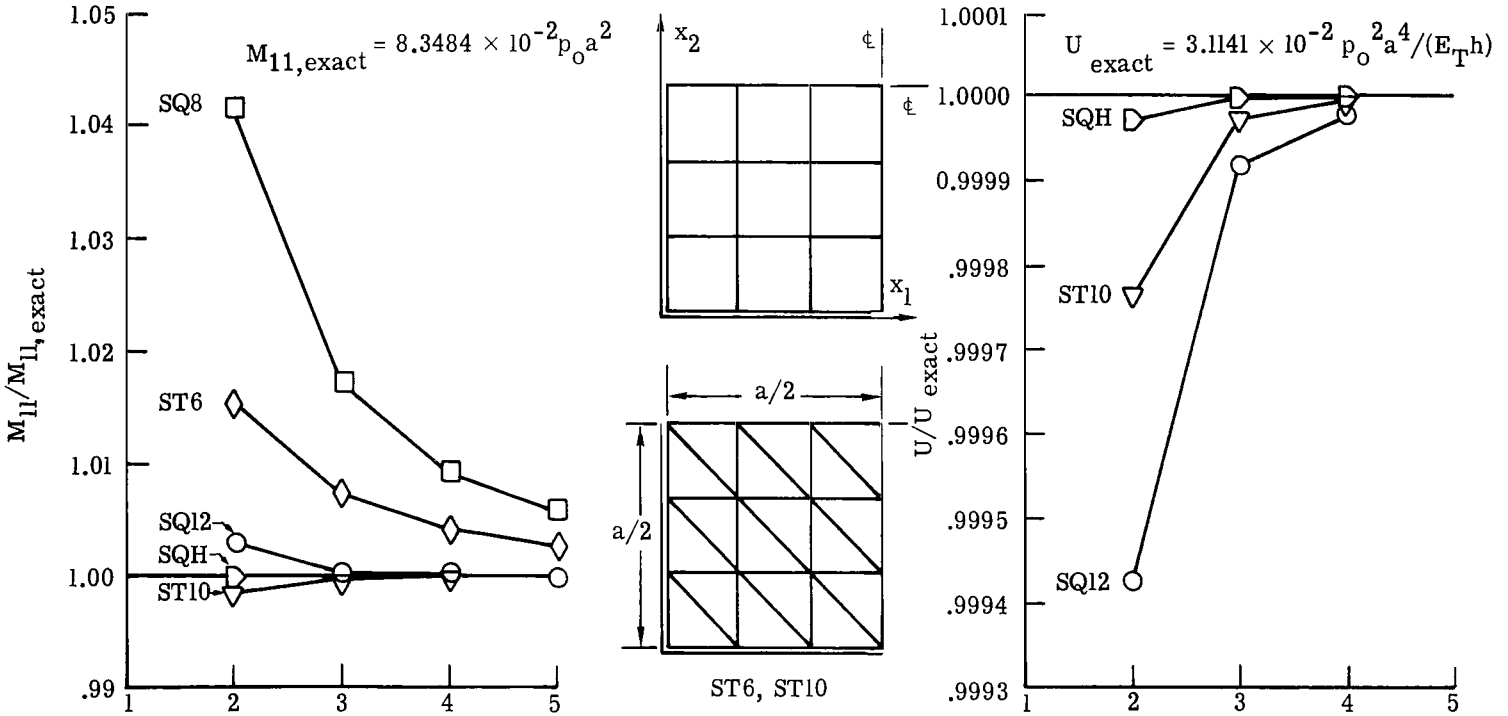

(c) M_{11} at center.

(d) Strain energy U in one-quarter of shell.

Figure 18.- Concluded.

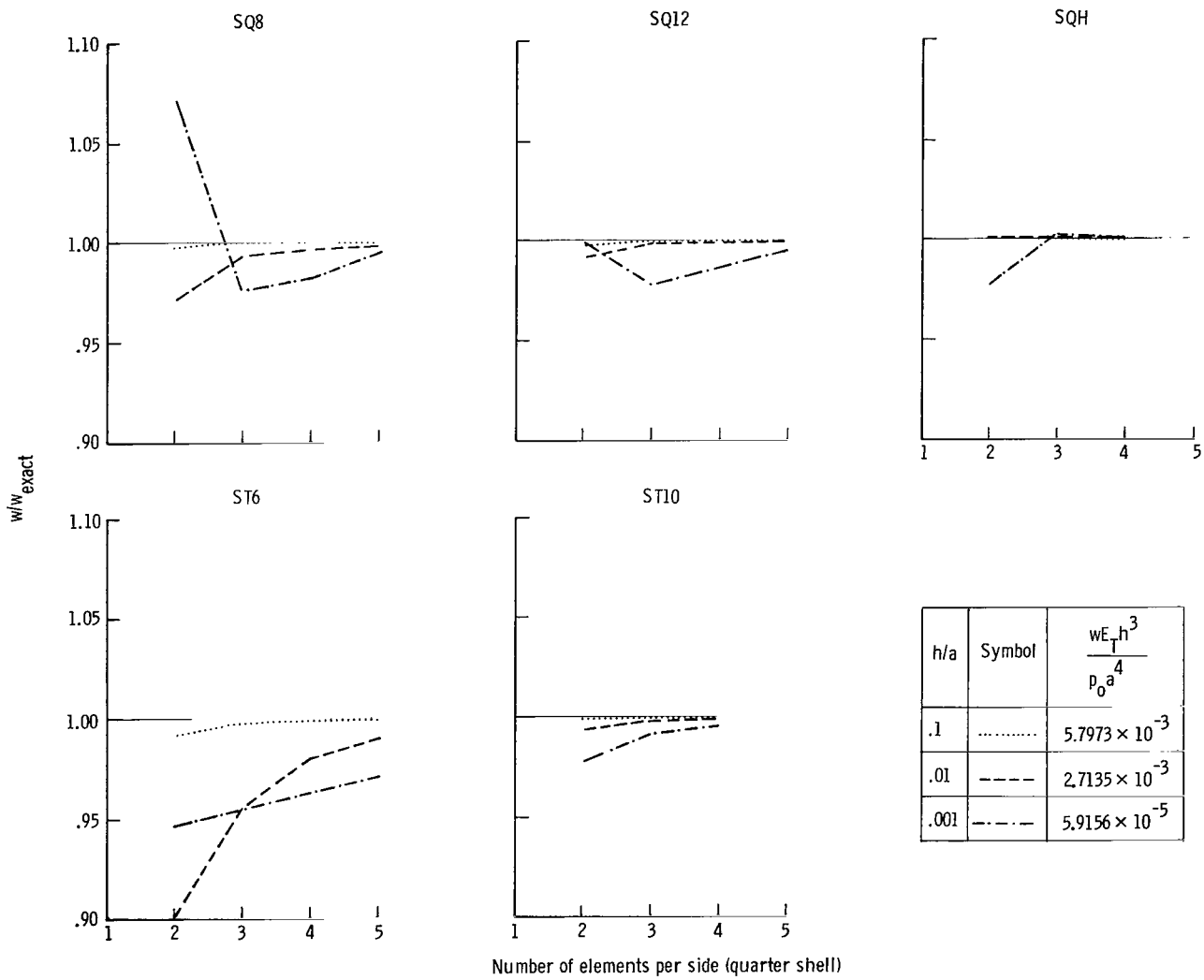

(a) Transverse displacement w at center.

Figure 19.- Effect of h/a on convergence of transverse displacement, stress resultants, and strain energy obtained by different stiffness models. Simply supported, nine-layered, orthotropic shallow-spherical segment.

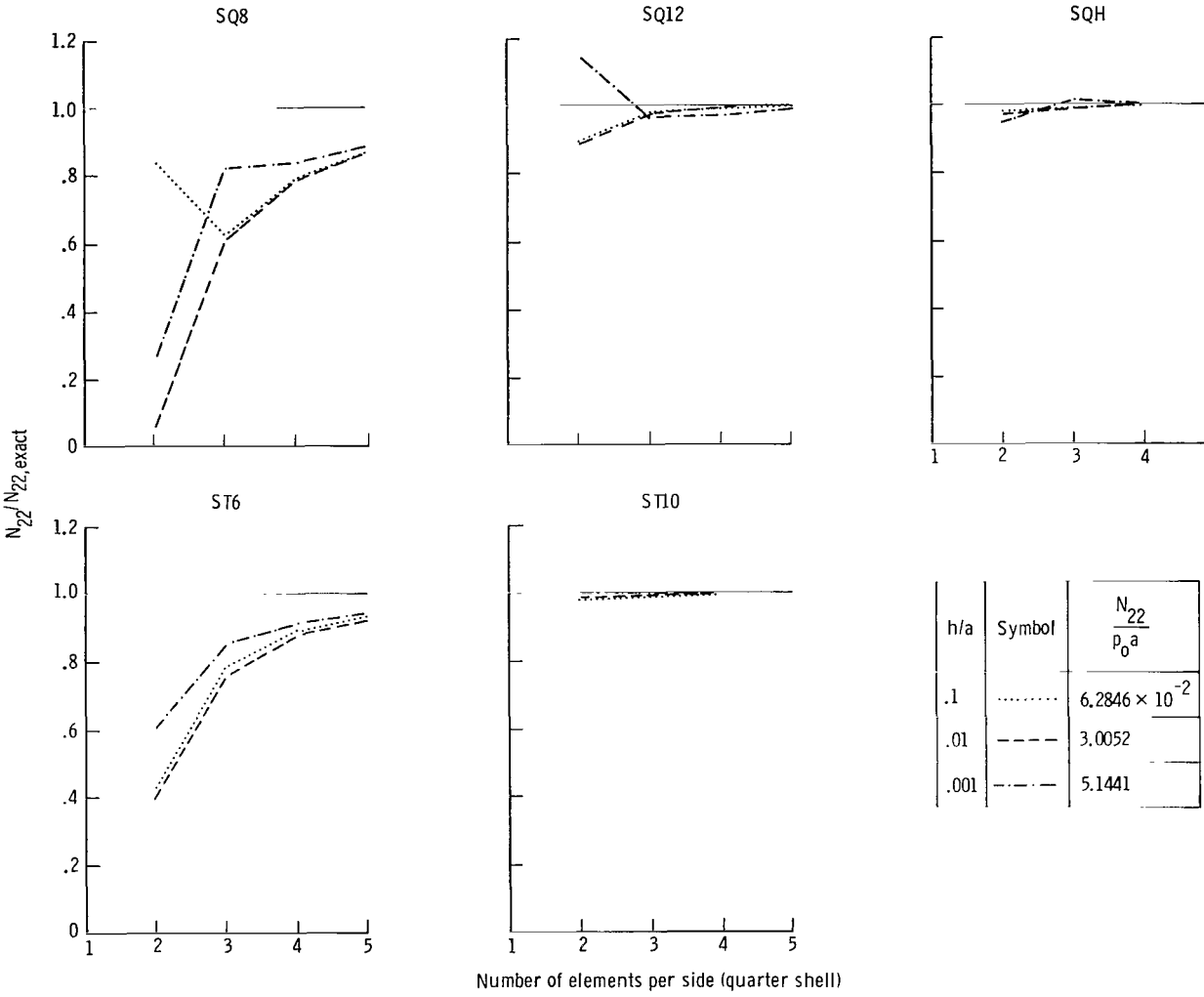

(b) Membrane stress resultant N_{22} at center.

Figure 19.- Continued.

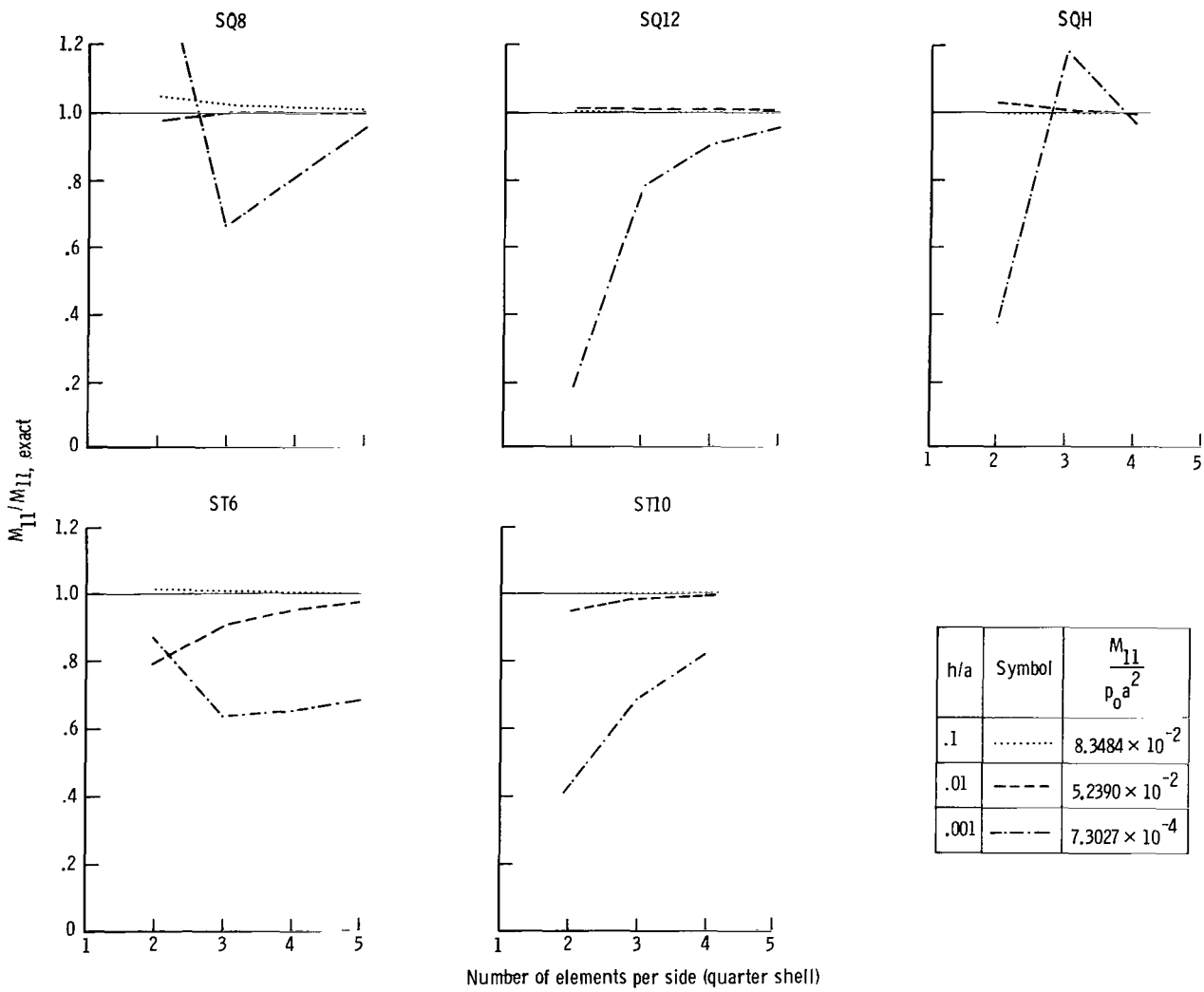

(c) Bending-moment resultant M_{11} at center.

Figure 19.- Continued.

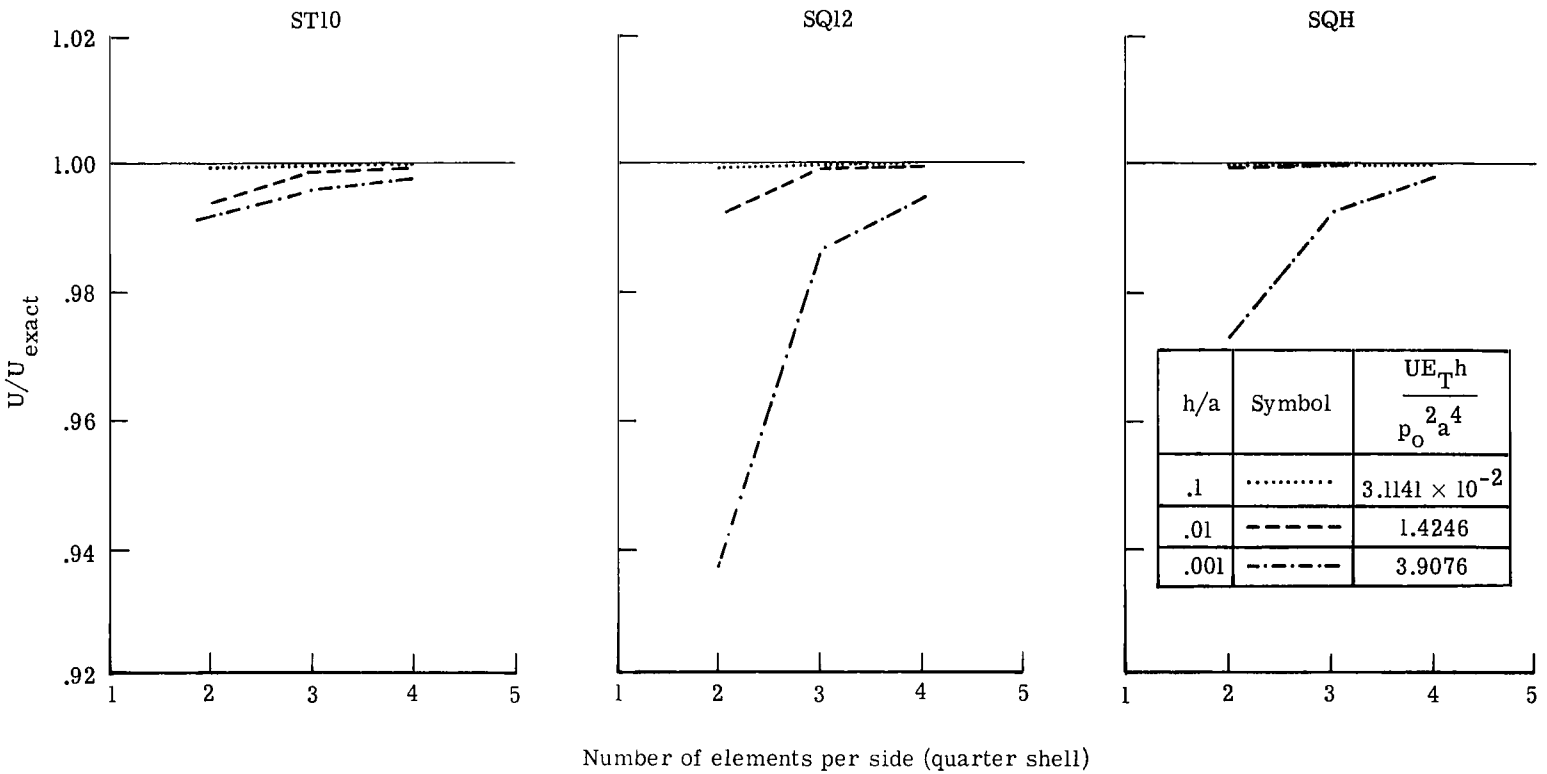

(d) Strain energy U in one-quarter of shell.

Figure 19.- Concluded.

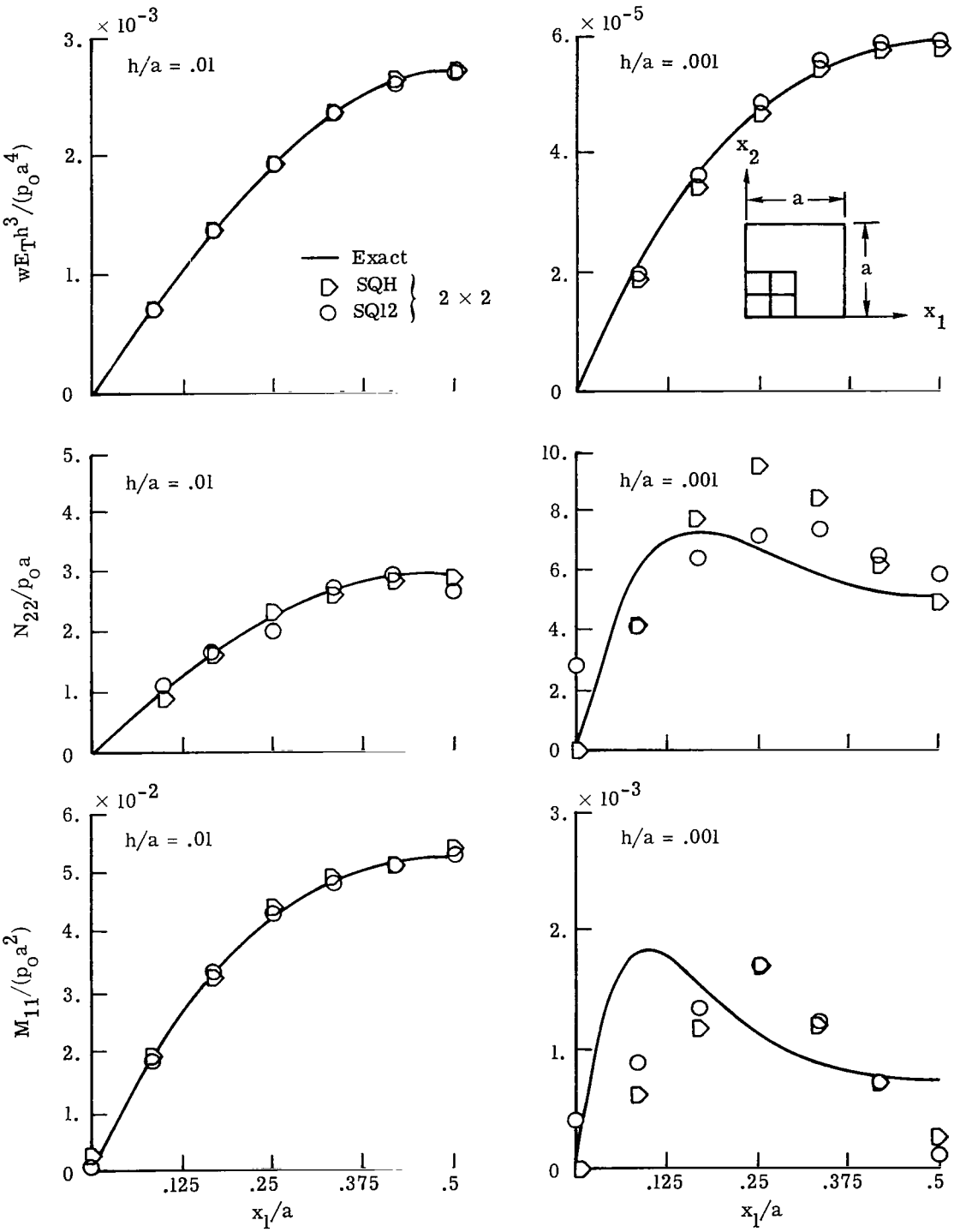

Figure 20.- Distribution of transverse displacement and stress resultants along center lines. Simply supported, nine-layered, orthotropic spherical segments. $\frac{h}{a}$ = 0.01 and 0.001.

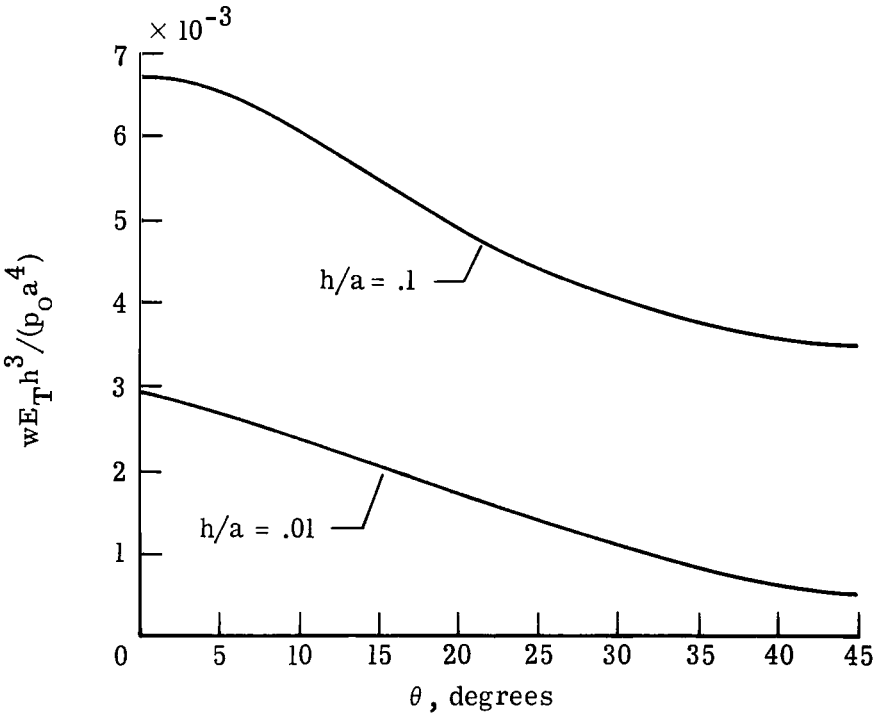

(a) Transverse displacement w at center of shell.

Figure 21.- Effect of fiber orientation on response of a simply supported nine-layered, anisotropic spherical segment with a square planform subjected to uniform loading.

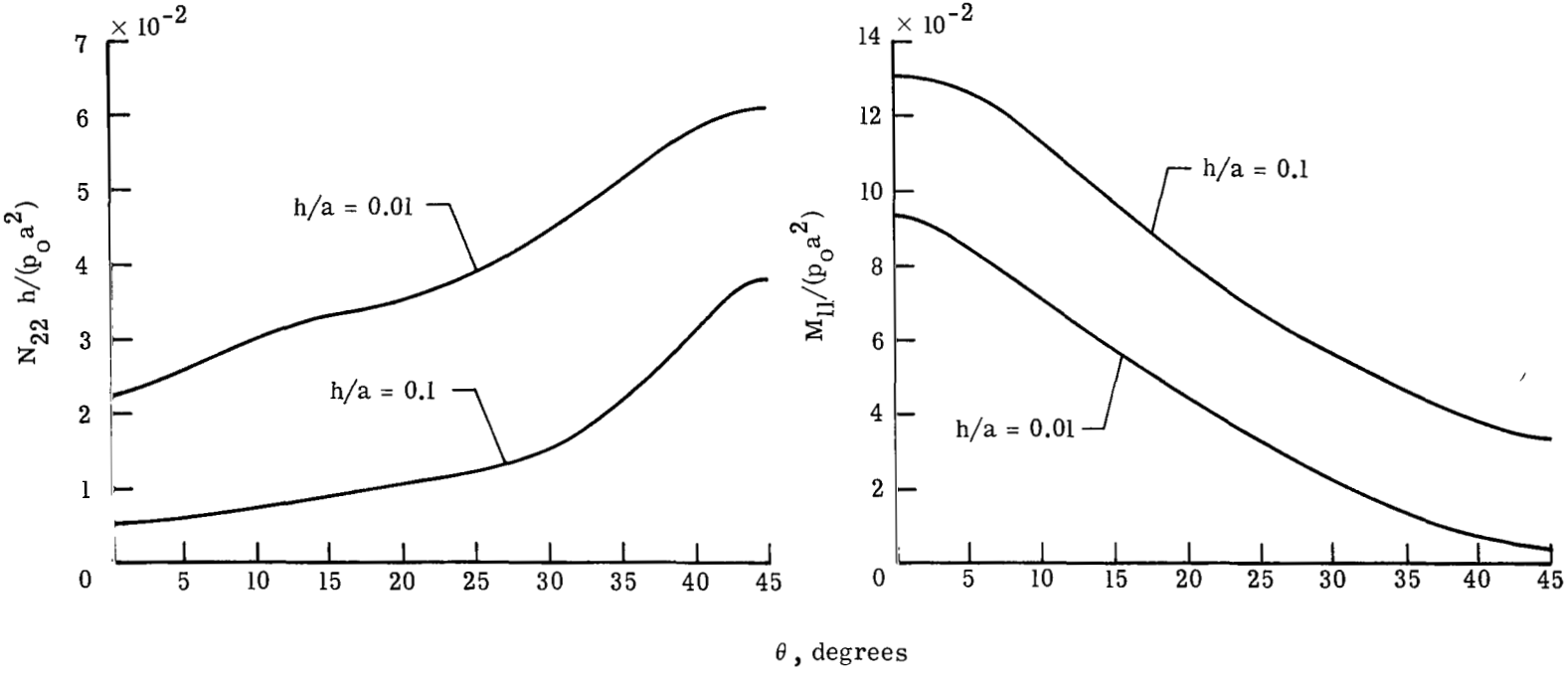

(b) Maximum membrane stress resultant N_{22} at center of shell.

(c) Maximum bending-moment resultant M_{11} at center of shell.

Figure 21.- Continued.

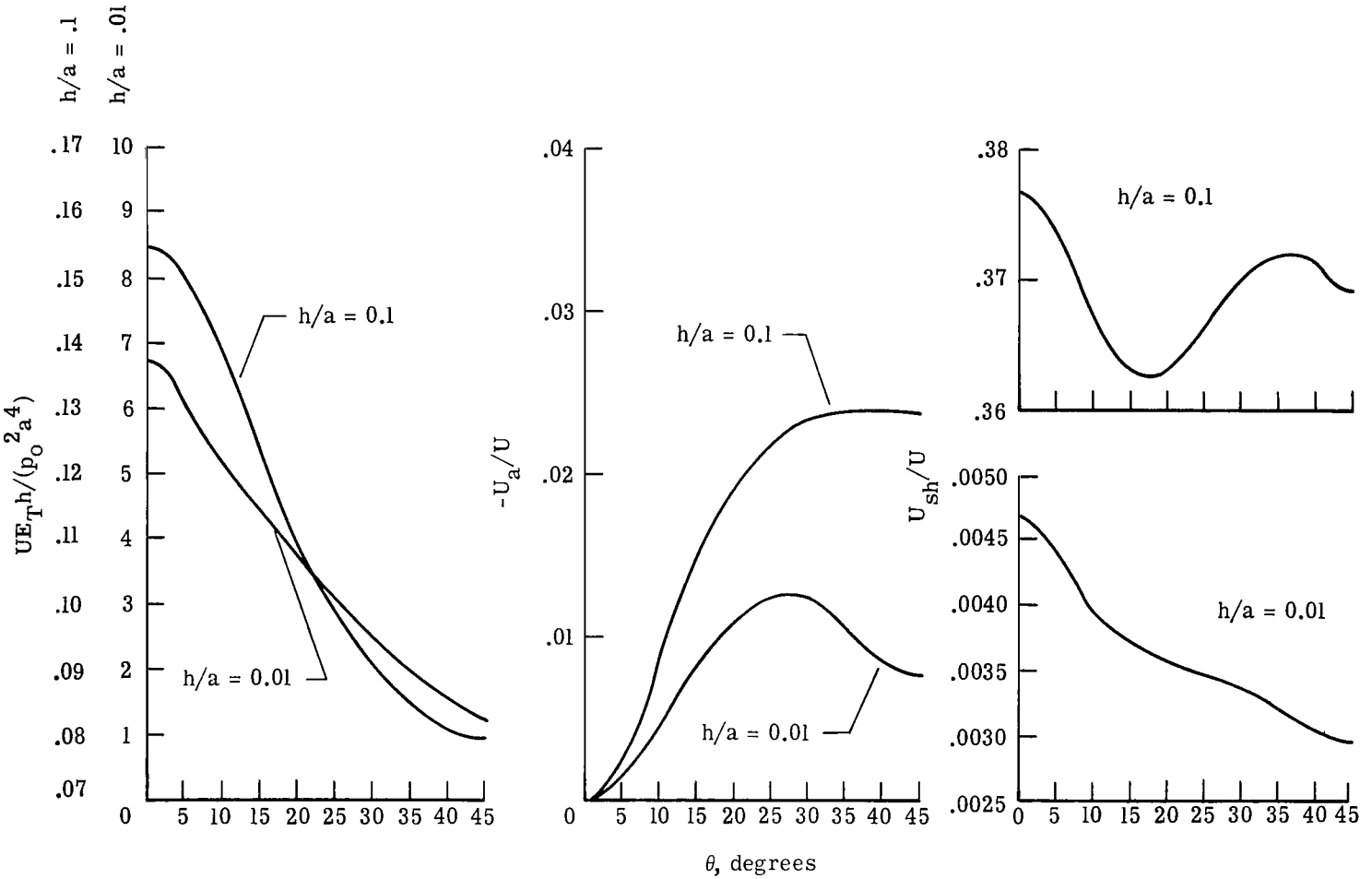

(d) Strain energy and measures of shear deformation and degree of anisotropy in shell as a function of fiber orientation.

Figure 21.- Concluded.

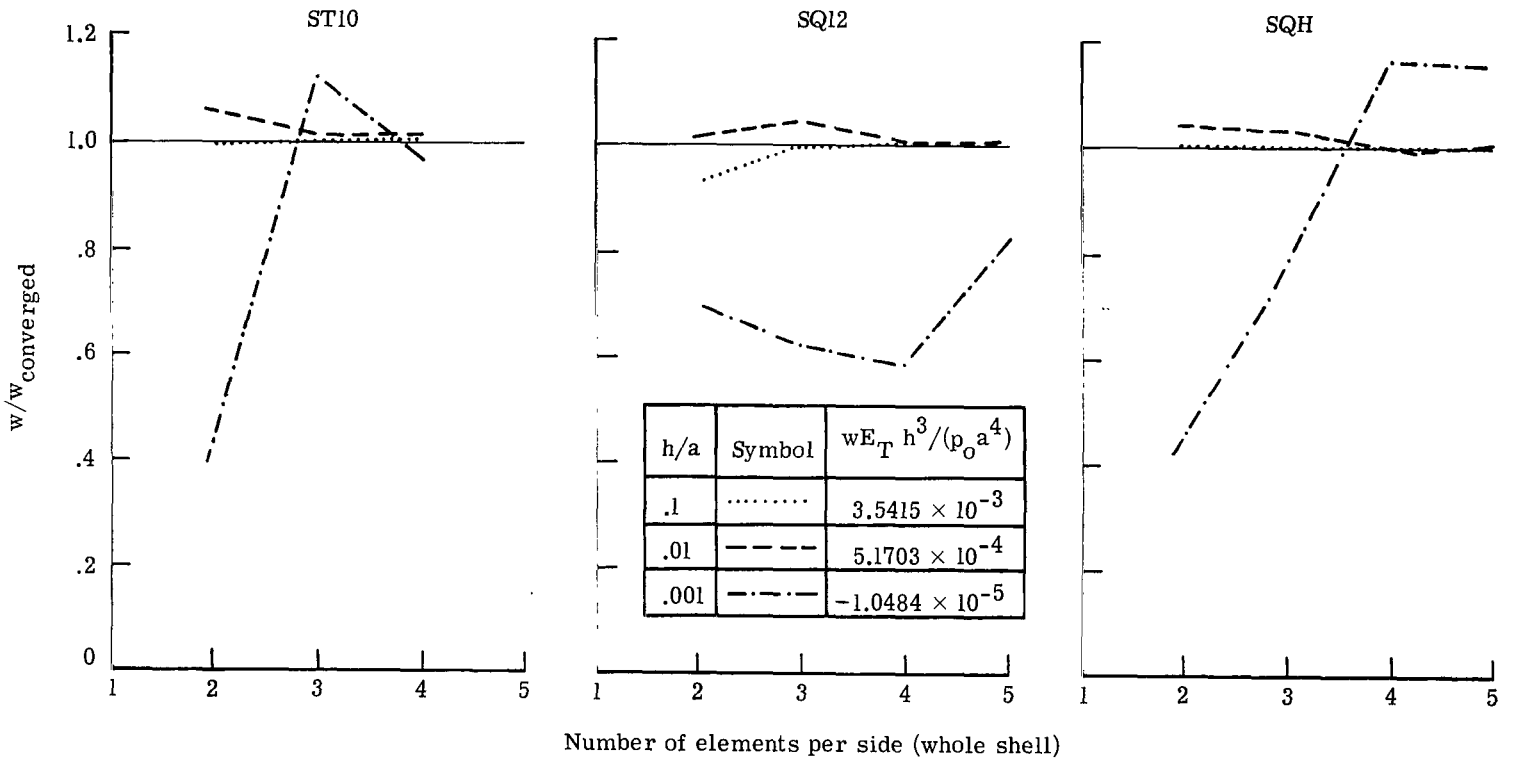

(a) w at center of shell.

Figure 22.- Effect of h/a on convergence of displacement and strain energy obtained by different stiffness models. Simply supported, nine-layered, anisotropic spherical segment with fiber orientation (45/-45/45/-45/45/-45/45/-45/45).

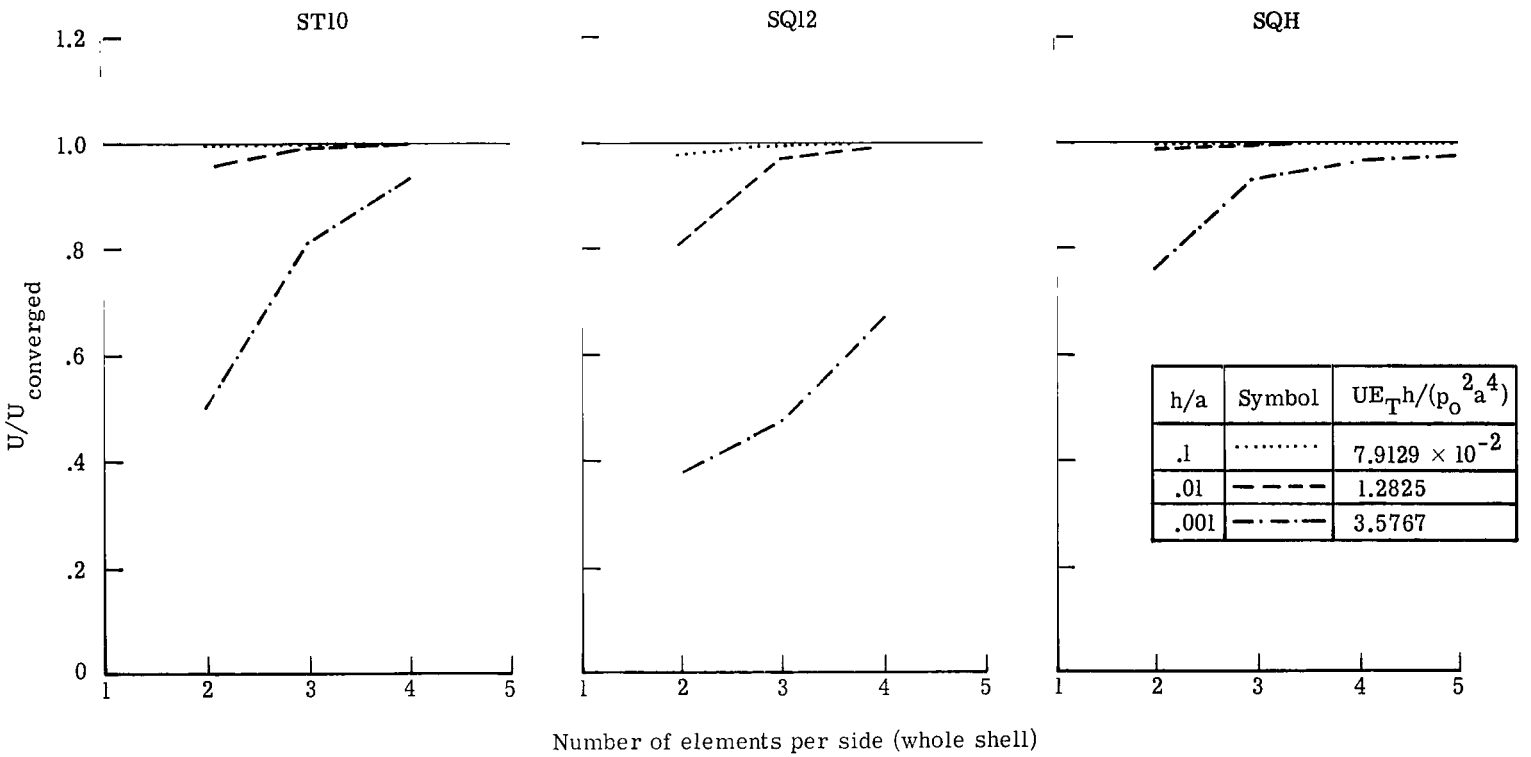

(b) Strain energy in shell.

Figure 22.- Concluded.

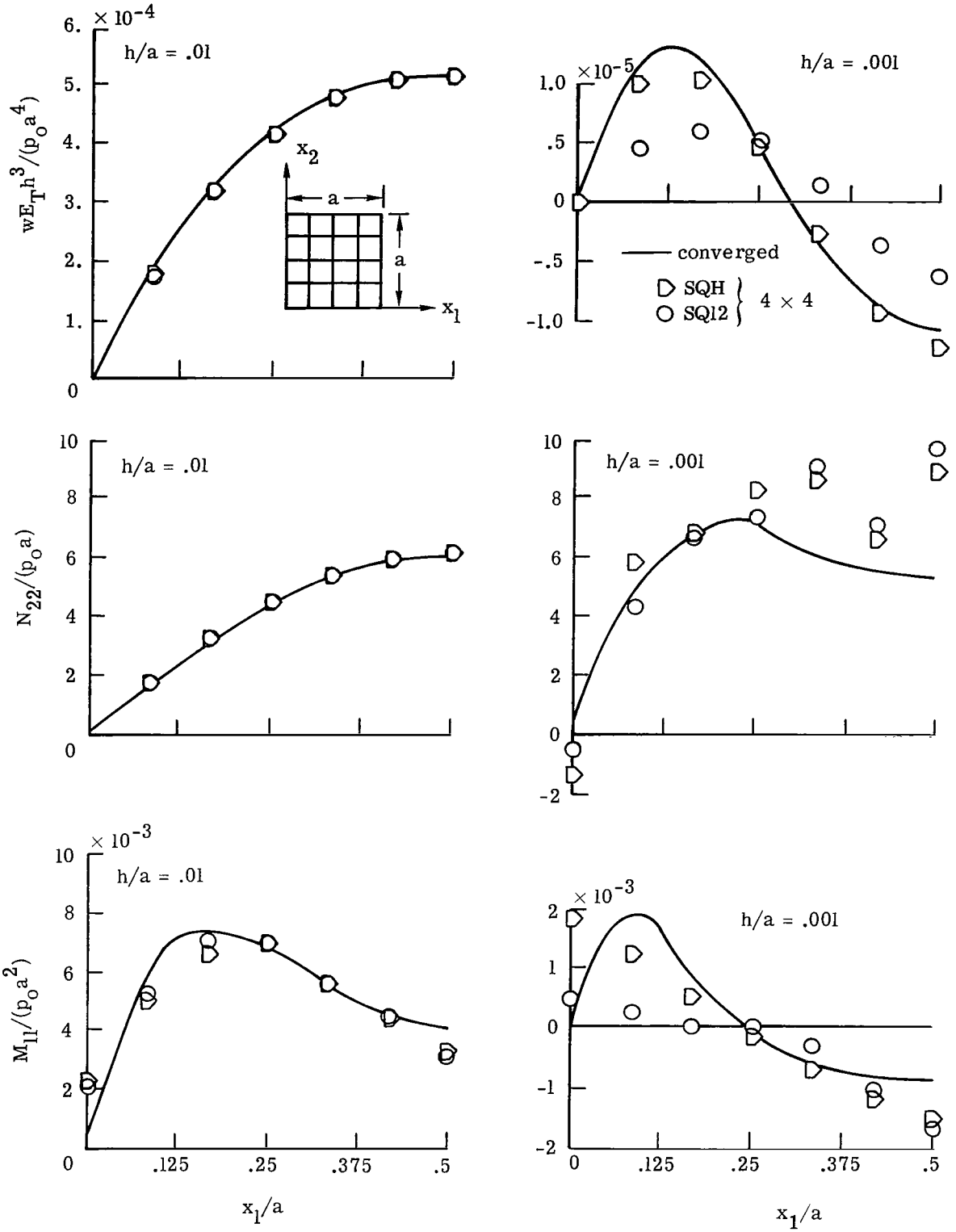

Figure 23.- Distribution of transverse displacement w and stress resultants N_{22} and M_{11} along $x_2 = \frac{a}{2}$. Simply supported, nine-layered, anisotropic spherical segments. $\frac{h}{a} = 0.01$ and 0.001.

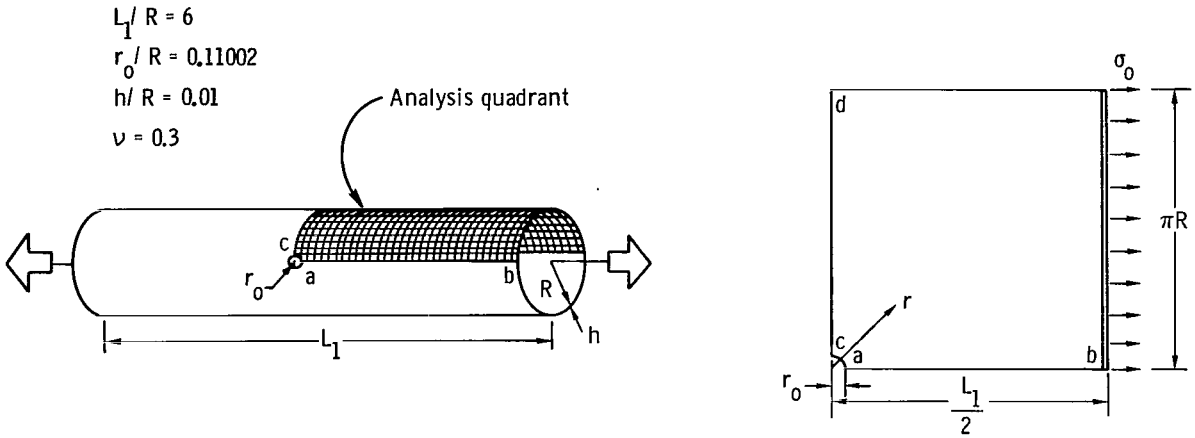

Figure 24.- Cylinder with a circular cutout loaded in tension.

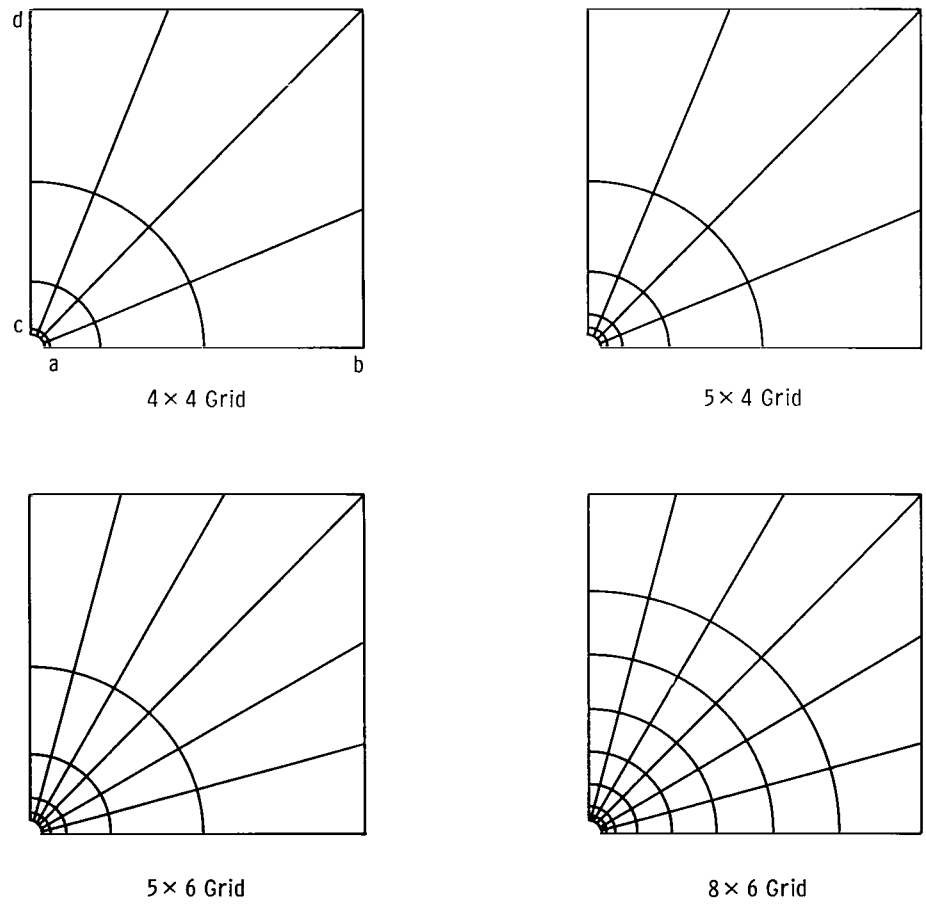

Figure 25.- Grids used in present study for cylinder with a cutout.

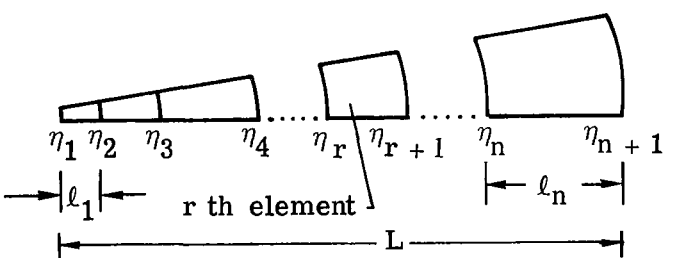

Grid	Number of elements	ℓ_1/r_o	ℓ_n/r_o
4 × 4	16	0.500	13.134
5 × 4	20	0.500	13.134
5 × 6	30	0.500	13.134
8 × 6	48	0.250	6.567

Figure 26.- Variable grid parameters.

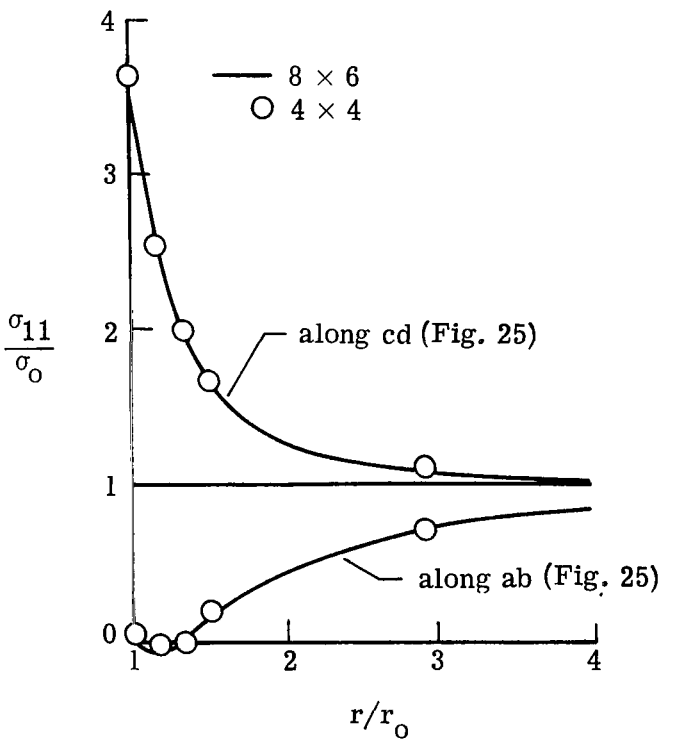

Figure 27.- Distribution of membrane stress concentration σ_{11}/σ_o obtained by isoparametric SQ12 elements.

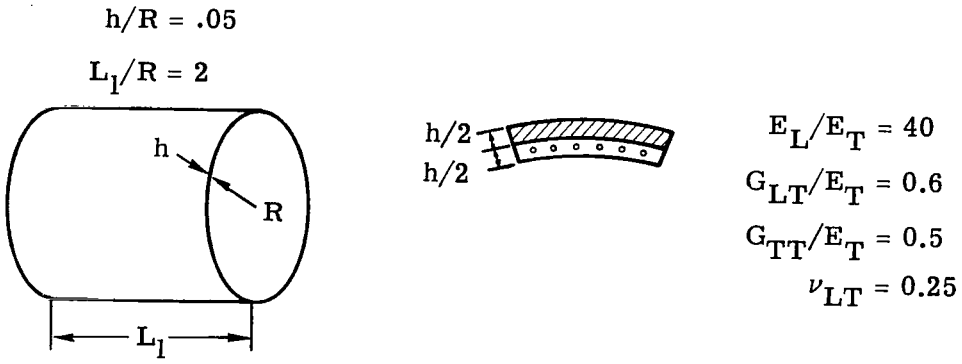

Figure 28.- Characteristics of two-layered graphite-epoxy cylinders.

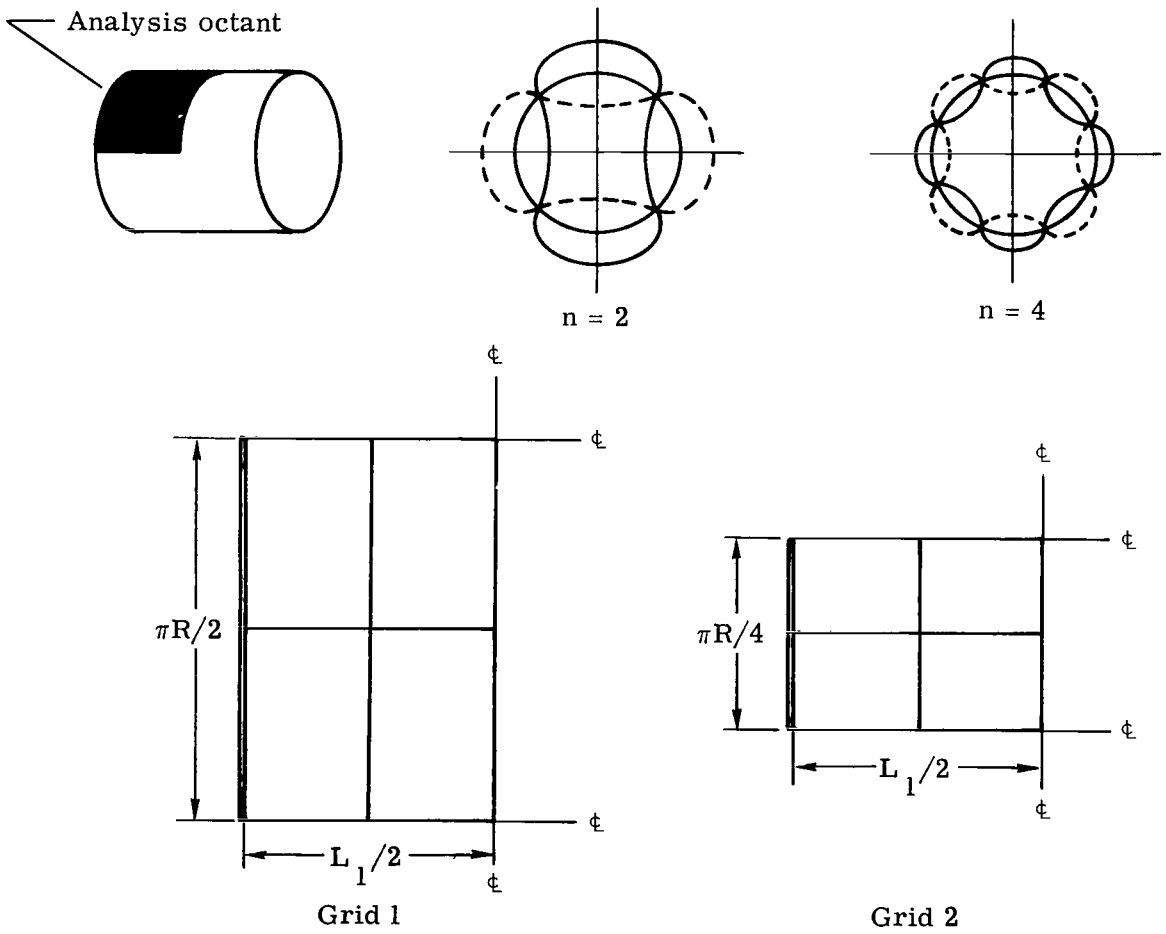

Figure 29.- Grids and modes for orthotropic cylinder.

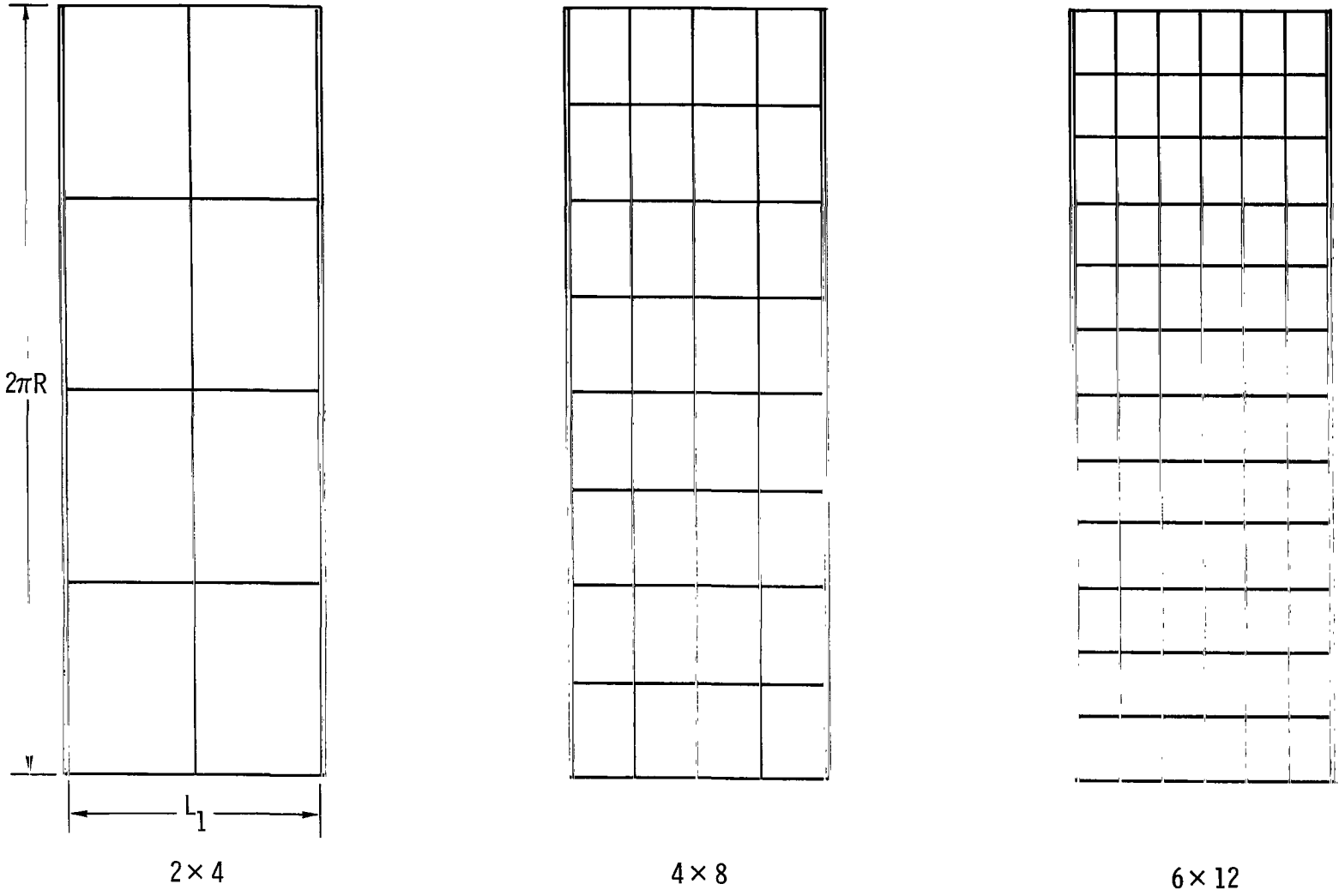

Figure 30.- Grids used for anisotropic cylinder.

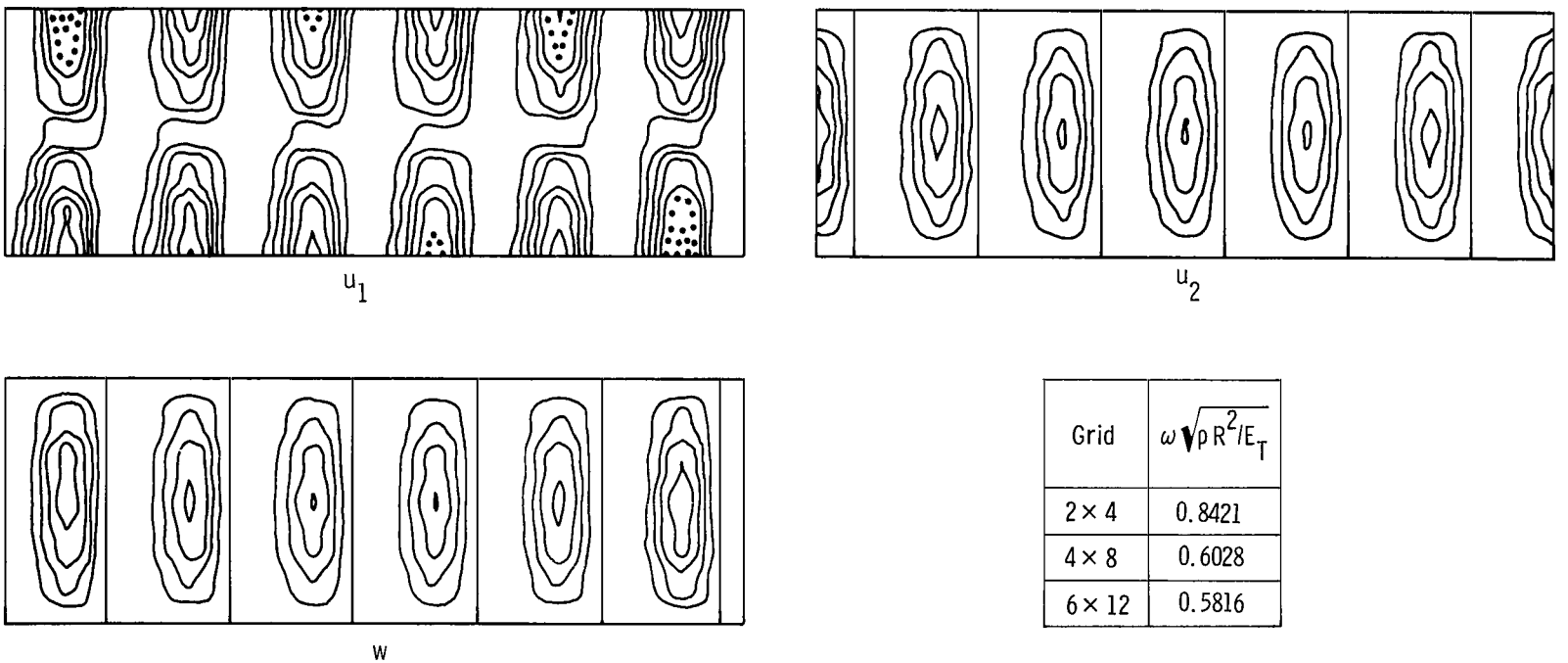

Grid	$\omega\sqrt{\rho R^2/E_T}$
2 × 4	0.8421
4 × 8	0.6028
6 × 12	0.5816

Figure 31.- Fundamental mode shapes and frequencies for simply supported, two-layered, anisotropic graphite-epoxy cylinder.

"The aeronautical and space activities of the United States shall be conducted so as to contribute . . . to the expansion of human knowledge of phenomena in the atmosphere and space. The Administration shall provide for the widest practicable and appropriate dissemination of information concerning its activities and the results thereof."

—NATIONAL AERONAUTICS AND SPACE ACT OF 1958

NASA SCIENTIFIC AND TECHNICAL PUBLICATIONS

TECHNICAL REPORTS: Scientific and technical information considered important, complete, and a lasting contribution to existing knowledge.

TECHNICAL NOTES: Information less broad in scope but nevertheless of importance as a contribution to existing knowledge.

TECHNICAL MEMORANDUMS: Information receiving limited distribution because of preliminary data, security classification, or other reasons. Also includes conference proceedings with either limited or unlimited distribution.

CONTRACTOR REPORTS: Scientific and technical information generated under a NASA contract or grant and considered an important contribution to existing knowledge.

TECHNICAL TRANSLATIONS: Information published in a foreign language considered to merit NASA distribution in English.

SPECIAL PUBLICATIONS: Information derived from or of value to NASA activities. Publications include final reports of major projects, monographs, data compilations, handbooks, sourcebooks, and special bibliographies.

TECHNOLOGY UTILIZATION PUBLICATIONS: Information on technology used by NASA that may be of particular interest in commercial and other non-aerospace applications. Publications include Tech Briefs, Technology Utilization Reports and Technology Surveys.

Details on the availability of these publications may be obtained from:

SCIENTIFIC AND TECHNICAL INFORMATION OFFICE

NATIONAL AERONAUTICS AND SPACE ADMINISTRATION

Washington, D.C. 20546